3D STRUCTURES BASED ON CARBON MATERIALS AND CONDUCTING POLYMERS FOR ELECTRORESPONSIVE CELL CULTURE

Antonio Dominguez-Alfaro
Ph.D Thesis
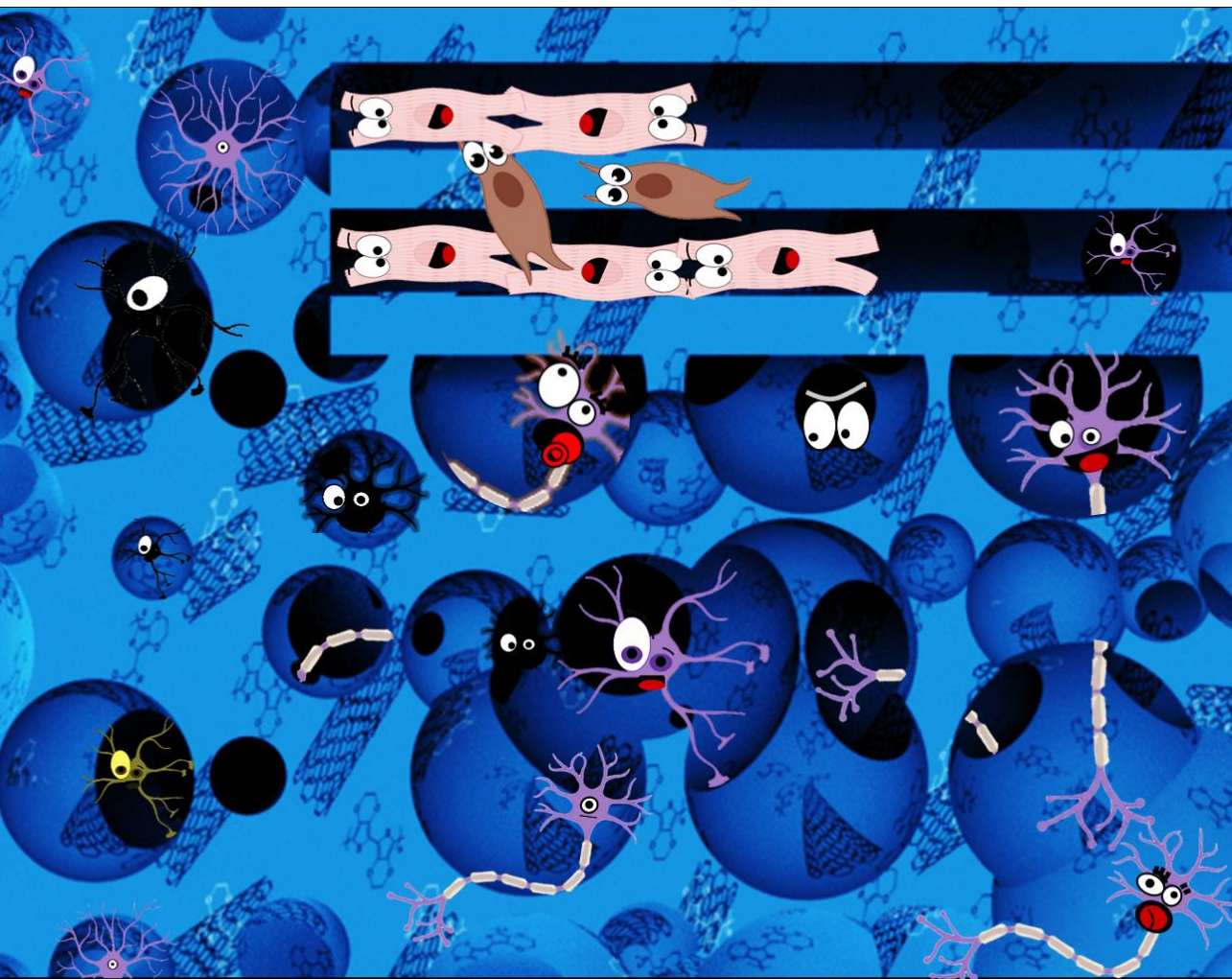Donosti, 2020

eman ta zabal zazu

Universidad del País Vasco

Euskal Herriko Unibertsitatea

3D structures based on carbon materials and conducting polymers for electroresponsive cell cultures

Antonio Domínguez Alfaro

Thesis Supervisor:
Prof. David Mecerreyes
Prof. Maurizio Prato

University Tutor:
Maria Paulis Lumbreras

University of the Basque Country UPV/EHU
Donostia-San Sebastian, Spain

A mis abuelos,

A mi Andalucía querida
"Estos días azules, y este sol de mi infancia"

Table of content

Conducting Polymers

Carbon Nanotubes (CNTs)

Conducting scaffolds for tissue engineering

Chapter 1: Introduction Conducting Scaffolds for Tissue Engineering

1.1 Tissue engineering

The aberrant increase in the population during the last century and future perspectives denote drastically limitations related with natural and social resources. Tissue engineering (TE) or regenerative medicine represent an interesting research field that requires the development of new health resources throughout new materials. The goal of this field is to manufacture structures that mimic the native organ for its functional replacement or reproduce a specific environment for its study. These structures rise from the combination of biomaterials, cells, and bioactive factors accurately selected to mimic and restore

a regular function of the body.[1] Up to date, tissue engineering has been used for skin, trachea, blood vessels,[2] bladder,[3] and urethra,[4] being successfully transplanted in humans.[5]

However, recreating functional biological tissues and/or organs is challenging due to the difficulties in simulating *in vitro* and *in vivo* environments that drive different cells to engineer a tissue. Hence, before manufacturing tissue or organs, there is a requirement to produce three-dimensional structure that fulfills the same properties as the complex human matrix.

1.2 About the tridimensionality

Take a moment and have a look into the world surrounding yourself. Doors, books, the TV, the computer, this thesis, our hands, people… everything that is around us is designed in three dimensions. Nevertheless, what is the exact meaning of the three dimensions or tridimensionality? According to the dictionary: "having three dimensions (such as height, width and depth), [means] looking real". Therefore, three dimensions represent everything that is in the universe and possess height, width and depth.

Three dimensions is not an isolate requirement of our macroscopic reality; inside living organism cells, the complex 3D tissue environment is forming intricate systems that impact the natural cellular response.[6] One of the main demonstration is that, current *in vitro* tests where material toxicity is evaluated, and generally carried out inside bidimensional petri dishes, do not fully support the complexity and heterogeneity of real systems.

In 1950, Leighton introduced by first time tridimensional porous structures in order to maintain the native tissue-like architecture, an important number of studies have

demonstrated that cells have a diverse behavior and response when cultured in a 3D organization, offering a more suitable *in vivo*-like environment.[7] These structures that provide cell-cell and cell-matrix communication are called scaffolds and must obey the following characteristics to mimic the *in vivo* environment: (i) porous structure in the three dimensions, with pore sizes large enough to allow cellular penetration and growth, as well as nutrient and metabolic waste flow; (ii) mechanical properties similar to the tissue of interest; (iii) an appropriate surface composition and morphology to allow cellular adhesion and interaction; and (iv) conductivity, related with electroactive tissue.[8]

1.3 Conducting materials for tissue engineering

On the basis of light microscopy, is estimated that inside of a mammalian body coexist around 210 different types of differentiated cell[5]. Within the different categories, the ones that respond to a pulsatile or continuous electrical stimulus are called electroactive cells. These biological tissues are electrically enhanced with endogenous electrical currents due to the flowing of charged ions through ion pumps, gap junctions, or simple leaking across individual cells. The difference in the ion concentration inside and outside the cells generates an electric field across cell membranes, named the membrane potential.[9] For example, neurons use electrical and electrochemical potentials to transmit information from neuron to neuron through synapses. Muscle cells produce electrical impulses that travel through the entire organ leading to muscle contraction, thus providing heart beats in the cardiac cells. As another example, some studies have demonstrated that bone marrow use conductivity to regenerate new tissue.[7]

Overall, for the development of scaffolds for electroactive tissue, conductivity is an essential requirement to enhance biological response, as well as cell-cell and cell-matrix interactions.

1.3.1 Conducting polymers and PEDOT

Conducting polymers (CP) are conjugated polymers that are able to move electrons throughout its backbone. Since the first conducting polymer (polyacetylene) was discovery at the early 70s, they have been explored in more than 124 research areas. After the awarded Nobel prized in chemistry in 2000 for the "discovery and development of electrically conductive polymers", new CPs have been synthesized improving some features as chemical stability, conductivity and biocompatibility, maintaining their main characteristic: their conjugation. **Figure 1.1** collects the most common conjugated polymers used so far: polyacetylene (PA), polypyrrole (PPy), polyaniline (PANI), poly(p-phenylene-vinylene) (PPV), poly (3,4-ethylene dioxythiophene) (PEDOT), polyfuran (PF) and other polythiophene (PTh) derivatives.
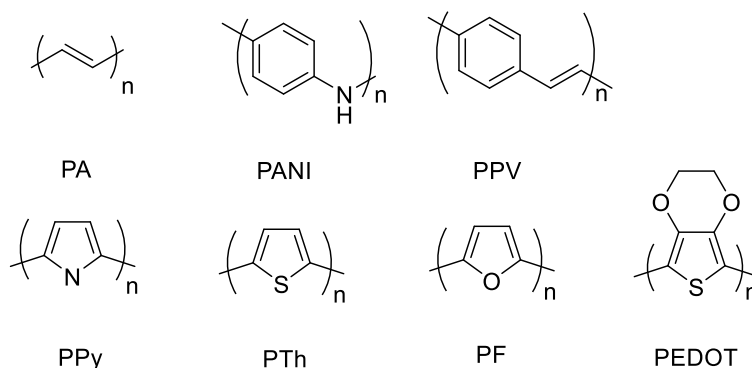
Figure 1.1 Schematic structure of the most common conductive polymers studied.

Due to its conjugation, they can be oxidized and reduced in a reversible manner modifying their conductivity. In fact, conductivity depends on the oxidation state: while neutral states present low electrical conductivity, oxidized states present the highest. As a consequence of oxidation/reduction, negatively or positively charged species, called dopants, can be incorporated as counterbalance species to

neutralize the overall charge. The presence of the dopants not only improves the conductivity, but also modulates the optical, magnetic and structural properties.

Among CPs, poly(3,4-ethylenedioxythiophene) (PEDOT) is the most used because its air-stability, derivatizability, high conductivity, biocompatibility and electrochromicity. However, the main problems when working with PEDOT are that it is not soluble, not processable and dopants are mandatory to obtain good conductivity.

Regarding the doping, when PEDOT is treated with a controlled oxidative environment two different states can be obtained (see **Figure 1.2**): the polaron that is the presence of a radical ion in the tiophene structure or bipolarons that presents dications which possess absorbance in the near infrared spectra and confer the highest conductivity state.

| Neutral state | Polaron state | Bipolaron state |
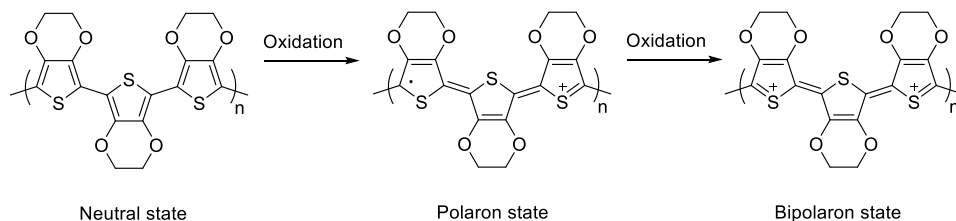
Figure 1.2 Different oxidation (neutral, polaron and bipolaron) states in PEDOT

Principally, exist two approaches to obtain PEDOT: *via* chemical oxidative polymerization, where reaction can take place in vapour or solution phase; or *via* electrochemical polymerization, which is performed in solution. The main difference between them is in the chemistry behind the removal of the proton of the monomer to generate the radical cation. In the chemical reaction, EDOT is oxidized by an iron based-oxidant to a cation radical, while in the electropolymerization the radical is formed electrochemically. Afterwards, both polymerization mechanism are similar, beyond slightly changes (see **Figure**

1.3.[9,10] Towards the oxidative polymerization, EDOT cation radicals form dimers that subsequently get deprotonated; then while the PEDOT polymeric chains are formed, they are doped with tosylate ion that resides on the film as a counterion.

D= Counterion/Dopant
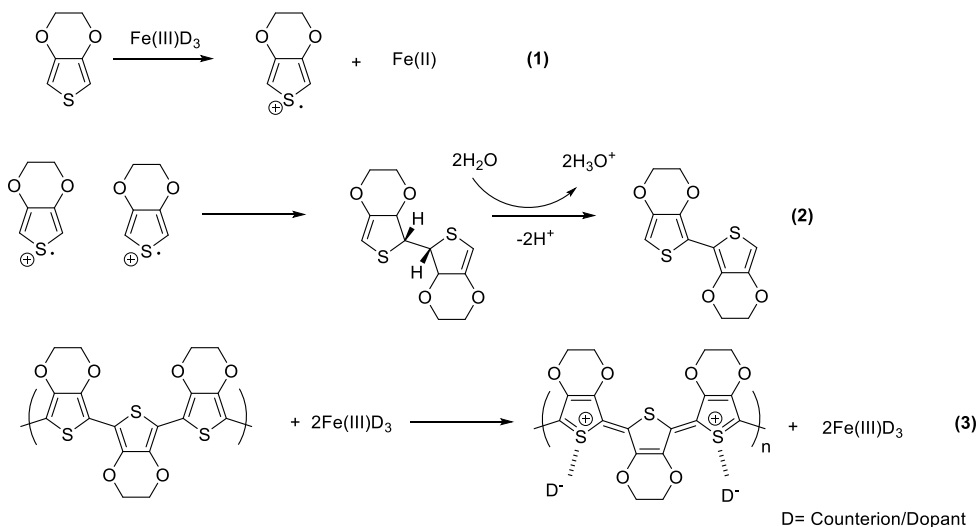
Figure 1.3 General polymerization mechanism of PEDOT by oxidative polymerization. (1) EDOT is oxidized by Fe(III) to a cation radical; (2) EDOT cation radicals form dimers that subsequently get deprotonated; (3) PEDOT polymer is doped and a tosylate ion resides in the film to act as a counter ion.

Generally, only films have been obtained using this technique. However, the way to polymerize PEDOT allows the introduction of additives as secondary dopants, which help to enhance properties as ionic conductivity, strength, capacitance or even the improvement of self-standing material. The use of carbon nanomaterials as secondary dopants will be described in more detail in the next sub-section.

1.3.2 Carbon nanomaterials and carbon nanotubes

Since E. Smalley, Harold W. Kroto and Robert F. Curl discovered the buckminsterfullerene in 1985,[11] carbon nanomaterials (CNMs) have become one of the materials more studied in the research field over years. (see **Figure 1.4**).

Focusing on materials with honeycomb structure, carbon nanotubes and graphene, are classified in literature as other type of conductive materials. As well as CPs, they have free electronic movement along their structure that confers their high conductivity.
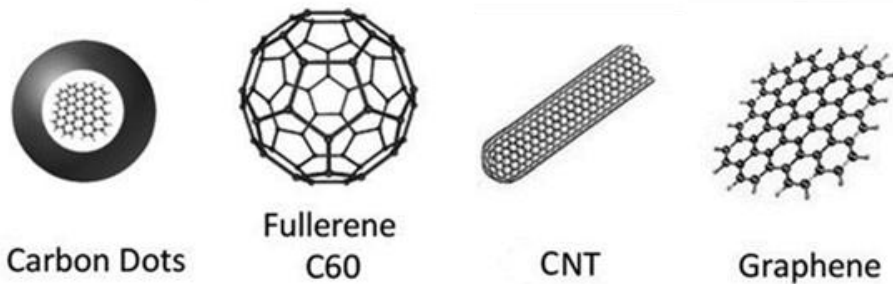
Figure 1.4 Carbon nanomaterials discovered along the last decades. Figure adapted from ref.[12]

In general, CNMs are very versatile materials with remarkable characteristics as easy hybridization to sp^3 atoms, low toxicity, high surface area, ultralight weight, electron-rich properties and excellent chemical and thermal stability. Specifically, carbon nanotubes (CNTs) are distinguished due to their tubular shape that possess extremely high aspect ratio ($\sim 1.32 \cdot 10^8$) and near zero weight. As a consequence, CNTs have been reported many times in literature as reinforcement in polymer composites.[11] CNTs can be divided in: single walled CNTs (SWCNTs), which contains shapes of diameter ranged from 0.7 to 1.4 nm and multi-walled CNTs (MWCNTs) that consist of multiple concentric cylinders with honeycombs

lattices of carbon that form tubes with diameters up to 100 nm and lengths from few hundreds of nm up to several μm for both cases.[13]

In the field of TE, CNTs are consider one of the most promising materials to interface with the central nervous system (CNS).[14,15] As consequence they have been used as growth substrates scaffolds for nerve tissue engineering, electrode coating, long-term implants, drug delivery agents, and molecular sensors.[16,13,17] In the last 20 years, CNTs have been demonstrated as promoters of neural growth and functional processes within axonal extension,[7] beside as modulators of neuronal behavior and inductors of neuronal differentiation. [18–22]

In particular, Prato *et al.* have demonstrated that the tight contact of the nanomaterial with the neuronal membranes boosts the neuronal survival and proliferation as well as promotes neuronal process outgrowth, axon excitability and synaptic activity of neuronal networks. [23–26] Due to their tubular morphology and electrical properties, CNTs have also been used for the stimulation of multiple neuronal cells, such as NG108 cell line, primary rat peripheral and hippocampal neurons.[27] Moreover, the inclusion of CNTs into scaffolds has addressed many requirements in TE as the reduction of astrocytic reactions, thus glial scar formation and the allowance of neuronal adhesion and axonal extension within the tridimensional architecture.

Overall, CNTs boost the growth and function of neurons, evoking postsynaptic responses on neurons, thus demonstrating huge potential for their electrical coupling.[28]

1.4 Conducting scaffolds of PEDOT and CNTs in tissue engineering

Conducting material could not only provide a structural and mechanical properties of natural-like tissues, but also transmit electrical signals between electroactive cells, promoting their adherence, migration, proliferation, and, when required, differentiation. In the field of tissue engineering, scaffolds have been manufactured in different ways, providing development of different conducting 3D architectures, as illustrated in **Figure 1.5**.

The major obstacle in using CPs and/or CNTs is the poor mechanical properties and their difficulties in manipulating and processing. Therefore, the manufacturing process of tridimensional porous structures containing CPs/CNTs individually or together represent a big challenge.

The employment of CPs and CNTs provides the final scaffold properties as biocompatibility and conductivity. The other requirements for TE, as porosity and suitable mechanical properties, need to be fulfilled choosing the right manufacturing method. Thus, within the classification presented in **Figure 1.5,** only two of the four 3D structures showed are able to accomplish this requirements: porous and 3D printed scaffolds. Hence a brief description above the methods and applications of this materials will be described.
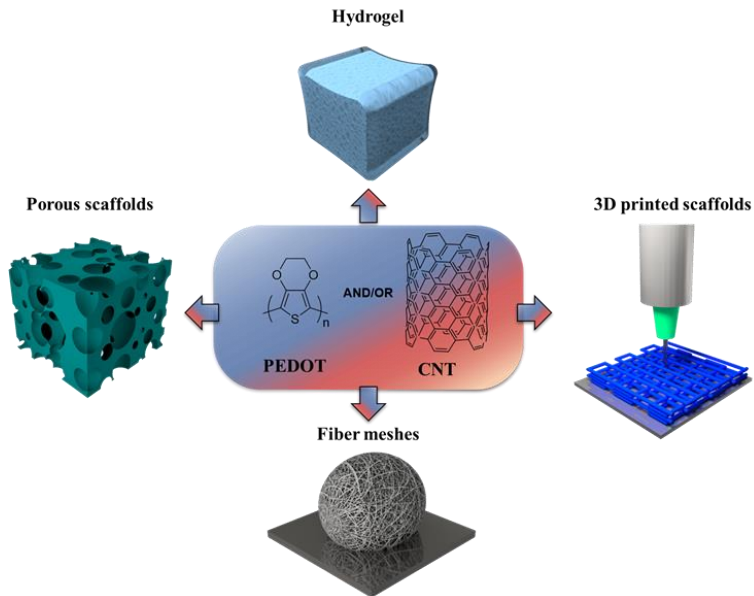
Figure 1.5 Different manufacturing techniques for the development of 3D conducting scaffolds. Figure adapted from ref.[29]

1.4.1 Porous conducting 3D scaffolds

There are different methods to produce porous scaffold as salt/sugar leaching, gas foaming, freeze drying or electrospinning, among others. All these examples involve the presence of a porogen as water, CO_2, salts or polymers.[10] Generally, this methodology allows an accurate porosity control in comparison with other techniques, as well as the possibility to make composites with ceramics, carbon nanomaterials, metals or even polymers.

As a representative example, CNTs have been included into three dimensional polymer matrices with a very high porosity while retaining the tridimensional structure, using polydimethylsiloxane (PDMS) and crystal sugar grains as

porogen.[30] In spite of the use of an isolating polymer, the large dimension of the CNTs and its concentration allows to retain the conductivity even along the three dimensions of the macrostructure. PDMS/CNTs scaffolds were studied as substrates for primary hippocampal neurons *in vitro* cultures and also implanted into adult rat visual cortex for long time. As a result, the scaffolds showed minimal immune response, demonstrating its good performance as neural interfaces.[28] These scaffolds will be refereed and deeply discussed in Chapter 2.

However, manufacturing porous conductive materials using PEDOT throughout a porogen presents important limitations due to the tiny polymer chains formed, producing scaffolds with high fragility and conductivity loss. PEDOT has always required the blending with another malleable non-conductive polymer, such as polystyrene sulfonate (PSS), to overcome such shortcoming. On the other side, freeze-drying represents an ultimate solution for the manufacturing of porous PEDOT:PSS scaffolds, allowing high conductivity while maintain soft properties and controlled porosity.[31] As main disadvantage, PEDOT:PSS solution is a patented product which does not allow the composition control; besides, the scaffold formation always require the action of a crosslinker as (3-glycidyloxypropyl)trimethoxysilane (GOPS) to retain the macrostructure[32].

As an example of the use of porous PEDOT scaffolds in biomedical applications, PEDOT:PSS scaffolds have been use for bone tissue engineering.[31] Moreover, Mecerreyes *et al.* substituted PSS with natural polymers such as xhantan gum[33], guar gum[34] and other glycosaminoglycans, as hyaluronic acid, chondroitin or heparine,[35] to form PEDOT:polysaccharides scaffolds for bioelectronics, cell growth monitoring, mixing ionic and electronic conductor or bioactive material for neural interfaces respectively.

1.4.2 3D printing of conducting polymers

3D printing consists on the deposition of a material layer by layer by using physicochemical changes until the formation of a tridimensional structure previously designed by computer aided manufacturing software. Physicochemical changes comprise temperature changes, chemical crosslinking and gelation process among others. Against other conventional manufacturing methods 3D printing has the advantage that allows fabrication of complex customized shapes easily. Therefore, 3D printing has stood out in areas such as tissue engineering, biomedical devices, aerospace, energy or soft-robotics.

Specially, 3D printing for tissue engineering represents a powerful tool since the possibility of create custom shapes inspired to the representative biological components. Two successful examples of 3D printing applications are the manufacturing of disease models before getting surgery and the fabrication of blood vessels implants.[36]

3D printing techniques can be summarized in the **Figure 1.6.** Each technique uses a source to produce the physicochemical change: light-based printing (SLA) use UV light, ink-jet use gelation or evaporation, extrusion based printing use temperature or evaporation of a solvent and electrohydrodynamic (EHD) printing use the differential of electrical current.

There are not many examples in the literature of 3D printing of conducting polymers. In a recent work, PEDOT:PSS was 3D printed by SLA forming an hydrogel with a crosslinked PEG diacrylate to create scaffolds for cell support while maintain the conductivity.[37] In another example, Phytic acid was mixed with PANI to produce at the same time gelation and subsequent doping; thus, controlling the deposition of both components it was possible to perform injecting printing.[38]

Finally, EHD printing manufacture of fibrous scaffolds was reported by deposition in layers made of PPy and polycaprolactone (PCL) for porous nerve guide conduits.[39]

Specifically, extrusion based printing is very popular in additive manufacturing. In this technique, in the first step the material is inserted in an extruder throughout a filament called fused filament fabrication (FFF) or throughout a direct way called direct ink writing (DIW); then the material flow down by the action of a mechanic gear, pneumatic or compression system. Recently, by a DIW a rheologically adapted PEDOT:PSS ink was printed and crosslinked through solvent evaporation, obtaining very high resolution structures that maintain the highly conducting performance of the polymer.[40] Another example took advantage of the viscous properties of PLLA solutions to blend and print PPy spheres and nanowires.[41] However, the use of this direct melting extrusion are quite unexplored for conducting polymers, and not reported yet in the case of PEDOT.
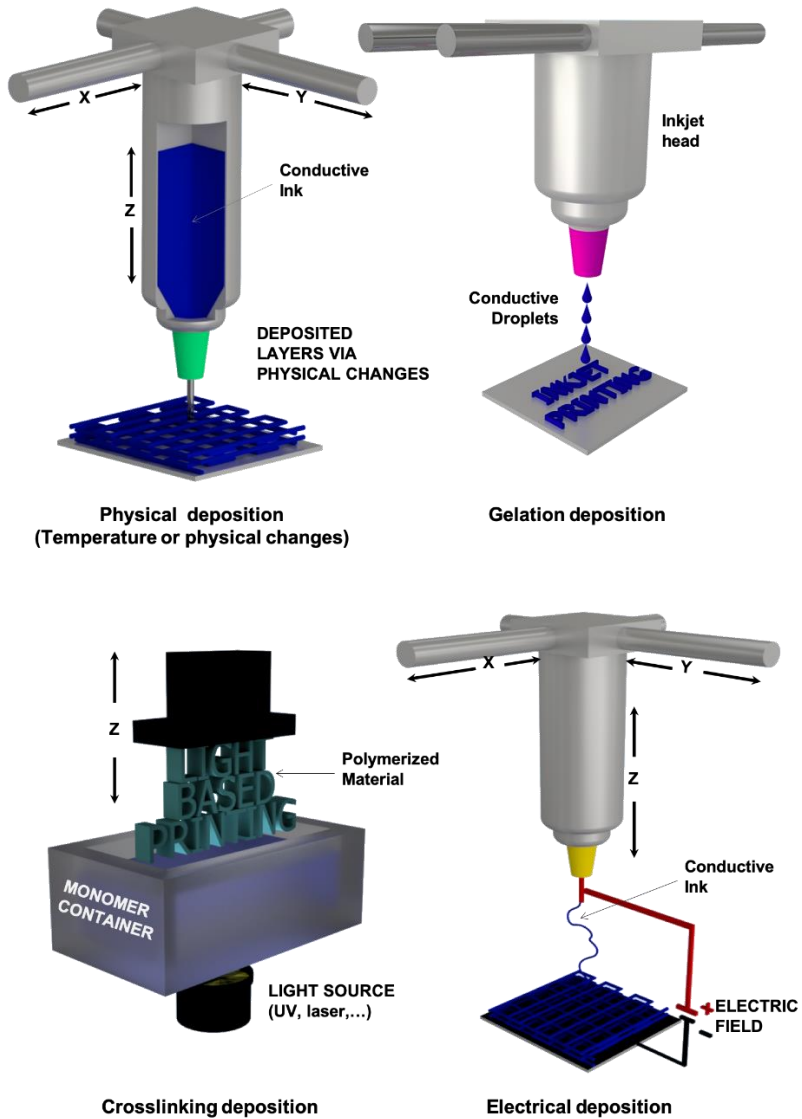
Figure 1.6 3D printing systems for development of conducting scaffolds. In the top, extrusion-based printing (left) and inkjet printing (right). In the bottom, light based printing (left) and electrohydrodynamic printing (right). Figure adapted from ref.[29]

1.5 Motivation, objectives and outline of the thesis

Innovative 3D materials are required in the field of tissue engineering for the development of conductive scaffolds for diseases models or body implants. The main problem observed with conductive materials is their poor processability, which limited the manufacture of real tridimensional structures.

Basically, we have addressed this disadvantage developing new manufacturing methods for scaffolds composed of conductive materials. Therefore, the aim of this thesis is to develop new tridimensional structures based on PEDOT that fulfill the tissue requirements. Such requirements would be the total biocompatibility, presence of controlled porosity for cell interconnectivity and flow of vital nutrients, specific soft mechanical properties to mimic tissue properties and electronic conductivity to enable and enhance cell adhesion and proliferation of electroactive cells.

This PhD thesis consists of five chapters. In the first, chapter the introduction to the thesis topics is presented. This introduction includes the description of the conducting materials used in this work such as CNTs and PEDOT, as well as the state-of-the art in the manufacturing of conductive scaffolds and the objectives of the PhD. After the introduction, three different innovative approaches to manufacture scaffolds are presented in three separate chapters. Thus, the second chapter deals with the investigation of novel PEDOT/CNTs scaffolds manufactured by an adaptation of the classical vapor phase polymerization method for films. In this case, the method was applied to a 3D scaffold which contain CNTs and sacrificial sugar porogens. The resulting conducting porous scaffolds based on PEDOT and CNTs were characterized and compared with previous semi-insulating PDMS/CNTs scaffolds. C8-D1A astrocytes, generally used as glial models, were cultured into both materials and its growth and attachment was compared.

In the third chapter, we have adapted another well-known film manufacturing technique of conducting polymers in order to develop PEDOT/CNTs scaffold by electrochemical polymerization. The PEDOT/CNTs porous scaffold was characterized and compared with a scaffold composed only by PEDOT. Neuroblastoma cells SH-SY5Y that are often used as in vitro models were cultured onto the electropolymerized scaffolds with and without CNT demonstrating differences in the growth and differentiation.

In the fourth chapter, a 3D printable conducting and biocompatible PEDOT-graft-PLA co-polymers for Direct Ink Writing were developed. Here, a novel graft copolymer between PEDOT with a tailored polylactide PLA macromonomer was synthesized by oxidative polymerization. The graft was characterized and its printability by direct ink writing throughout melting extrusion was studied. Patterns with specific shapes were printed and co-culture with primary cardiomyocytes and cardiac fibroblast as proof of concept for future cardiac patches.

To conclude, chapter five shows the most relevant findings, future work, and conclusions of this PhD thesis.
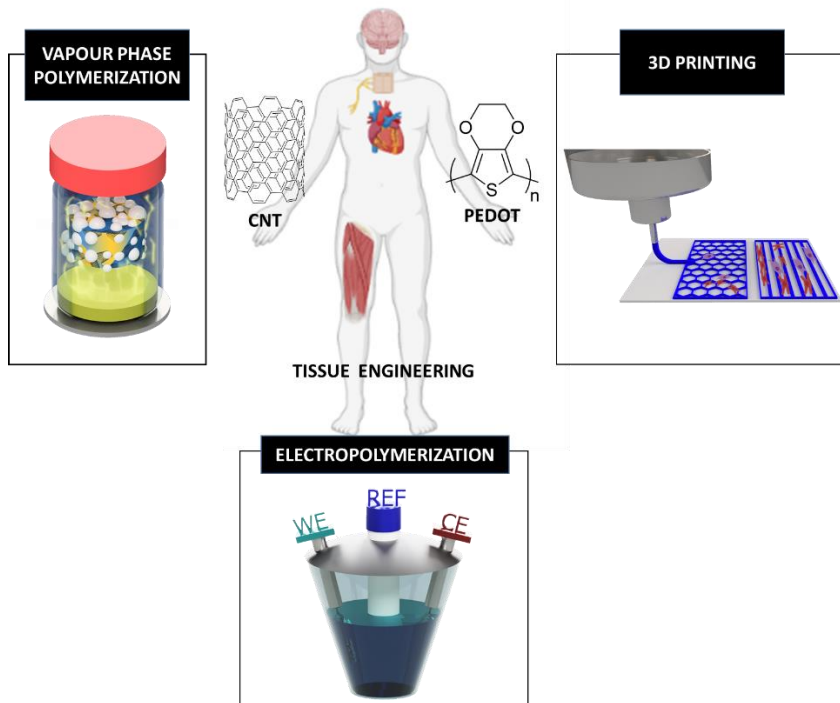
Figure 1.7 Work outline

1.6 References

(1)   LANGER, R.; VACANTI, J. P. TISSUE ENGINEERING. *Science (80-.).* **1993**, *260* (5110), 920–926. https://doi.org/10.1126/science.8493529.

(2)   Zhu, W.; Qu, X.; Zhu, J.; Ma, X.; Patel, S.; Liu, J.; Wang, P.; Lai, C. S. E.; Gou, M.; Xu, Y.; Zhang, K.; Chen, S. Direct 3D Bioprinting of Prevascularized Tissue Constructs with Complex Microarchitecture. *Biomaterials* **2017**, *124*, 106–115. https://doi.org/10.1016/j.biomaterials.2017.01.042.

(3)   Atala, A.; Bauer, S. B.; Soker, S.; Yoo, J. J.; Retik, A. B. Tissue-Engineered Autologous Bladders for Patients Needing Cystoplasty. *Lancet* **2006**, *367*

(9518), 1241–1246. https://doi.org/https://doi.org/10.1016/S0140-6736(06)68438-9.

(4) Raya-Rivera, A.; Esquiliano, D. R.; Yoo, J. J.; Lopez-Bayghen, E.; Soker, S.; Atala, A. Tissue-Engineered Autologous Urethras for Patients Who Need Reconstruction: An Observational Study. *Lancet* **2011**, *377* (9772), 1175–1182. https://doi.org/10.1016/S0140-6736(10)62354-9.

(5) Lo, C.; Hickerson, D.; Yoo, J. J.; Atala, A.; Allickson, J. Chapter 3 - Moving into the Clinic. In *Principles of Tissue Engineering (Fifth Edition)*; Lanza, R., Langer, R., Vacanti, J. P., Atala, A., Eds.; Academic Press, 2020; pp 53–61. https://doi.org/https://doi.org/10.1016/B978-0-12-818422-6.00003-4.

(6) Romo-Morales, A.; Przyborski, S. An Introduction to the Third Dimension for Routine Cell Culture. *Technology Platforms for 3D Cell Culture*. March 29, 2017, pp 1–19. https://doi.org/doi:10.1002/9781118851647.ch1.

(7) Mattson, M. P.; Haddon, R. C.; Rao, A. M. Molecular Functionalization of Carbon Nanotubes and Use as Substrates for Neuronal Growth. *J. Mol. Neurosci.* **2000**. https://doi.org/10.1385/JMN:14:3:175.

(8) Alegret, N.; Dominguez-Alfaro, A.; Mecerreyes, D. 3D Scaffolds Based on Conductive Polymers for Biomedical Applications. *Biomacromolecules* **2019**, *20* (1), 73–89. https://doi.org/10.1021/acs.biomac.8b01382.

(9) Levin, M. Large-Scale Biophysics: Ion Flows and Regeneration. *Trends Cell Biol.* **2007**, *17* (6), 261–270. https://doi.org/https://doi.org/10.1016/j.tcb.2007.04.007.

(10) Mueller, M.; Fabretto, M.; Evans, D.; Hojati-Talemi, P.; Gruber, C.; Murphy, P. Vacuum Vapour Phase Polymerization of High Conductivity PEDOT: Role of PEG-PPG-PEG, the Origin of Water, and Choice of Oxidant. *Polymer (Guildf).* **2012**, *53* (11), 2146–2151. https://doi.org/https://doi.org/10.1016/j.polymer.2012.03.028.

(11) Mittal, G.; Rhee, K. Y.; Mišković-Stanković, V.; Hui, D. Reinforcements in

Multi-Scale Polymer Composites: Processing, Properties, and Applications. *Compos. Part B Eng.* **2018**, *138*, 122–139. https://doi.org/https://doi.org/10.1016/j.compositesb.2017.11.028.

(12) Baptista, F. R.; Belhout, S. A.; Giordani, S.; Quinn, S. J. Recent Developments in Carbon Nanomaterial Sensors. *Chem. Soc. Rev.* **2015**, *44* (13), 4433–4453. https://doi.org/10.1039/C4CS00379A.

(13) Rauti, R.; Musto, M.; Bosi, S.; Prato, M.; Ballerini, L. Properties and Behavior of Carbon Nanomaterials When Interfacing Neuronal Cells: How Far Have We Come? *Carbon N. Y.* **2019**, *143*, 430–446. https://doi.org/https://doi.org/10.1016/j.carbon.2018.11.026.

(14) Fabbro, A.; Sucapane, A.; Toma, F. M.; Calura, E.; Rizzetto, L.; Carrieri, C.; Roncaglia, P.; Martinelli, V.; Scaini, D.; Masten, L.; Turco, A.; Gustincich, S.; Prato, M.; Ballerini, L. Adhesion to Carbon Nanotube Conductive Scaffolds Forces Action-Potential Appearance in Immature Rat Spinal Neurons. *PLoS One* **2013**, *8* (8), e73621. https://doi.org/10.1371/journal.pone.0073621.

(15) Fabbro, A.; Villari, A.; Laishram, J.; Scaini, D.; Toma, F. M.; Turco, A.; Prato, M.; Ballerini, L. Spinal Cord Explants Use Carbon Nanotube Interfaces to Enhance Neurite Outgrowth and to Fortify Synaptic Inputs. *ACS Nano* **2012**, *6* (3), 2041–2055. https://doi.org/10.1021/nn203519r.

(16) Yang, N.; Chen, X.; Ren, T.; Zhang, P.; Yang, D. Carbon Nanotube Based Biosensors. *Sensors Actuators B Chem.* **2015**, *207*, 690–715. https://doi.org/https://doi.org/10.1016/j.snb.2014.10.040.

(17) Silva, G. A. Neuroscience Nanotechnology: Progress, Opportunities and Challenges. *Nat. Rev. Neurosci.* **2006**, *7* (1), 65–74. https://doi.org/10.1038/nrn1827.

(18) Pampaloni, N. P.; Scaini, D.; Perissinotto, F.; Bosi, S.; Prato, M.; Ballerini, L. Sculpting Neurotransmission during Synaptic Development by 2D Nanostructured Interfaces. *Nanomedicine Nanotechnology, Biol. Med.*

2018, *14* (7), 2521–2532. https://doi.org/https://doi.org/10.1016/j.nano.2017.01.020.

(19) Malarkey, E. B.; Fisher, K. A.; Bekyarova, E.; Liu, W.; Haddon, R. C.; Parpura, V. Conductive Single-Walled Carbon Nanotube Substrates Modulate Neuronal Growth. *Nano Lett.* **2009**, *9* (1), 264–268. https://doi.org/10.1021/nl802855c.

(20) Hu, H.; Ni, Y.; Montana, V.; Haddon, R. C.; Parpura, V. Chemically Functionalized Carbon Nanotubes as Substrates for Neuronal Growth. *Nano Lett.* **2004**, *4* (3), 507–511. https://doi.org/10.1021/nl035193d.

(21) Fabbro, A.; Bosi, S.; Ballerini, L.; Prato, M. Carbon Nanotubes: Artificial Nanomaterials to Engineer Single Neurons and Neuronal Networks. *ACS Chem. Neurosci.* **2012**, *3* (8), 611–618. https://doi.org/10.1021/cn300048q.

(22) Fabbro, A.; Prato, M.; Ballerini, L. Carbon Nanotubes in Neuroregeneration and Repair. *Adv. Drug Deliv. Rev.* **2013**, *65* (15), 2034–2044. https://doi.org/10.1016/j.addr.2013.07.002.

(23) Gazzi, A.; Fusco, L.; Orecchioni, M.; Ferrari, S.; Franzoni, G.; Yan, J. S.; Rieckher, M.; Peng, G.; Lucherelli, M. A.; Vacchi, I. A.; Chau, N. D. Q.; Criado, A.; Istif, A.; Mancino, D.; Dominguez, A.; Eckert, H.; Vázquez, E.; Ros, T. Da; Nicolussi, P.; Palermo, V.; Schumacher, B.; Cuniberti, G.; Mai, Y.; Clementi, C.; Pasquali, M.; Feng, X.; Kostarelos, K.; Yilmazer, A.; Bedognetti, D.; Fadeel, B.; Prato, M.; Bianco, A.; Delogu, L. G. Graphene, Other Carbon Nanomaterials and the Immune System: Toward Nanoimmunity-by-Design. *J. Phys. Mater.* **2020**, *3* (3), 34009. https://doi.org/10.1088/2515-7639/ab9317.

(24) Bianco, A.; Kostarelos, K.; Prato, M. Making Carbon Nanotubes Biocompatible and Biodegradable. *Chem. Commun.* **2011**, *47* (37), 10182–10188. https://doi.org/10.1039/C1CC13011K.

(25) Webster, T. J.; Waid, M. C.; McKenzie, J. L.; Price, R. L.; Ejiofor, J. U.

Nano-Biotechnology: Carbon Nanofibres as Improved Neural and Orthopaedic Implants. *Nanotechnology* **2003**, *15* (1), 48–54. https://doi.org/10.1088/0957-4484/15/1/009.

(26)   Mattson, M. P.; Haddon, R. C.; Rao, A. M. Molecular Functionalization of Carbon Nanotubes and Use as Substrates for Neuronal Growth. *J. Mol. Neurosci.* **2000**, *14* (3), 175–182. https://doi.org/10.1385/JMN:14:3:175.

(27)   Lovat, V.; Pantarotto, D.; Lagostena, L.; Cacciari, B.; Grandolfo, M.; Righi, M.; Spalluto, G.; Prato, M.; Ballerini, L. Carbon Nanotube Substrates Boost Neuronal Electrical Signaling. *Nano Lett.* **2005**, *5* (6), 1107–1110. https://doi.org/10.1021/nl050637m.

(28)   Aurand, E. R.; Usmani, S.; Medelin, M.; Scaini, D.; Bosi, S.; Rosselli, F. B.; Donato, S.; Tromba, G.; Prato, M.; Ballerini, L. Nanostructures to Engineer 3D Neural-Interfaces: Directing Axonal Navigation toward Successful Bridging of Spinal Segments. *Adv. Funct. Mater.* **2018**, *28* (12), 1700550. https://doi.org/10.1002/adfm.201700550.

(29)   Alegret, N.; Dominguez-Alfaro, A.; Mecerreyes, D. Chapter 10 Conductive Polymers Building 3D Scaffolds for Tissue Engineering. In *Redox Polymers for Energy and Nanomedicine*; The Royal Society of Chemistry, 2021; pp 383–414. https://doi.org/10.1039/9781788019743-00383.

(30)   Bosi, S.; Rauti, R.; Laishram, J.; Turco, A.; Lonardoni, D.; Nieus, T.; Prato, M.; Scaini, D.; Ballerini, L. From 2D to 3D: Novel Nanostructured Scaffolds to Investigate Signalling in Reconstructed Neuronal Networks. *Sci. Rep.* **2015**, *5*, 9562.

(31)   Guex, A. G.; Puetzer, J. L.; Armgarth, A.; Littmann, E.; Stavrinidou, E.; Giannelis, E. P.; Malliaras, G. G.; Stevens, M. M. Highly Porous Scaffolds of PEDOT:PSS for Bone Tissue Engineering. *Acta Biomater.* **2017**, *62*, 91–101. https://doi.org/10.1016/j.actbio.2017.08.045.

(32)   Wan, A. M.-D.; Inal, S.; Williams, T.; Wang, K.; Leleux, P.; Estevez, L.; Giannelis, E. P.; Fischbach, C.; Malliaras, G. G.; Gourdon, D. 3D

Conducting Polymer Platforms for Electrical Control of Protein Conformation and Cellular Functions. *J. Mater. Chem. B* **2015**, *3* (25), 5040–5048. https://doi.org/10.1039/C5TB00390C.

(33) del Agua, I.; Marina, S.; Pitsalidis, C.; Mantione, D.; Ferro, M.; Iandolo, D.; Sanchez-Sanchez, A.; Malliaras, G. G.; Owens, R. M.; Mecerreyes, D. Conducting Polymer Scaffolds Based on Poly(3,4-Ethylenedioxythiophene) and Xanthan Gum for Live-Cell Monitoring. *ACS Omega* **2018**, *3* (7), 7424–7431. https://doi.org/10.1021/acsomega.8b00458.

(34) del Agua, I.; Mantione, D.; Casado, N.; Sanchez-Sanchez, A.; Malliaras, G. G.; Mecerreyes, D. Conducting Polymer Iongels Based on PEDOT and Guar Gum. *ACS Macro Lett.* **2017**, *6* (4), 473–478. https://doi.org/10.1021/acsmacrolett.7b00104.

(35) Mantione, D.; del Agua, I.; Schaafsma, W.; Diez-Garcia, J.; Castro, B.; Sardon, H.; Mecerreyes, D. Poly(3,4-Ethylenedioxythiophene):GlycosAminoGlycan Aqueous Dispersions: Toward Electrically Conductive Bioactive Materials for Neural Interfaces. *Macromol. Biosci.* **2016**, *16* (8), 1227–1238. https://doi.org/10.1002/mabi.201600059.

(36) Yan, Q.; Dong, H.; Su, J.; Han, J.; Song, B.; Wei, Q.; Shi, Y. A Review of 3D Printing Technology for Medical Applications. *Engineering* **2018**, *4* (5), 729–742. https://doi.org/https://doi.org/10.1016/j.eng.2018.07.021.

(37) Heo, D. N.; Lee, S.-J.; Timsina, R.; Qiu, X.; Castro, N. J.; Zhang, L. G. Development of 3D Printable Conductive Hydrogel with Crystallized PEDOT:PSS for Neural Tissue Engineering. *Mater. Sci. Eng. C* **2019**, *99*, 582–590. https://doi.org/https://doi.org/10.1016/j.msec.2019.02.008.

(38) Pan, L.; Yu, G.; Zhai, D.; Lee, H. R.; Zhao, W.; Liu, N.; Wang, H.; Tee, B. C.-K.; Shi, Y.; Cui, Y.; Bao, Z. Hierarchical Nanostructured Conducting Polymer Hydrogel with High Electrochemical Activity. *Proc. Natl. Acad. Sci.*

2012, *109* (24), 9287–9292. https://doi.org/10.1073/pnas.1202636109.

(39)   Vijayavenkataraman, S.; Kannan, S.; Cao, T.; Fuh, J. Y. H.; Sriram, G.; Lu, W. F. 3D-Printed PCL/PPy Conductive Scaffolds as Three-Dimensional Porous Nerve Guide Conduits (NGCs) for Peripheral Nerve Injury Repair. *Front. Bioeng. Biotechnol.* **2019**, *7*, 266. https://doi.org/10.3389/fbioe.2019.00266.

(40)   Yuk, H.; Lu, B.; Lin, S.; Qu, K.; Xu, J.; Luo, J.; Zhao, X. 3D Printing of Conducting Polymers. *Nat. Commun.* **2020**, *11* (1), 1604. https://doi.org/10.1038/s41467-020-15316-7.

(41)   Ma, C.; Jiang, L.; Wang, Y.; Gang, F.; Xu, N.; Li, T.; Liu, Z.; Chi, Y.; Wang, X.; Zhao, L.; Feng, Q.; Sun, X. 3D Printing of Conductive Tissue Engineering Scaffolds Containing Polypyrrole Nanoparticles with Different Morphologies and Concentrations. *Materials (Basel).* **2019**, *12* (15). https://doi.org/10.3390/ma12152491.

CHAPTER 2
VAPOUR PHASE
POLYMERIZATION

Chapter 2: Vapour Phase Polymerized Scaffolds

2.1 Introduction

Vapor phase polymerization (VPP) is one of the first documented methodologies employed for the manufacturing of bidimensional films of conductive polymers (CP). This technique was discovered at the earliest of 2000 and allows to synthesize PEDOT-based materials with the highest conductivities (up to 1000 S/cm).[1,2]

VPP is based on the polymerization reaction that occur when an EDOT monomer unit in gaseous phase is placed intimately in contact with an oxidant, typically iron tosylate (($Fe(Tos)_3$), yielding PEDOT. Chemically, EDOT is oxidized by the Fe(III) forming at the initial step EDOT radicals, then dimers, oligomers and finally

PEDOT, as it was indicated in the introduction. Commonly, the iron-based oxidant is drop-casted or spin-coated onto a substrate and then the polymerization takes place on the surface.

The main problem of this methodology resides in the low reproducibility, since PEDOT under harsh conditions of temperature can suffer overoxidation, thus decreasing its conductivity and film delamination.[3,4] Hence, during last years, an important number of publications[5] have appeared showing how different additives, such as pyridine[6], surfactants or poly (ethyleneglycol)[7], can improve the reproducibility and electronic performance and film formation, and have been predominantly applied for organic photovoltaics and fuel cells.[8]

However, up to date, only planar substrates have been reported using this method.[5,9] The major obstacle in manufacturing 3D structures composed uniquely of conducting polymers by VPP is that during the process, the oligomers are produced within the lattices, producing short polymer chains with high conductivity and low mechanical properties, thus decreasing the capability to hold the macrostructure and collapsing. As an alternative, conductive structures can be produced by the formation of an external coating through VPP of the conducting polymer, being the latter polymerized around a previous manufactured 3D structure Such approach has been achieved in 3D printed scaffolds,[10] fibers,[11] or even cellulose aerogels, among others.[12] However, a thin layer of CP is formed on the 3D structure and the conductivity performance is very poor.

Hence, the only way to solve this problem is to use secondary nanocomposites that could improve the weak structure. In this line, there are only a few studies published, one of which fabricated a hybrid PEDOT-SiO_2 3D porous structure *in situ* by VPP with polystyrene microparticles as template.[13–15]

Carbon Nanotubes (CNTs), composed of sp[2] carbon atoms, confer not only an improvement of the mechanical properties, but also an improvement in terms of electrical conductivity. Moreover, the presence of conjugation along the outer structure of the tube allow the formation of pi-pi interaction with the conjugated polymers.[16–19] Therefore, the presence of CNT in tridimensional structures can be used as nucleation points within the z axis during the polymerization.[20]

Regarding biocompatibility, both PEDOT and CNT have been demonstrated as excellent interfaces for the growth of neurons and others electroactive cells.[21,22] Therefore, the combination of carbon nanomaterials and conducting polymers might represent a powerful tool to generate biohybrid tridimensional materials for tissue regeneration purposes.

In this chapter, we have modulated the classical VPP methodology to manufacture 3D hybrid PEDOT/CNT materials instead of films. This large tridimensional material has been tested as biological platforms culturing C8-astrocytes. Herein, the good biological results obtained, *i.e.*, spreading of cells, have been compared with the previous PDMS/CNT scaffold developed.

2.2 Results and discussion

2.2.1 Fabrication and optimization of PEDOT/CNT scaffolds

Free-standing scaffolds made of PEDOT/CNT were fabricated by vapour phase polymerization (VPP). In order to optimize the synthetic pathway, temperature and iron-based oxidant percentage was evaluated within the fabrication of PEDOT/CNT scaffolds. It is remarkable to underline that PEDOT alone scaffolds were not able to maintain the 3D structure: all the conditions tried collapsed the structure.

Figure 2.1 shown the general procedure to fabricate VPP scaffolds using a similar strategy previously reported in our group.[22,23] First, sugar as porogen was mashed and sifted to obtain a crystal grain dispersion between 100 µm and 250 µm. 500 mg of crystal sugar grains were collected, mixed with CNTs (15 mg) and shaken overnight. Then, 7% of oxidant (Fe(Tos)$_3$ or FeCl$_3$) were incorporated and blended until obtaining a homogeneous powder. Finally, a little amount of MilliQ water (5 µL approximately) was added and mixed thoroughly. After this step, the mixture presented a malleable consistency, was molded inside a hollow plastic cylinder (Ø=5 mm) and compacted from both sides to form a cylindrical-shape template. Then the structure was held with a thread and hanged inside a schlenk flask. 400 µL of EDOT monomer was introduced at the bottom of the flask and the VPP was carried out under vacuum, varying two conditions: temperature (120ºC and 140ºC) and reaction time (6h and overnight).

After the polymerization was completed, the scaffolds were immersed overnight into MilliQ water and then cleaned with ethanol for five days in a Soxhlet system to remove sucrose and the excess of oxidant, respectively.
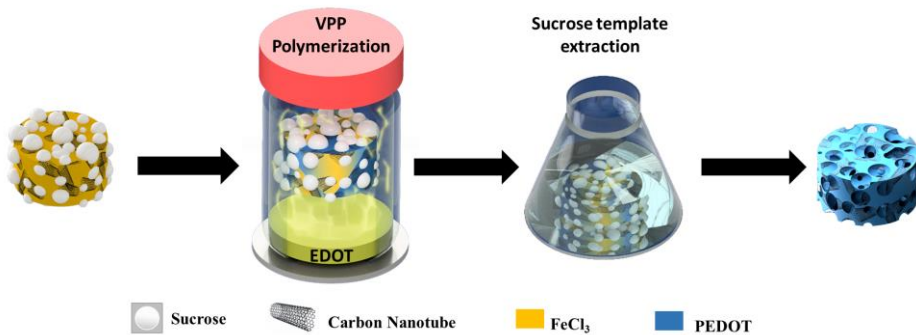

Figure 2.1 General scheme to manufacture PEDOT/CNT scaffolds. From left to right: molding of CNT with iron chloride and CNT; reaction at certain temperature

and time; sucrose and iron residue cleaning by water and ethanol respectively; final scaffold resulted.

Special attention has been addressed in obtaining self-standing scaffolds, thus we have extensively evaluated the VPP conditions. For instance, lower temperatures and shorter reaction times lead to collapse of the structures after sucrose removal, suggesting that the amount of polymer produced was not enough to hold the tridimensional structure. Moreover, as already mentioned, scaffolds composed exclusively of PEDOT were not self-standing structures.

Among the variables, the amount and type of oxidant was also studied. We used $Fe(TOS)_3$ and $FeCl_3$ at 20 mg, 40 mg or 80 mg. Nevertheless, only scaffolds polymerized using 20 mg of $FeCl_3$ were stable enough to keep the 3D structure after the cleaning step. Since the effective oxidation strength that refers to cation reduction (Fe^{3+} to Fe^{2+}) is constant, the anion in the iron species (*i.e.* Tos^-, Cl^-) has a huge impact in the polymerization rate. Therefore, as it is reported in literature, $FeCl_3$ is a more powerful oxidant when compared to $Fe(Tos)_3$.[5] Furthermore, for tridimensional structures, $FeCl_3$ has shown excellent results in the previously synthesized PPy/CNTs 3D scaffolds.[23]

On the other hand, iron-based oxidants are very hygroscopic. During the VPP, water has a dual role: i) it can act as proton scavenger, stabilizing dimers that participate in the polymer growth and ii) increases the formation of crystallite regions within the oxidant layer, which are not able to participate in an effective polymerization of EDOT[3,7]. Thus, larger amount of hygroscopic iron-based oxidant does not control the humidity rate and hinders the polymerization during the reaction.

2.2.2 Composition and structural characterization of PEDOT/CNT scaffolds

First, scaffold's composition, namely PEDOT and CNTs percentages, was calculated for each condition using TGA. As it can be observed in **Figure 2.2a**, the materials show two well-separated degradation curves by derivative evaluation: PEDOT is degraded between 100-500 ºC while CNTs start its degradation above 500 ºC. Hence, this behavior represents an ideal condition for quantitative composition calculation. PEDOT was estimated in terms of percentage of weight loss per gram of sample at 500 ºC, right before the degradation of CNTs begins, as observed in **Figure 2.2b.** Modulating the synthetic conditions, PEDOT can be incorporated into the scaffold between 42 and 68 wt%. Comparatively, at 120ºC, PEDOT percentage (%) is ranging from (47.39 ± 5.09)% after 6 hours to (53.48 ± 6.10) for overnight reaction. While for 140ºC, PEDOT the percentage is ranging from (62.84 ± 9.89) for 6 hours to (69.04 ± 4.62) for overnight reaction. Clearly, the most significant effect is obtained for 120ºC while at 140ºC the changes are similar. On the other hand, the major effect is observed within the temperature change: an increase of 20 ºC gives rise to *ca*. 25% more PEDOT deposition, while time of reaction from 6h to overnight, results only in a 6% increase of PEDOT deposited. These results suggest two ideas: the polymerization occurs mainly within the first six hours of reaction, and temperature of 140 ºC pushes more aggressively the polymerization reaction within the lattices.

As can be appreciated, the amount of CNT during the synthesis was kept constant due to simplifications during in the methodology evaluation.
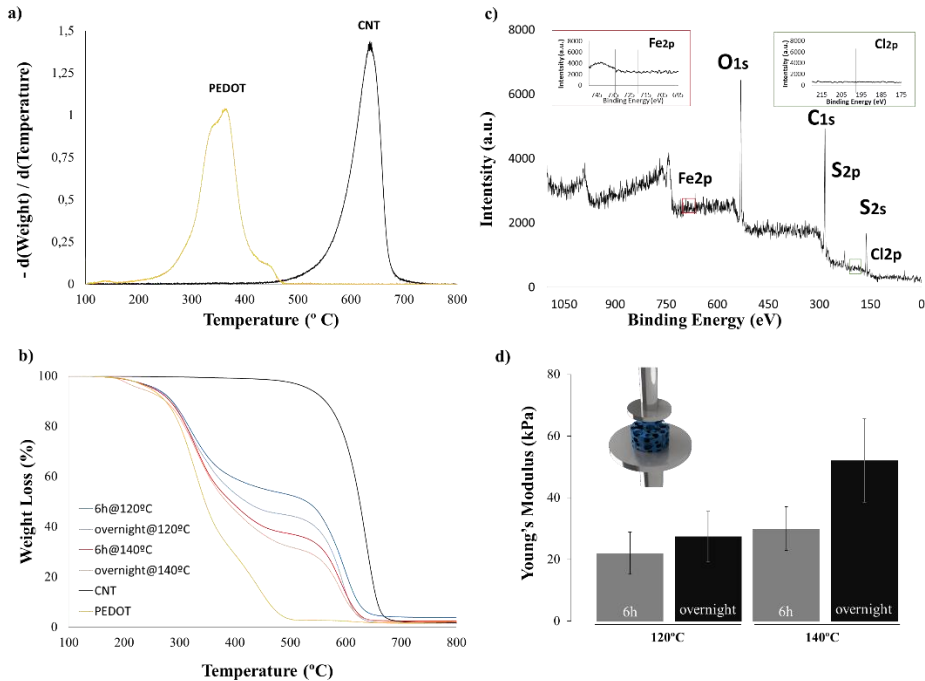
Figure 2.2 Derivative plot of the TGA in air (top picture, **a**) and different synthesis conditions used within the VPP reaction (bottom, **b**). XPS analysis of PEDOT/CNT scaffold after cleaning (top picture, **c**) and Young's Modulus (wet) of the scaffolds synthesized in different conditions (n=5), (bottom, **d**)

Figure 2.2d shows Young's modulus (YM) calculated for compressive studies performed in wet conditions. As it can be observed, values are very low, indicating the soft nature of the material. Stiffness has a direct dependence on the conditions used, *i. e.*, the time of reaction and temperature. So, following the TGA results, we can conclude that the stiffness of the scaffolds is correlated with the amount of polymer deposited within the interstitial structure. Despite slightly differences can be observed at low temperature (120ºC) and short times (6h), the significant differences are revealed for high temperatures (140 ºC) and large polymerization times (overnight), reaching the highest values *ca.* 50kPa.

PEDOT/CNT scaffolds present similar YM, *i.e.* 45kPa, as the previous PDMS/CNT scaffolds indicating his fantastic performance as a soft material and its potential use in neural cell cultures. Actually, such values fit perfectly for neural or spinal cord implants due to Young's modulus for human brains is estimated in a range from 0.1 to 20 kPa while around 40kPa in the spinal cord.[24] Overall, this result underlines PEDOT/CNT scaffolds as potentially applicable in soft neural tissue.[25,26]

On the other hand, conductivity was also evaluated. Electrochemical impedance spectroscopy (EIS) is a powerful tool to evaluate tridimensional conductivity without destroying the scaffold. Usually, conductivity evaluation is performed by conventional multimeter, although some authors used four-point probe technique that, but this method is only applicable on films, since porous structures would require its collapse. EIS generates a signal as a function of the frequency at a constant potential, providing a complex information on many variables (frequency, voltage, phase, current, etc.). Thanks to this, EIS could have been used to evaluate the tridimensional conductivity in conductive scaffolds while supporting cellular activity.[27–30]

Figure 2.3a shows the Bode plot of the 3D scaffolds analyzed. It is important to mention that all scaffolds were compared in the same conditions, *i.e.,* 5 mm height cylinders with 5 mm diameter and placed inside the electrochemical cell compartment which gold electrodes were in contact in a sandwich-like configuration. As a control, the previously mentioned PDMS/CNT scaffolds were used due to similarities in its composition respect to amount of CNT and properties as value of young modulus and porosity. Our results (**Figure 2.3b**) show that the impedance of PEDOT/CNT (6 kΩ) scaffolds at 0.1 Hz was approximately ten times lower than PDMS/CNT (50 kΩ). We hypothesize that impedance behavior of the PEDOT/CNT scaffolds might arise not only from the presence of the CNT or the

PEDOT themselves, but also from the conductive bridges formed between the conjugated thiophene chains of the PEDOT matrix and the CNT during the polymerization process.

The Bode plot in **Figure 2.3b** shows that PEDOT/CNT scaffold presents two responses in the phase: a maximum near medium frequencies, ca. 100 kHz, corresponding to a phase of 52°, and a small shoulder at lower frequencies. At the same time, PDMS/CNT present a band close to 10kHz, although the maximum phase is placed at 62°. The PEDOT/CNT scaffolds phase Bode plot can be associated to a Randle circuit behavior due to the electrons flow through the entire matrix.

Additionally, the phase movement shows a capacitance behavior at high frequencies and a resistor contribution (Phase = 0°) at lower frequencies. In contrast, the PDMS/CNT scaffolds have capacitor behavior at low frequencies. Furthermore, the porous morphology of the scaffolds allows for a significantly higher surface-to-volume ratio, resulting in low impedance that is promising for neural probe applications.
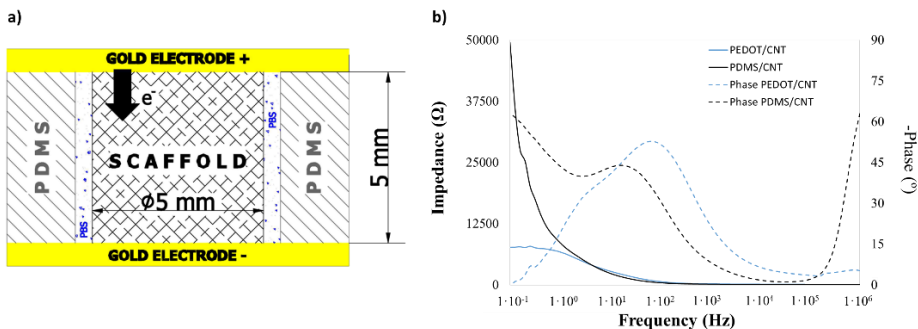

Figure 2.3 a) Representation of the EIS cell for the measures on the scaffolds **b)** Conductivity measurement through impedance (solid line) and phase angle

2.2.3 Nano- and micro- morphology of 3D PEDOT/CNT porous scaffolds

The principal aim of this work is to use PEDOT/CNT scaffold tridimensional structures for neuronal tissue engineering; thus, our scaffolds should allow cell support and attachment. As we mention in Chapter 1, cells cultured on 3D structures exhibit more similar conditions to *in vivo* tissue than cells cultured on 2D substrates. Hence, apart from tridimensionality, the scaffolds need to fill the requirement of porosity. In general, the number and size of pores among interconnectivity improve cellular parameters as secretion, infiltration, tissue ingrowth, and molecular delivery.[31]

Scanning electron microscopy (SEM) was used to qualitatively evaluate the number and size of pores upon removal of sucrose. Moreover, microcomputer tomography (μCT) was used to quantify the real porosity of the structure.

Figure 2.4a reveals a high number of heterogeneous porous with folded morphology; indeed, they present high interconnection within the holes and folds. Going into details, above the structure two types of surface are differentiated **Figure 2.4b-c**: one smooth and continuous surface which may be related to PEDOT, and a second brush-like structure, predominantly founded around the frame of the cavities. We suggest that the brush-like structures correspond to disorganized assemblies of CNTs, as confirmed with higher magnifications analysis **Figure 2.4d**. It is remarkable to say that, despite mechanical properties showed a dependence respect to the composition, in SEM images were not found significant differences between scaffolds synthesized with different conditions.
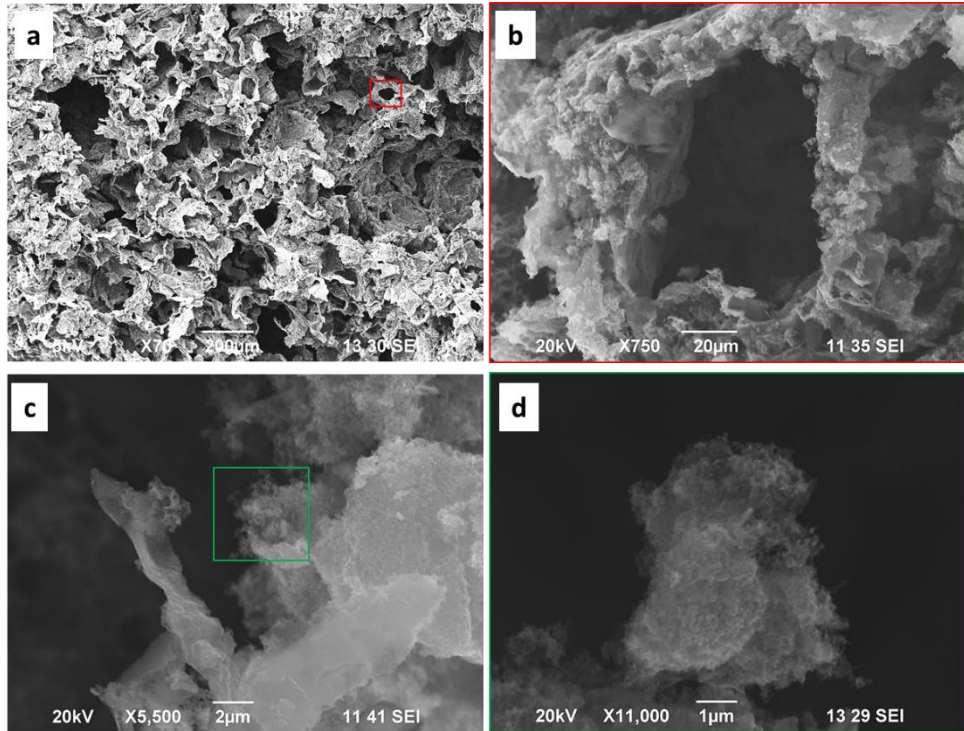
Figure 2.4 SEM images of the PEDOT/CNT scaffolds (synthesized overnight at 140ºC) at different magnifications **a)** show the homogeneous micro-porosity. **b)** represent the distributed CNT around the polymeric surface **c-d)** different magnification of the brush-like structures corresponding to CNT.

Micro-computed tomography (µCT) was used to quantify the micro-porosity of PEDOT/CNT scaffolds and analyze its internal 3D structure. Internal porosity of two different examples were found very similar -between 14 and 16 slices were evaluated for each sample. The data show that around 45% of the sample area corresponds to pores and 55% to matter. Moreover, statistical analysis of the pores diameter showed that 25% of the total pores are meso/micro pores (<50 µm), almost 60% between 50 and 100 µm, around 20% between 100 and 150 µm and less than 7% above 150 µm. (see **Figure 2.5)**. Two different conclusions can be

noted from these data. First, sifted method of the sugar crystal grain confers to the scaffold a controlled porosity. Secondly, when compared with the previously manufactured PDMS/CNT scaffolds, we observed that both materials possess similar porosity (46% for PEDOT/CNT and 40% for PDMS/CNT).
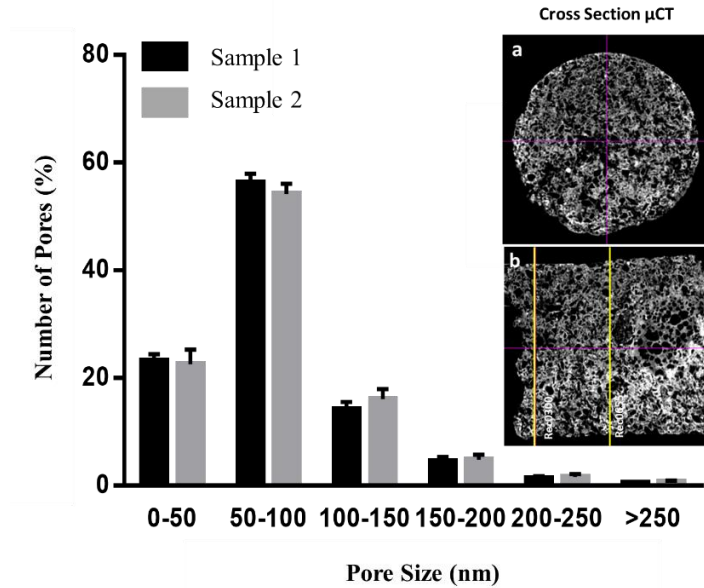

Figure 2.5 Porosity analysis performed by micro-computer tomography of scaffolds crossed sections

Once the porosity was evaluated, intimate interaction between CNT and PEDOT was studied using transmission electron microscopy (TEM). As previously reported, depending on the dopant and polymerization conditions, PEDOT can polymerize in several nanometric forms, like nanorods, nanowires or nanoparticles, among others.[32–34]

Figure 2.6 presents three sub-structures: (i) thick tubes, which are assumed to be PEDOT/CNT hybrids with the polymer wrapping the cylindrical structures; (ii) thin tubes with diameters around 15-20 nm, corresponding to naked CNTs and (iii)

polymer film agglomerates, determined as PEDOT. TEM revealed that most of the CNT presented in the scaffold are coated with the polymer, increasing their diameters. We think that such a heterogeneity underpins the whole structure, being responsible for the scaffolds' structural integrity. Non-covalent π-π stacking of the aromatic polymer backbone and the surface of the nanotubes represent the most remarkable interactions between this high rich electron material. Such electrostatic interaction between conductive polymers through non-covalent functionalization has already been observed.[35,36]
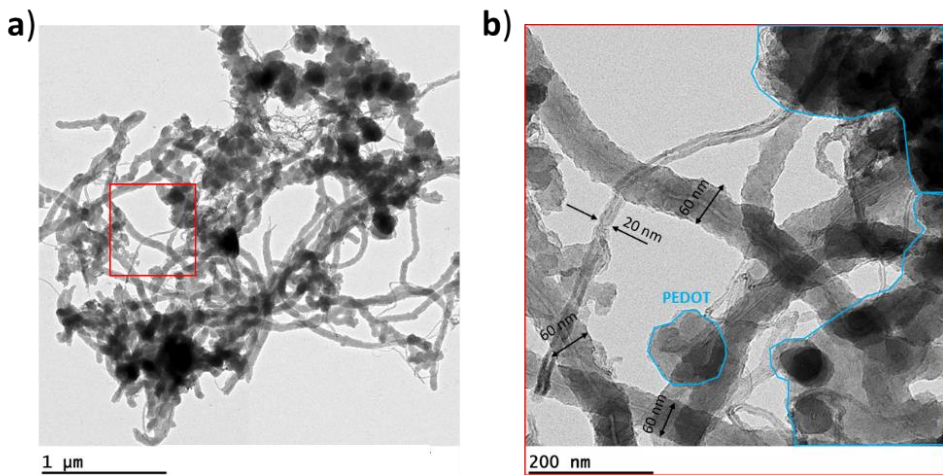
Figure 2.6 TEM images of PEDOT/CNT materials obtained. Right image corresponds to the magnification selected in the left image.

2.2.4 Cell culturing of C8-D1A

Before the use of PEDOT/CNT scaffolds in further studies for tissue engineering applications, cytotoxicity of the material was evaluated throughout modified lactate dehydrogenase assay (LDH). It is worthy to note that for this purpose, modified LDH is required because CNT can interact with conventional LDH or MTT assay test.[37]

Hence, C8-D1A cell line was cultured *in vitro* onto scaffolds for 3 and 6 days and compared with previous PDMS/CNT scaffolds. We choose astrocytes because they form part of the glia, providing support and nutrients to neurons, thus they have an essential function in the regeneration of neuronal tissue and represent an ideal model to test the biocompatibility and the potential of our conductive scaffolds in neural prostheses for spinal cord injury.[38]

As it is well known, LDH is a semiquantitative measurement of the number of viable cells growing on the scaffolds. Thus, scaffolds were seeded in the same way and with same number of astrocytes ($5·10^5$ C8-D1A); besides, given their similar values of porosity and mechanical properties, the differences observed *in vitro* can be directly attributed to the effect of the materials.

In a first experiment, the effect of the different polymerization conditions employed was evaluated, *i.e.*, different PEDOT/CNT ratios, and showed no significant differences between the different kind of scaffolds (**Figure 2.7a**). In a second step, the PEDOT/CNT scaffolds were compared with the previously synthesized PDMS/CNT scaffolds, and, again, no significant differences in the absorbance were observed (see **Figure 2.7b**). In conclusion, we have demonstrated that the PEDOT/CNT scaffolds do not affect the cell viability, and that the scaffolds manufactured have a positive impact on the C8-D1A growth within the first three days of culture.
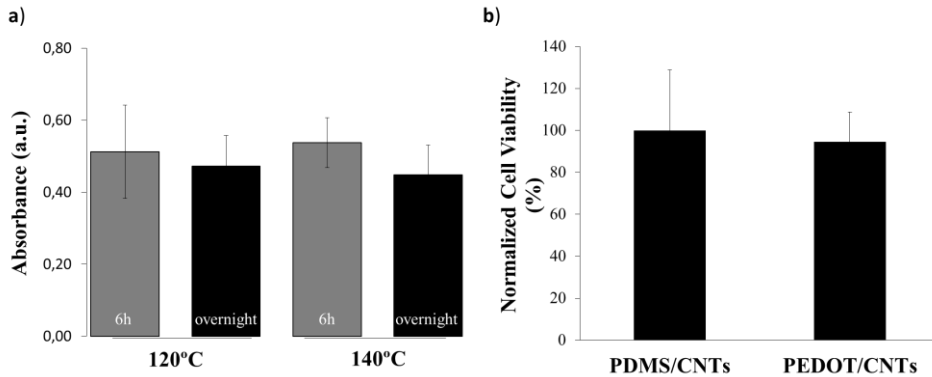
Figure 2.7 a) *In vitro* LDH assay of C8-D1A astrocytes cultured for 3 days on PEDOT/CNT scaffolds manufactured by different conditions. **b)** Comparative LDH assay of in vitro C8-D1A astrocytes cultivated for 3 days on PEDOT/CNT *versus* PDMS/CNT. (All values are expressed as means ± SD from 4 independent experiments (n=3). P>0.05, results are considered statistically non-significant by Student's t test.)

In addition, confocal imaging was employed to analyze the cellular viability and attachment to the PEDOT/CNT scaffold. Calcein-AM stains only living cells with green fluorophore while F-actin stain is employed to evaluate adhesion throughout cytoskeleton staining. Immunofluorescence was performed at 3 and 6 days. Furthermore, z-stacks were carried out and showed certain degree of cell penetration within the range of visualization allowed (up to 100 µm).
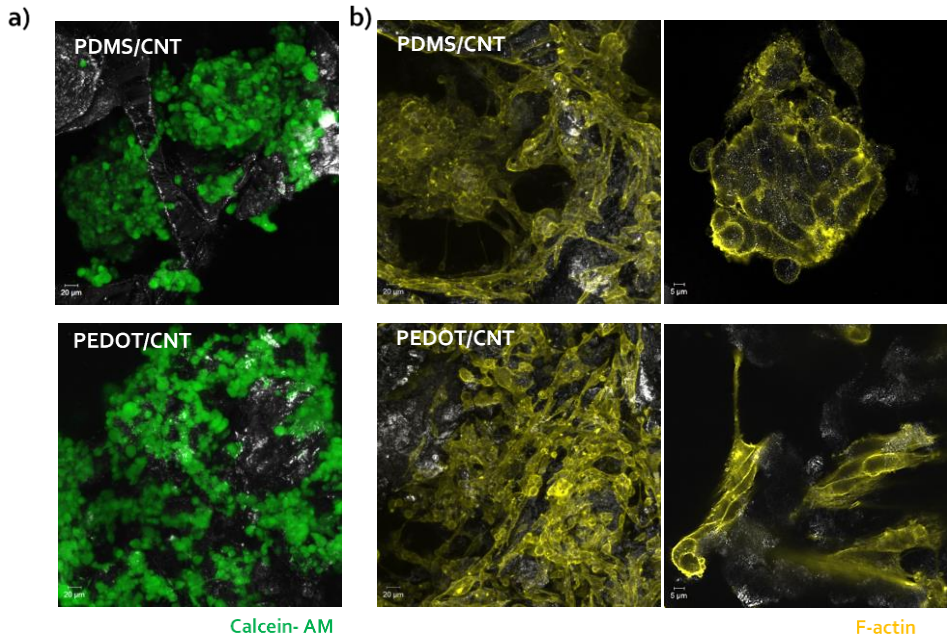
Figure 2.8 a) Calcein-AM stain of viable cells (green) and **b)** cytoskeleton F-actin (yellow) staining of PEDOT/CNT and PDMS/CNT scaffolds after 3 days of culture

As can be observed in **Figure 2.8a**, calcein staining presents differences related with cell growth behavior. Meanwhile astrocytes clusters are formed on PDMS/CNT scaffolds, PEDOT/CNT scaffolds present higher spreading level over the whole surface. Cluster formation are disadvantageous for synthetic biological active surface due to the reduction of their own growth stretching and the long-distance communication, presumably affecting their natural activity.[39]

Moreover, in accordance with calcein staining, the cytoskeleton imaged by F-actin staining present large elongations of the filamentous axons on PEDOT/CNT scaffolds, indicating the typical phenotype of astrocytic cells. (**Figure 2.8b**). From our point of view, this data was a clear indicator that the cells keep their original function, despite other experiments should be carried out in this direction.

These observations were also corroborated by SEM images, where cells cultured on PEDOT/CNT (**Figure 2.9**) showed a normal morphology. Large elongations, as well as abundant cell-to-cell contacts (highlighted with green arrows) can be distinguished (left-bottom image). This observation suggests higher guidance and enhancement of the astrocytes to the material during their growth and expansion, as previously reported. These experiments not only confirm the low cytotoxicity of the material, but also let us anticipate that the cells are also able to maintain their function.
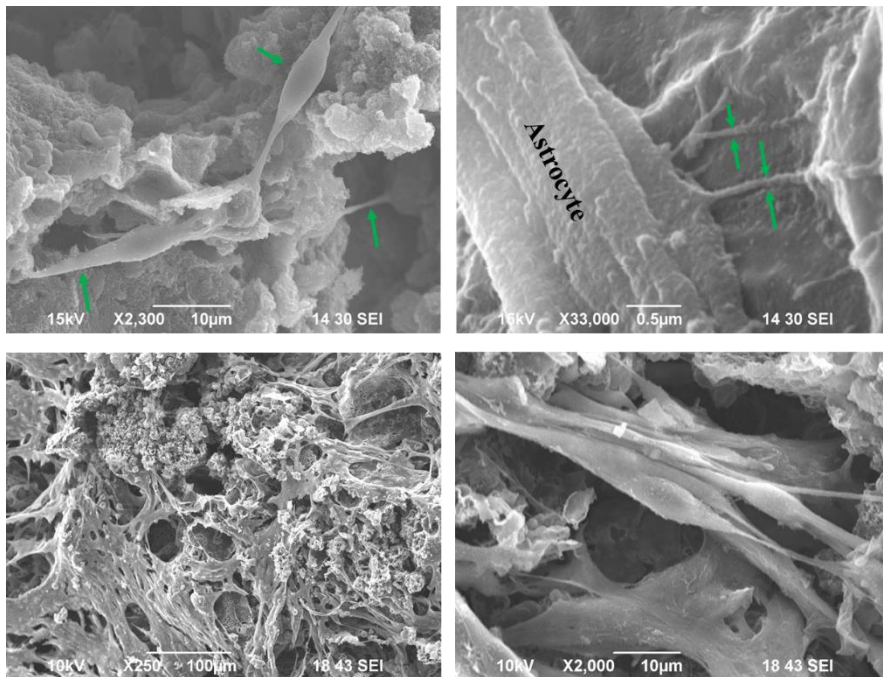
Figure 2.9 SEM images of the astrocytes grown in the 3D PEDOT/CNT scaffolds for 3 days. Higher magnifications show the close interaction and adhesion of the astrocytic filaments to the scaffold.

2.3 Conclusions

In this chapter, PEDOT/CNT porous scaffolds have been manufactured through VPP methodology. Crystal sugar grain were used as a template as in previous works carried out in our laboratory. The procedure represents a powerful method to manufacture 3D scaffolds controlling such as important properties as polymer composition, porosity, conductivity, and compressive toughness. Crucial role of CNTs has been demonstrated for this manufacturing technique due to structures composed uniquely of PEDOT collapsed. Moreover, PEDOT/CNT scaffolds were compared with previous synthesized in our group composed of PDMS/CNT.

VPP method can modulate the scaffold composition from 42% to 68% of PEDOT through different reactions conditions, as determined by TGA. At the same time, VPP can produce different scaffolds with variable YMs, within the range of 20-50 kPa, typical values of soft materials. Moreover, PEDOT/CNT scaffolds possess 45% porosity with homogeneous distribution of pore diameters and excellent interconnectivity between them. As well, EIS analyses showed that PEDOT/CNT scaffolds are highly conductive, more than ten times below the previously reported.

Finally, high viability was demonstrated with the incubation of astrocytes, showing similar cell viability than previous PDMS/CNT scaffolds, pointing out that prepared scaffolds are suitable candidates for a widely number of applications within the field of neural cell cultures.

2.4 Experimental and protocol section

2.4.1 Composition and structural characterization

Compressive modulus testing

First, scaffolds were soaked in Milli-Q water for 1-2 min, and the excess of water was carefully removed. Deformation was measured by correlation between height displacement at each point with the scaffolds' initial height (strain, %). Obtained force curve was normalized to the specimens' diameter (stress, kPa). Then, young's modulus (YM) was obtained as the slope of the stress/strain curve of the linear elastic section in the initial stages (typically from 15 to 40% strain in our case). Data were collected from 4-5 repetitions of each condition measured.

Micro-computed Tomography (µCT)

Scaffolds were segmented using a thresholding procedure. Values corresponding to scaffold segment were extracted from background and optimized comparing the 2D grey scale image. Therefore, binary images were created and porosity values for each slice assessed. Thus the porosity was calculated in 14 randomly selected slices (n=14) for the first sample, and 16 randomly selected slices (n=16) for the second.

Conductivity measurements (EIS)

EIS measurement were carried out in a homemade device was developed. The scaffolds were cut in cylinders of 5 x 5 mm (LxD), and then immersed in phosphate-buffered saline (PBS, 10 mM). Moreover, they were degassed for 5 minutes to ensure the complete permeation inside of the porous lattices. Then, scaffolds were placed inside a PDMS container with few drops of 10 mM of PBS buffer solution between two coplanar gold electrodes in a sandwich configuration. We ensure that the full structure was constantly in contact with the material, allowing electricity flow within the material.

2.4.2 Nano and micro morphology

Scanning electron microscope (SEM)

Scaffold were slices in 2 mm thickness and mounted on an aluminum holder with double-sided carbon tape. Then, sample was evaluated in point by point mode at different magnifications

Transmission electron microscopy (TEM)

PEDOT/CNT scaffolds were smashed and dispersed in miliQ water (ca. 0.1 mg·mL-1 in milliQ water). Then a single drop (0.5 µL) was deposited onto a copper grid. Water was evaporated at room temperature and then inserted.

2.4.3 Cell culture

Biocompatibility assay

Scaffolds were placed in the soxhlet during one day before the in vitro assays, to ensure the absence of ethanol from the previous removal steps. They were left in air at room temperature to dry and cut into disks of 2mm thickness. In the case of PDMS/CNT, they were cleaned each side under low-pressure oxygen plasma treatment for 6 min (Pico Plasma Cleaner, Diener electronic). Just before the seeding, all the scaffolds were sterilized during 20 min with UV light on each side.

SEM imaging of the cells

After culture, scaffolds were dehydratated with ethanol and deionized water gradient (60%, 70%, 80%, 90%, and 100%), each for 30min at room temperature. Then, a second dehydration was performed with a hexamethyldisilazane (HMDS) in ethanol gradient solutions (30%, 50%, 70%, 90%, 100%) using again 30 minutes incubation for each step. HMDS 100% samples were air-dried, sputter-coated with gold (Alto 1000, Gatan Inc.), and visualized by SEM.

2.5 References

(1)   Winther-Jensen, B.; Chen, J.; West, K.; Wallace, G. Vapor Phase Polymerization of Pyrrole and Thiophene Using Iron(III) Sulfonates as Oxidizing Agents. *Macromolecules* **2004**, *37* (16), 5930–5935. https://doi.org/10.1021/ma049365k.

(2)   Winther-Jensen, B.; West, K. Vapor-Phase Polymerization of 3,4-Ethylenedioxythiophene: A Route to Highly Conducting Polymer Surface Layers. *Macromolecules* **2004**, *37* (12), 4538–4543. https://doi.org/10.1021/ma049864l.

(3)   Fabretto, M.; Zuber, K.; Hall, C.; Murphy, P.; Griesser, H. J. The Role of Water in the Synthesis and Performance of Vapour Phase Polymerised PEDOT Electrochromic Devices. *J. Mater. Chem.* **2009**, *19* (42), 7871–7878. https://doi.org/10.1039/B912324E.

(4)   Zuber, K.; Fabretto, M.; Hall, C.; Murphy, P. Improved PEDOT Conductivity via Suppression of Crystallite Formation in Fe(III) Tosylate During Vapor Phase Polymerization. *Macromol. Rapid Commun.* **2008**, *29* (18), 1503–1508. https://doi.org/10.1002/marc.200800325.

(5)   Brooke, R.; Cottis, P.; Talemi, P.; Fabretto, M.; Murphy, P.; Evans, D. Recent Advances in the Synthesis of Conducting Polymers from the Vapour Phase. *Prog. Mater. Sci.* **2017**, *86*, 127–146. https://doi.org/https://doi.org/10.1016/j.pmatsci.2017.01.004.

(6)   Winther-Jensen, B.; Breiby, D. W.; West, K. Base Inhibited Oxidative Polymerization of 3,4-Ethylenedioxythiophene with Iron(III)Tosylate. *Synth. Met.* **2005**, *152* (1), 1–4. https://doi.org/https://doi.org/10.1016/j.synthmet.2005.07.085.

(7)   Jimison, L. H.; Hama, A.; Strakosas, X.; Armel, V.; Khodagholy, D.; Ismailova, E.; Malliaras, G. G.; Winther-Jensen, B.; Owens, R. M. PEDOT:TOS with PEG: A Biofunctional Surface with Improved Electronic

Characteristics. *J. Mater. Chem.* **2012**, *22* (37), 19498–19505. https://doi.org/10.1039/C2JM32188B.

(8) Jiang, Y.; Liu, T.; Zhou, Y. Recent Advances of Synthesis, Properties, Film Fabrication Methods, Modifications of Poly(3,4-Ethylenedioxythiophene), and Applications in Solution-Processed Photovoltaics. *Adv. Funct. Mater.* *n/a* (n/a), 2006213. https://doi.org/10.1002/adfm.202006213.

(9) Strakosas, X.; Wei, B.; Martin, D. C.; Owens, R. M. Biofunctionalization of Polydioxythiophene Derivatives for Biomedical Applications. *J. Mater. Chem. B* **2016**, *4* (29), 4952–4968. https://doi.org/10.1039/C6TB00852F.

(10) Iandolo, D.; Ravichandran, A.; Liu, X.; Wen, F.; Chan, J. K. Y.; Berggren, M.; Teoh, S.-H.; Simon, D. T. Development and Characterization of Organic Electronic Scaffolds for Bone Tissue Engineering. *Adv. Healthc. Mater.* **2016**, *5* (12), 1505–1512. https://doi.org/10.1002/adhm.201500874.

(11) Marroquin, J. B.; Coleman, H. A.; Tonta, M. A.; Zhou, K.; Winther-Jensen, B.; Fallon, J.; Duffy, N. W.; Yan, E.; Abdulwahid, A. A.; Jasieniak, J. J.; Forsythe, J. S.; Parkington, H. C. Neural Electrodes Based on 3D Organic Electroactive Microfibers. *Adv. Funct. Mater.* **2018**, *28* (12), 1700927. https://doi.org/10.1002/adfm.201700927.

(12) Françon, H.; Wang, Z.; Marais, A.; Mystek, K.; Piper, A.; Granberg, H.; Malti, A.; Gatenholm, P.; Larsson, P. A.; Wågberg, L. Ambient-Dried, 3D-Printable and Electrically Conducting Cellulose Nanofiber Aerogels by Inclusion of Functional Polymers. *Adv. Funct. Mater.* **2020**, *30* (12), 1909383. https://doi.org/10.1002/adfm.201909383.

(13) Fernandez, F. D. M.; Khadka, R.; Yim, J.-H. Highly Porous, Soft, and Flexible Vapor-Phase Polymerized Polypyrrole–Styrene–Ethylene–Butylene–Styrene Hybrid Scaffold as Ammonia and Strain Sensor. *RSC Adv.* **2020**, *10* (38), 22533–22541. https://doi.org/10.1039/D0RA03592K.

(14) Park, J. S.; Kim, B.; Lee, B.-T.; Choi, J. S.; Yim, J.-H. Fabrication of an Electroconductive{,} Flexible, and Soft Poly(3,}4-Ethylenedioxythiophene)–

Thermoplastic Polyurethane Hybrid Scaffold by in Situ Vapor Phase Polymerization. *J. Mater. Chem. B* **2018**, *6* (24), 4082–4088. https://doi.org/10.1039/C8TB00311D.

(15) Choi, J. S.; Park, J. S.; Kim, B.; Lee, B.-T.; Yim, J.-H. In Vitro Biocompatibility of Vapour Phase Polymerised Conductive Scaffolds for Cell Lines. *Polymer (Guildf).* **2017**, *124*, 95–100. https://doi.org/https://doi.org/10.1016/j.polymer.2017.07.047.

(16) Kormányos, A.; Hursán, D.; Janáky, C. Photoelectrochemical Behavior of PEDOT/Nanocarbon Electrodes: Fundamentals and Structure–Property Relationships. *J. Phys. Chem. C* **2018**, *122* (25), 13682–13690. https://doi.org/10.1021/acs.jpcc.8b00145.

(17) Tahir, M.; He, L.; Haider, W. A.; Yang, W.; Hong, X.; Guo, Y.; Pan, X.; Tang, H.; Li, Y.; Mai, L. Co-Electrodeposited Porous PEDOT–CNT Microelectrodes for Integrated Micro-Supercapacitors with High Energy Density{,} High Rate Capability{,} and Long Cycling Life. *Nanoscale* **2019**, *11* (16), 7761–7770. https://doi.org/10.1039/C9NR00765B.

(18) Hu, X.; Chen, L.; Tan, L.; Ji, T.; Zhang, Y.; Zhang, L.; Zhang, D.; Chen, Y. In Situ Polymerization of Ethylenedioxythiophene from Sulfonated Carbon Nanotube Templates: Toward High Efficiency ITO-Free Solar Cells. *J. Mater. Chem. A* **2016**, *4* (17), 6645–6652. https://doi.org/10.1039/C6TA00287K.

(19) Sun, D.; Li, H.; Li, M.; Li, C.; Dai, H.; Sun, D.; Yang, B. Electrodeposition Synthesis of a NiO/CNT/PEDOT Composite for Simultaneous Detection of Dopamine, Serotonin, and Tryptophan. *Sensors Actuators B Chem.* **2018**, *259*, 433–442. https://doi.org/https://doi.org/10.1016/j.snb.2017.12.037.

(20) Guo, F.; Jiang, Y.; Xu, Z.; Xiao, Y.; Fang, B.; Liu, Y.; Gao, W.; Zhao, P.; Wang, H.; Gao, C. Highly Stretchable Carbon Aerogels. *Nat. Commun.* **2018**, *9* (1), 881. https://doi.org/10.1038/s41467-018-03268-y.

(21) Aurand, E. R.; Usmani, S.; Medelin, M.; Scaini, D.; Bosi, S.; Rosselli, F. B.;

Donato, S.; Tromba, G.; Prato, M.; Ballerini, L. Nanostructures to Engineer 3D Neural-Interfaces: Directing Axonal Navigation toward Successful Bridging of Spinal Segments. *Adv. Funct. Mater.* **2018**, *28* (12), 1700550. https://doi.org/10.1002/adfm.201700550.

(22)   Bosi, S.; Rauti, R.; Laishram, J.; Turco, A.; Lonardoni, D.; Nieus, T.; Prato, M.; Scaini, D.; Ballerini, L. From 2D to 3D: Novel Nanostructured Scaffolds to Investigate Signalling in Reconstructed Neuronal Networks. *Sci. Rep.* **2015**, *5*, 9562.

(23)   Alegret, N.; Dominguez-Alfaro, A.; González-Domínguez, J. M.; Arnaiz, B.; Cossío, U.; Bosi, S.; Vázquez, E.; Ramos-Cabrer, P.; Mecerreyes, D.; Prato, M. Three-Dimensional Conductive Scaffolds as Neural Prostheses Based on Carbon Nanotubes and Polypyrrole. *ACS Appl. Mater. Interfaces* **2018**, *10* (50), 43904–43914. https://doi.org/10.1021/acsami.8b16462.

(24)   Tyler, W. J. The Mechanobiology of Brain Function. *Nat. Rev. Neurosci.* **2012**, *13* (12), 867–878. https://doi.org/10.1038/nrn3383.

(25)   Karimi, A.; Shojaei, A.; Tehrani, P. Mechanical Properties of the Human Spinal Cord under the Compressive Loading. *J. Chem. Neuroanat.* **2017**, *86*, 15–18. https://doi.org/https://doi.org/10.1016/j.jchemneu.2017.07.004.

(26)   Budday, S.; Nay, R.; de Rooij, R.; Steinmann, P.; Wyrobek, T.; Ovaert, T. C.; Kuhl, E. Mechanical Properties of Gray and White Matter Brain Tissue by Indentation. *J. Mech. Behav. Biomed. Mater.* **2015**, *46*, 318–330. https://doi.org/10.1016/j.jmbbm.2015.02.024.

(27)   Wang, S.; Guan, S.; Zhu, Z.; Li, W.; Liu, T.; Ma, X. Hyaluronic Acid Doped-Poly(3,4-Ethylenedioxythiophene)/Chitosan/Gelatin (PEDOT-HA/Cs/Gel) Porous Conductive Scaffold for Nerve Regeneration. *Mater. Sci. Eng. C* **2017**, *71*, 308–316. https://doi.org/https://doi.org/10.1016/j.msec.2016.10.029.

(28)   Wei, B.; Liu, J.; Ouyang, L.; Martin, D. C. POSS-ProDOT Crosslinking of PEDOT. *J. Mater. Chem. B* **2017**, *5* (25), 5019–5026.

https://doi.org/10.1039/C7TB00598A.

(29)   Wang, S.; Guan, S.; Xu, J.; Li, W.; Ge, D.; Sun, C.; Liu, T.; Ma, X. Neural Stem Cell Proliferation and Differentiation in the Conductive PEDOT-HA/Cs/Gel Scaffold for Neural Tissue Engineering. *Biomater. Sci.* **2017**, *5* (10), 2024–2034. https://doi.org/10.1039/C7BM00633K.

(30)   Wang, S.; Sun, C.; Guan, S.; Li, W.; Xu, J.; Ge, D.; Zhuang, M.; Liu, T.; Ma, X. Chitosan/Gelatin Porous Scaffolds Assembled with Conductive Poly(3{,}4-Ethylenedioxythiophene) Nanoparticles for Neural Tissue Engineering. *J. Mater. Chem. B* **2017**, *5* (24), 4774–4788. https://doi.org/10.1039/C7TB00608J.

(31)   Huang, G.; Li, F.; Zhao, X.; Ma, Y.; Li, Y.; Lin, M.; Jin, G.; Lu, T. J.; Genin, G. M.; Xu, F. Functional and Biomimetic Materials for Engineering of the Three-Dimensional Cell Microenvironment. *Chem. Rev.* **2017**, *117* (20), 12764–12850. https://doi.org/10.1021/acs.chemrev.7b00094.

(32)   Mao, H.; Liu, X.; Chao, D.; Cui, L.; Li, Y.; Zhang, W.; Wang, C. Preparation of Unique PEDOT Nanorods with a Couple of Cuspate Tips by Reverse Interfacial Polymerization and Their Electrocatalytic Application to Detect Nitrite. *J. Mater. Chem.* **2010**, *20* (45), 10277–10284. https://doi.org/10.1039/C0JM01745K.

(33)   Choi, J. W.; Han, M. G.; Kim, S. Y.; Oh, S. G.; Im, S. S. Poly(3,4-Ethylenedioxythiophene) Nanoparticles Prepared in Aqueous DBSA Solutions. *Synth. Met.* **2004**, *141* (3), 293–299. https://doi.org/https://doi.org/10.1016/S0379-6779(03)00419-3.

(34)   Bai, X.; Hu, X.; Zhou, S.; Yan, J.; Sun, C.; Chen, P.; Li, L. Controlled Fabrication of Highly Conductive Three-Dimensional Flowerlike Poly (3{,}4-Ethylenedioxythiophene) Nanostructures. *J. Mater. Chem.* **2011**, *21* (20), 7123–7129. https://doi.org/10.1039/C1JM10335K.

(35)   Zengin, H.; Zhou, W.; Jin, J.; Czerw, R.; Smith Jr., D. W.; Echegoyen, L.; Carroll, D. L.; Foulger, S. H.; Ballato, J. Carbon Nanotube Doped

Polyaniline. *Adv. Mater.* **2002**, *14* (20), 1480–1483. https://doi.org/10.1002/1521-4095(20021016)14:20<1480::AID-ADMA1480>3.0.CO;2-O.

(36) Arcila-Velez, M. R.; Emmett, R. K.; Karakaya, M.; Podila, R.; Díaz-Orellana, K. P.; Rao, A. M.; Roberts, M. E. A Facile and Scalable Approach to Fabricating Free-Standing Polymer—Carbon Nanotube Composite Electrodes. *Synth. Met.* **2016**, *215,* 35–40. https://doi.org/https://doi.org/10.1016/j.synthmet.2016.02.005.

(37) Ali-Boucetta, H.; Al-Jamal, K. T.; Kostarelos, K. Cytotoxic Assessment of Carbon Nanotube Interaction with Cell Cultures. *Methods Mol. Biol.* **2011**, *726*, 299–312. https://doi.org/10.1007/978-1-61779-052-2_19.

(38) Zhou, T.; Ming, Y.; Perry, S. F.; Tatic-Lucic, S. Estimation of the Physical Properties of Neurons and Glial Cells Using Dielectrophoresis Crossover Frequency. *J. Biol. Phys.* **2016**, *42* (4), 571–586. https://doi.org/10.1007/s10867-016-9424-5.

(39) Katiyar, K. S.; Winter, C. C.; Struzyna, L. A.; Harris, J. P.; Cullen, D. K. Mechanical Elongation of Astrocyte Processes to Create Living Scaffolds for Nervous System Regeneration. *J. Tissue Eng. Regen. Med.* **2017**, *11* (10), 2737–2751. https://doi.org/10.1002/term.2168.
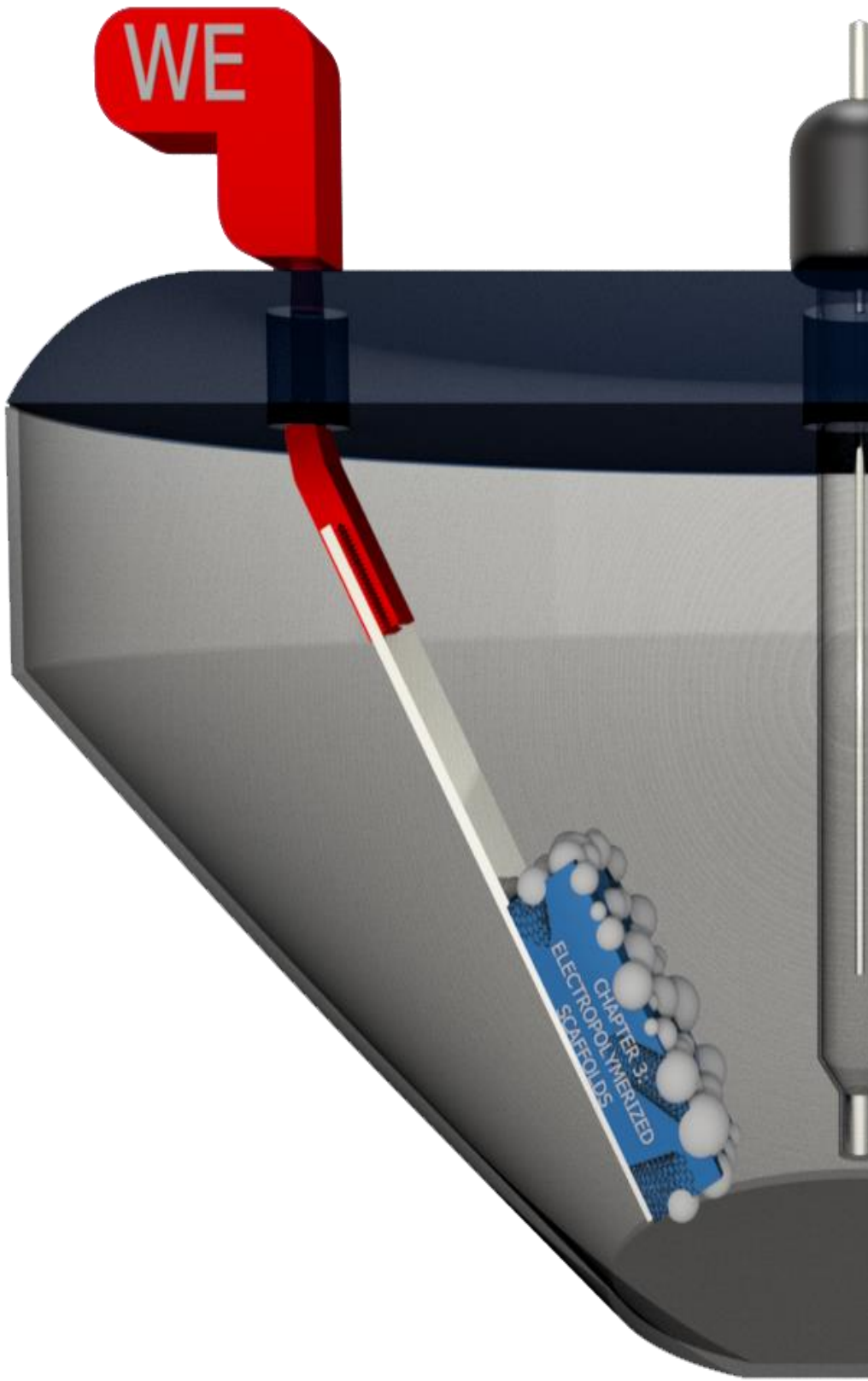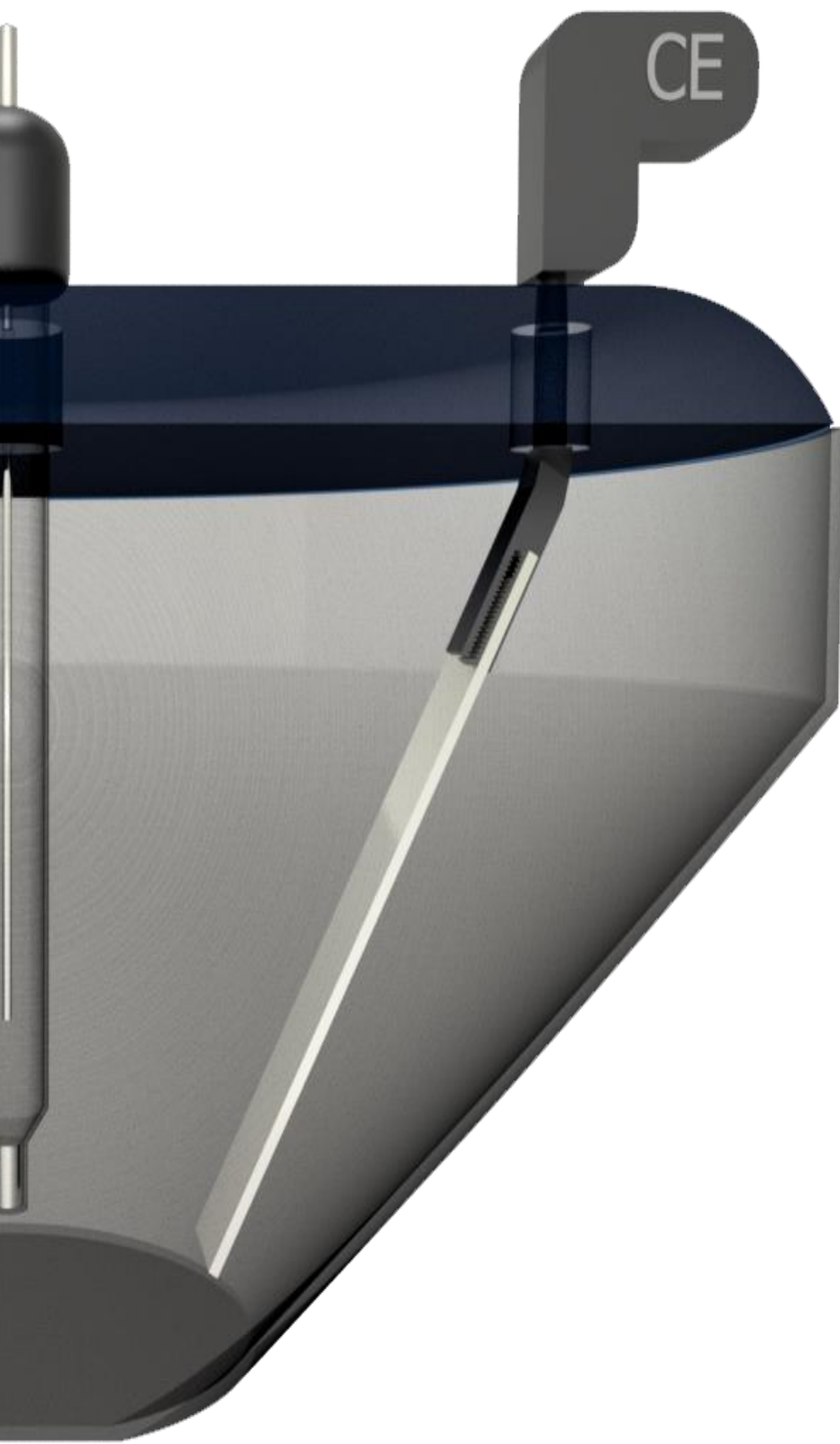
Chapter 3: Electropolymerized Scaffolds

3.1 Introduction

While vapour phase polymerization described in the previous chapter requires the action of an oxidant for PEDOT polymerization, electropolymerization (EP) is based on an electrochemical reaction and requires the action of an electrical input. Therefore, conventional EP is carried out in a three-electrode cell where polymerization reaction takes place on the working electrode, while the counter electrode and reference balance the charge of the system.

The EP mechanism is similar to the previous explained: 1) radical cation formation, 2) oligomerization, 3) deposition (including nucleation and growth) and 4) coupling under solid-state conditions.[1,2] The main difference with the chemical oxidative

method reside in the final steps, where larger oligomers are deposited onto the electrode surface acting as further nucleation points for the coupling in solid state conditions of the conductive polymer.

EP provides several advantages *vs* chemical methods as: it is faster, allows a better control of the amount of polymer deposited, does not require toxic oxidant reagents and produces polymers with increased doping, conductivity, purity and homogeneity.

Generally, the reaction can be performed by two different pathways: cyclic voltammetry, where a voltage range is applied on the working electrode at a certain scan rate; and chronoamperometry, which involves a constant current during a period of time. These two methods lead the polythiophene polymer structure in two different states, the neutral state or the oxidized doped state, having an important impact on the final electrode morphology.[3,4]

In biomedical applications, this doping mechanism at different oxidation states have been used in drug delivery systems or cell culture studies. Drugs as risperidone,[5] nerve growth factors,[6] neurotrophin-3,[7] or dexamethasone[8] can be introduced as dopants during the polymerization and be released later with a voltage input. Meanwhile, changes in the redox state of the film have been used to evaluate mammalian cell adhesion, or control protein folding, among others.[9–13]

Remarkably, two- (2D) or three-dimensional (3D) type of polymer growth can be involved during the EP. The main difference resides in the nuclei: 2D growth preferably undergoes in parallel to the electrode, while in 3D the polymerization process occurs in perpendicular and parallel to the electrode. Besides, a sacrificial template can be used in order to produce channels, holes, or cavities on the electrode morphology.[14,15]

As in Chapter 2, CNTs has an important role on this approach. To the best of our knowledge, the manufacture of electrodes made of PEDOT and carbon nanomaterials (CNM) by EP has been only focused in the development of thin film coated devices.[16–21] We have fabricated our own electrodes molding a mixture of CNT and crystal sugar grain as described before. Moreover, in this approach we were able to manufacture thin scaffolds of PEDOT, but its growth within the tridimensionality is limited to the presence of CNT. Hence, after the electropolymerization, we have observed that in PEDOT/CNT scaffolds, polymer growth occurs not only nearby of the electrode but also in the tridimensional structured formed by the template. Therefore, in presence of CNT we have achieve the manufacturing of large structures, *i.e.* higher than 1mm, improving results reported in literature.

Hence, in this chapter we have developed and characterized large PEDOT/CNT scaffolds and compared with his homonymous PEDOT control. Thus, using this technique we can manufacture 3D scaffolds made of commercially available monomers and other derivatives. Finally, we have tested our conductive 3D scaffolds as substrates to induce SH-SY5Y cellular differentiation without the use of any additional chemical or factor.

3.2 Results and discussion

3.2.1 Fabrication and optimization of PEDOT and PEDOT/CNT scaffolds

In the same way as in the Chapter 2, 15 mg CNT was mixed with 500 mg of sieved crystal sugar grain (100-250µm). Then, a little amount of water was added and molded on a ITO electrode at different shapes. Finally, they were inserted in a three electrode cell and the polymerization was performed throughout a chrono amperometry (constant potential) (**Figure 3.1**) After polymerization, sucrose was removed by immersing the electrode in water and the amount of PEDOT deposited

was quantified by TGA. It is important remark to that, CNTs and sugar maintain the structure during the polymerization, avoiding the release of themselves in the solution.
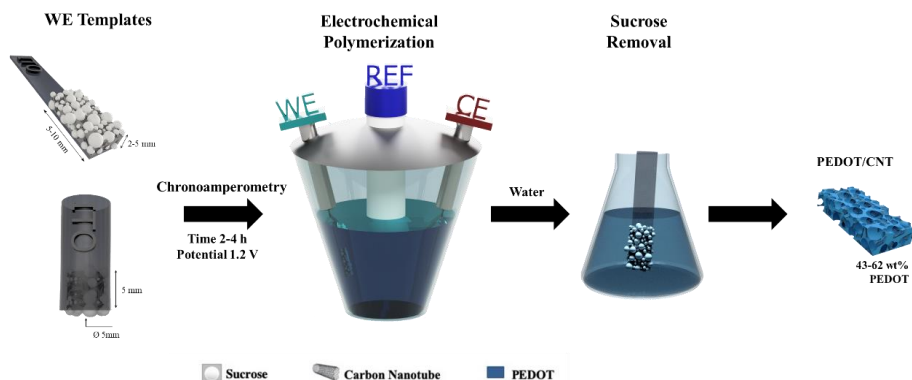

Figure 3.1 Scheme of manufacture PEDOT/CNT scaffolds through electropolymerization of EDOT

First, electrode template with 5x5x2 mm of shape was prepared onto ITO coated-PET slides and reaction conditions were evaluated in order to obtain a self-standing scaffold (Scheme 1). Chrono amperometry was carried out at different voltages, 1.0V, 1.2V and 1.4V at different reaction times, from 2h to 4h. As we have shown in the Chapter 2, PEDOT and CNT possess well separated degradation curves. Therefore, the amount of PEDOT was estimated in percentage of weight loss at 500 ºC.

Oxidation potential of 1.2V was chosen for the general manufacturing process due to different considerations. First, is the most common potential applied in literature for PEDOT films manufactured by EP, then, because at 1.0V none of the scaffolds prepared maintained the structural integrity after the sucrose removal, even though the amount of polymer deposited was theoretically sufficient, *i.e.* 50.8% after 4h. Hence we think that only small oligomers are deposited, which are not large

enough to keep the 3D structure. Finally, because comparative current on the chronoamperometry present equal deposition rate than 1.4V, thus same PEDOT amount (**Figure 3.2a**). Scaffolds manufactured using 1.2V, 0.1M conditions shown composition percentage between 44.5%, 52.9% and 59.0% for 2h, 3h, and 4h, respectively. (**Figure 3.2b**). Moreover, all the resulting scaffolds kept their tridimensionality and shape.

Once the optimum voltage was established, the concentration of the monomer was evaluated at different times of electrodeposition at 1.2V in the range between 0.05-0.5M of monomer. We observed that effect of the initial monomer concentration is not significant. In summary, we determined that amount PEDOT deposited show significant increases with time, but does not shown differences between monomer concentrations.

Scalable X-Y-Z axys of the scaffold were studied, larger surface area and height were evaluated: first X-Y rectangular shape was studied (10x5x2 mm), and second Z cubic shape (5x5x5 mm). Compared with previous studies, wider width scaffold was achieved at same polymerization conditions but longer times (1.2V, 4h, 0.1M EDOT), as conclusion the method is scalable along XY axis. However, for the cubic shape self-standing material was not possible to achieved, even different conditions reaction was tried. We think that, in spite of there is a polymerization process due to nucleation points within the third dimension as demonstrated, the intensity of the current is exponentially lost as the mixture of CNT-sucrose is far from the ITO surface and, consequently, the polymerization in that region is hindered and less efficient.

Thus, in order to obtain Z-scalable structures we designed a cilindrical electrode increasing the contact surface and achieving a real height scaffold. In this case, all mixture CNT-sugar was in contact with the electrode and polymerization was

produced in the third dimension. As height, volume of material and dimension were not comparable with previous, the successfully scaffold required more heavy conditions. Therefore, after 16h of chronoamperometry at 1.2V and 1M of EDOT monomer, scaffold was achieved. Furthermore, EDOT was gradually added to the electrolyte solution through an automated syringe pump in order to avoid polymer degradation.

Under such condition, PEDOT scaffold was polymerized. The polymerization rate obtained in the chronoamperometry resulted the double compared with cube 5x5x2. Moreover, pump addition improve the polymerization rate up to 300% as can be observed in the chronoamperometry plot. (**Figure 3.2c**). In addition, this polymerization control throughout pump addition can be observed by TGA. The amount of PEDOT deposited is also increased, from 30 to 60% respectively as shown in **Figure 3.2d**.
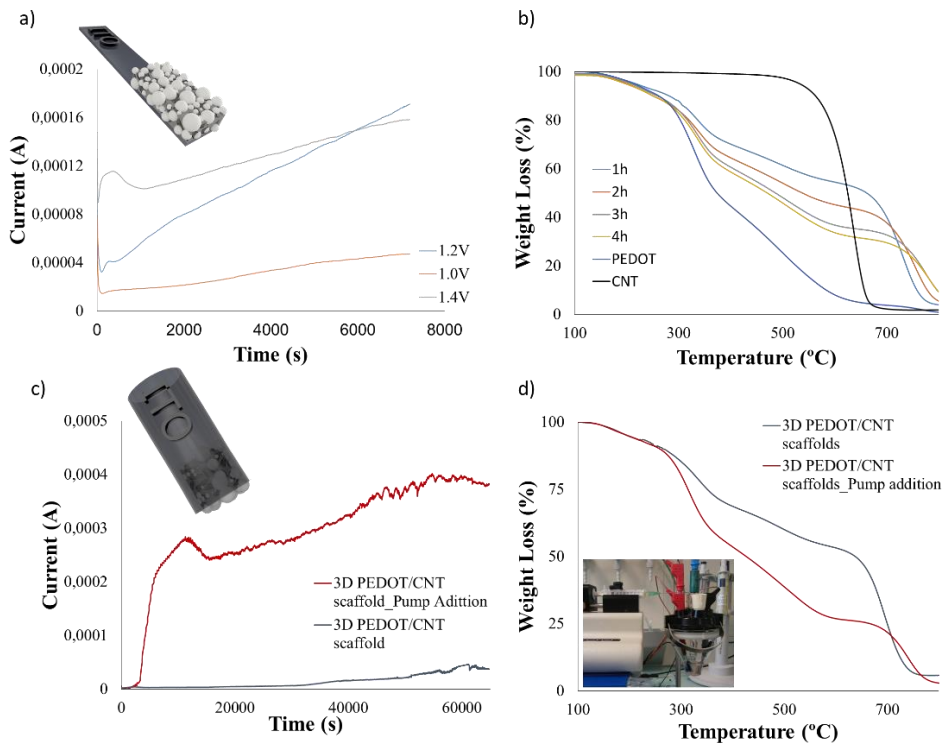
Figure 3.2 a) Chrono amperometry of rectangular shape (5x5x2) at different voltages b) TGA measurement of rectangular (5x5x2) scaffolds at manufactured at 1.2V, 0.1M for different reaction time c) Chronoamperometry of cylindrical electrode shape at 16h, 1M with and without addition pump d) TGA measurement of large Z scaffolds at manufactured at 1.2V, 1M, 16h for manufacturing scaffolds with and without addition pump

3.2.2 Nano, Micro- morphology and electrical characterization of 3D PEDOT/CNT scaffolds

As it was described in the introduction of the chapter, tridimensional scaffolds made by EP are challenge and CNT have been the key to achieve large dimensions. In contraposition to Chapter 1, PEDOT scaffold (in absence of CNT)

was manufacture following same conditions, 1.2V, 2h and 0.1M EDOT and used as control. The main difference during its electropolymerization resides on the absence of CNT within the sugar template. After polymerization, big differences in the height were observed by eye naked. Therefore, scaffold profile of the electrodes was analyzed in SEM images (**Figure 3.3**). As can be observed, thickness of the PEDOT/CNT scaffolds is double size than PEDOT scaffold. This fact agrees on the hypothesize made during the optimization conditions, CNT not only provide conductivity in the third dimension but also act as nucleation points, favoring the oxidation of EDOT monomers along the whole template. Moreover, TEM helped to confirm this theory due to, as well as Chapter 2, strong π-π interactions between both materials are present during the electropolymerization process. Thus, different structures can be observed, by one hand PEDOT cover several CNT increasing their diameter and by other hand forms hybrid clusters of conducting polymers.

Composition was studied in detail and both samples present the expected C, O and S peaks. Moreover, the presence of the CNT was observed after analysis of the deconvolution of the C1s peak. As can be observed in **Figure 3.3**, C=C band is higher for the PEDOT/CNT sample than PEDOT, 31% compared to the 25% of the CNT-free scaffold. As well, the π-π band, which is not present in the PEDOT scaffolds, is clearly visible in the CNT-containing sample. All these facts determined the presence of CNT on the scaffolds surface, thus confirming our previous conjectures.
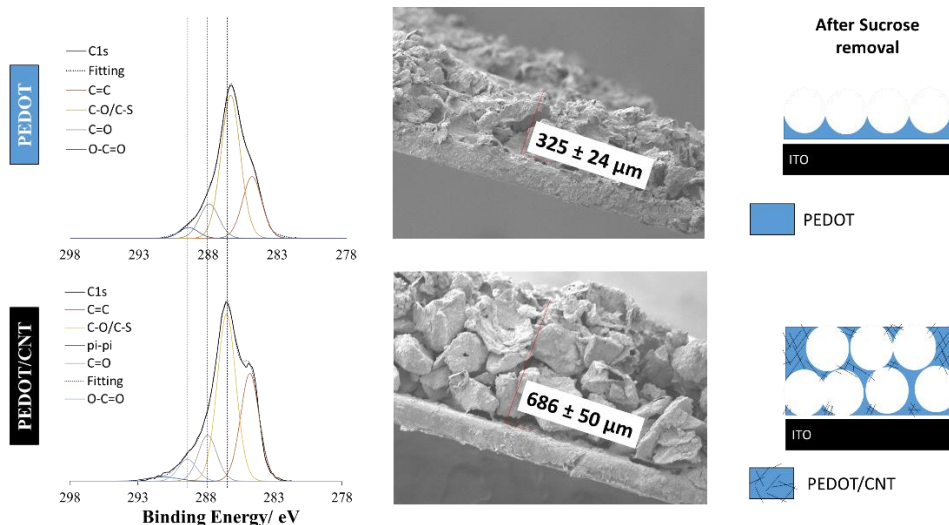
Figure 3.3 From the left to the right, XPS deconvolution analysis of the different PEDOT and PEDOT/CNT scaffold, SEM images of the profile and structural representation of the final 3D structure

SEM was used to analyze comparatively interconnectivity, size and shape after the sugar removal of PEDOT and PEDOT/CNT scaffolds. The images in **Figure 3.4** show grain-like homogeneous internal structure of the PEDOT/CNT scaffolds while homogeneous presence of open cavities in PEDOT scaffolds. Moreover, PEDOT/CNT scaffolds at higher magnification present particles structures with higher roughness while totally smooth surface in the absence of roughness is observed in PEDOT scaffolds. Comparatively, above nanometric magnification PEDOT/CNT revealed the brush-like assembly of the CNT along the internal surface of the whole structure.
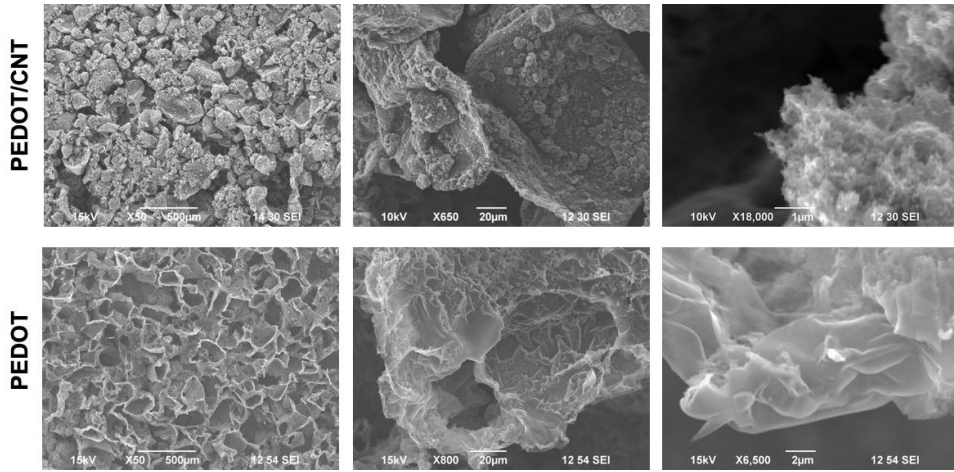
Figure 3.4 SEM images of the PEDOT/CNT (top) scaffolds and PEDOT (bottom) after sucrose removal. Synthesis conditions: 1.2V, 0.1M of EDOT and 2h of electrodeposition

Once the structures are formed and remain stuck to the electrode, they can be used not only as implants but also as three dimensional electrodes for recording or stimulating. Thus, as in the previous chapter, EIS of the PEDOT and PEDOT/CNT scaffolds was evaluated in a PBS solution simulating electrophysiological conditions. **Figure 3.5a** show conductivity of PEDOT/CNT scaffolds that present 5 times less resistance than the PEDOT scaffolds. However, as it was shown in the SEM morphology, PEDOT/CNT scaffolds are higher and possess higher surface area in contact with the electrolyte than the PEDOT scaffolds. Hence, in order to provide more comparable conductivity measurement, the materials were demounted, morter and deposited onto a glass substrate. Resistance differences were measured with 4PP technique. The obtained conductivity is in line with the values of EIS, since PEDOT (2.54 ± 1.06 Ω·m) is among ten times less conductor than PEDOT/CNT material (0.23 ± 0.02 Ω·m). (**Figure 3.5b**)
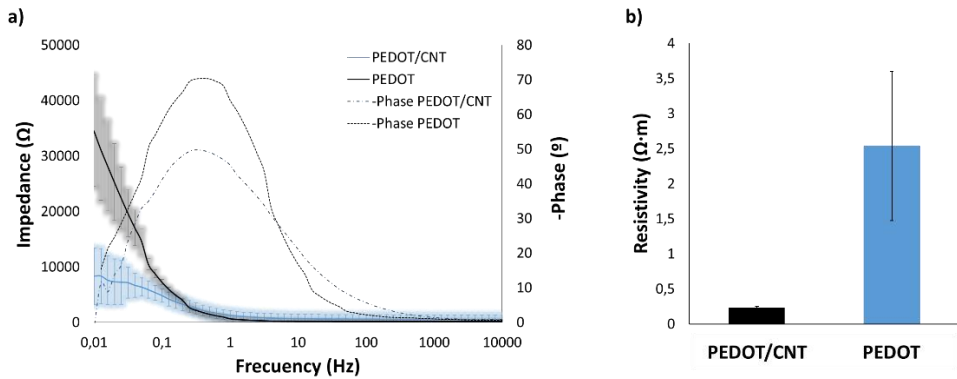
Figure 3.5 a) EIS of the PEDOT (black) and PEDOT/CNT (blue) scaffolds. Geometry of the scaffolds: cubic rectangular, 5x5x5mm b) Resistivity of PEDOT and PEDOT/CNT composites measured by 4PP

3.2.3 Spontaneous cell differentiation of neuroblastoma SH-SY5Y cells

SH-SY5Y is a human neuroblastoma-derived cell line that are commonly used as models *in vitro* for the study of different neurodegenerative diseases. If conditions are suitable, or chemicals as retinoic acid or neurotropic factors are added, this cells proliferate until differentiation, resulting in mature neurons with clear phenotype, *i.e.*, large axons and lamelipodia.[22–26] Therefore, by using the structures developed here, we have tried to make them differentiate in mature neurons because the action of our PEDOT and PEDOT/CNT electroactive material.

SH-SY5Y were cultured on scaffolds during 3 and 7 days and *in vitro* cytotoxicity was analyzed using same LDH assay as the previous chapter and immunostaining calcein-AM/F-actin. As in the previous work, cytotoxicity was not observed, beside as high confluence cells were observed using calcein-AM staining over both

scaffolds (**Figure 3.6a**). In addition, large neuron elongations are clearly presented in both PEDOT and PEDOT/CNT materials, by F-actin labeling. In fact, the presence of these elongations is remarkable numerous in the CNT-containing material, suggesting the cell ability to maintain their normal morphology and their function when CNTs are present (see **Figure 3.6**).
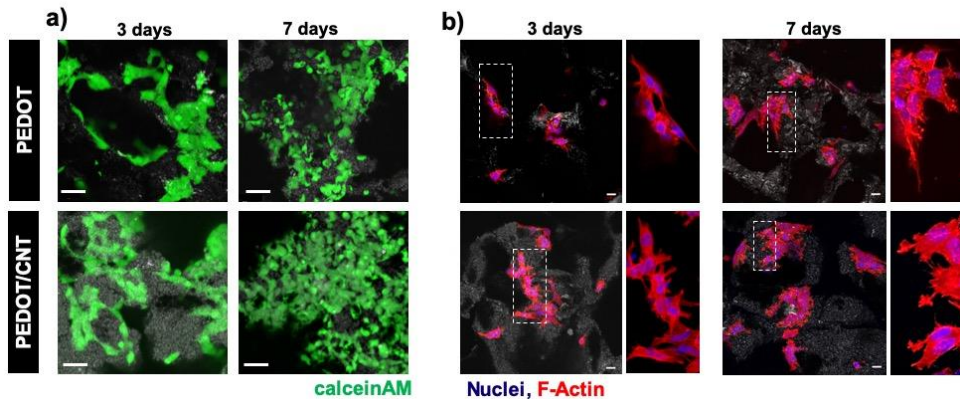
Figure 3.6 Confocal imaging of SH-SY5Y cells grown on the PEDOT and PEDOT/CNT scaffolds after 3 and 7 days of culture whith a) Calcein-AM labeling (green) and b) F-actin (red, 555) staining.

SEM images are in agreement with these observations, which show high confluence and adhered cells in both PEDOT and PEDOT/CNT electrodes. In addition, SEM images (**Figure 3.7**) of SH-SY5Y cultured at 3 or 7 days onto PEDOT/CNT scaffolds show much more expanded cytoskeleton (highlighted with red arrows) with the typical neuron-like morphology, while such morphology is not present in the PEDOT scaffolds. Moreover, some round-shaped cells are observed in PEDOT scaffolds, indicating that in absence of CNT not all the cells were able to expand and differentiate. This observation let us anticipate that the cells are also able to properly differentiate into neuronal cells.
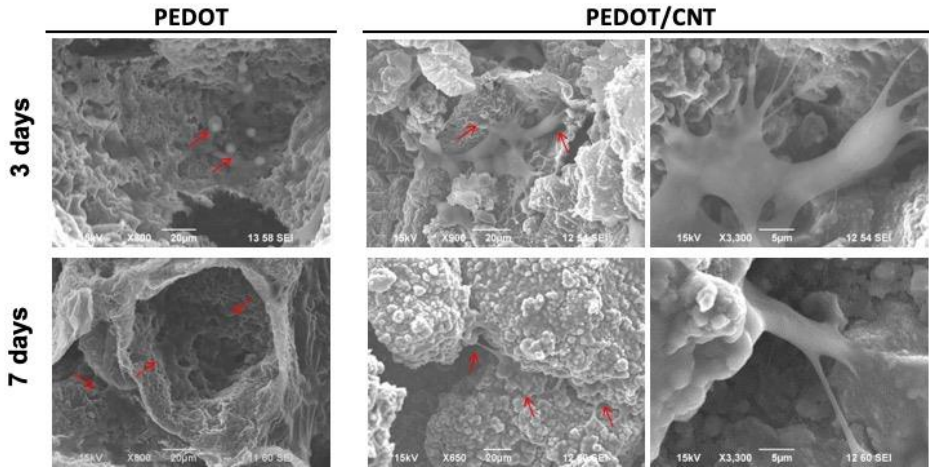
Figure 3.7 SEM images of the SH-SY5Y cells grown on the PEDOT and PEDOT/CNT scaffolds after 3 and 7 days of culture. Red arrows point the cells.

In order to confirm this observation, β-Tubulin class III (β-III-Tub) was labeled. β-III-Tub is a protein well-known in literature that is expressed in neurons and is involved in neurogenesis process, axon guidance and maintenance. We have stained our cells cultured after 3 and 7 days and evaluate the differentiation into mature neurons by immunofluorescence assay and signal/noise ratio analysis on the manufactured substrates. (see **Figure 3.8a**) The intensity was measured using signal/noise ratio for both materials which confirm the increased presence of tubulin while an important reduction after two weeks is appreciate, that can be associated to confluence within the incubation well and/or the lack of specific neuron media. According to the images and the plot collected in **Figure 3.8b**, the β-III-Tub is expressed in both materials at day 7 but highly intense in PEDOT/CNT scaffolds.
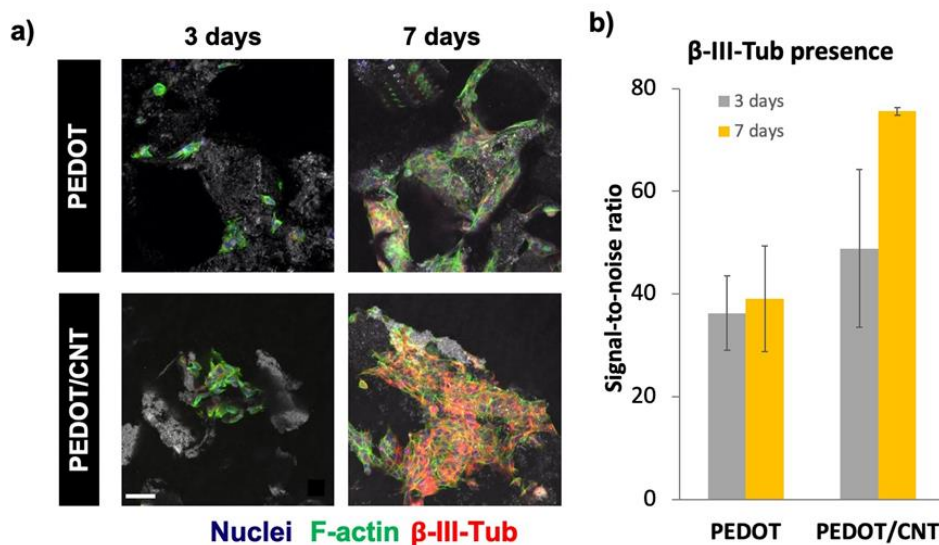
Figure 3.8 a) Immunofluorescence assay of the SH-SY5Y cells cultured on the PEDOT and PEDOT/CNT scaffolds after 3 and 7 days **b)** Intensity signal-to-noise ratio of amount of β-III-Tub expressed of the incubated cells, taken from the immunostaining images.

Finally, differentiation to mature neuronal cells was also corroborated with other neuron-like phenotype which is microtubule-associated protein MAP-II. Differentiated matured neurons are expected to express β-III-Tub and MAP-II in their elongated neurites. As well as before, immunofluorescence assay and analysis of signal-to noise ratio was performed. The dendritic elongations are clearly observed with this staining, see white narrows in **Figure 3.9a**, thus supporting the previous results observed with the β-III-Tub staining. The cells grown on the PEDOT/CNT scaffold show increased number of elongated neurites, in comparison with the low number observed for the PEDOT scaffolds. Moreover, we observe that the intensity of the MAP-II increase significantly over the time as happens with the β-III-Tub (see **Figure 3.9b**).

With all these facts, we can confirm that proliferation within the PEDOT scaffolds is higher since the number of undifferentiated cells is higher. This results are in line too with the higher confluence observed in calcein images. Overall, we can conclude that the cells do differentiate to neuronal cells faster when cultured in the PEDOT/CNT scaffolds achieving higher degree of maturity and differentiation into neurons.
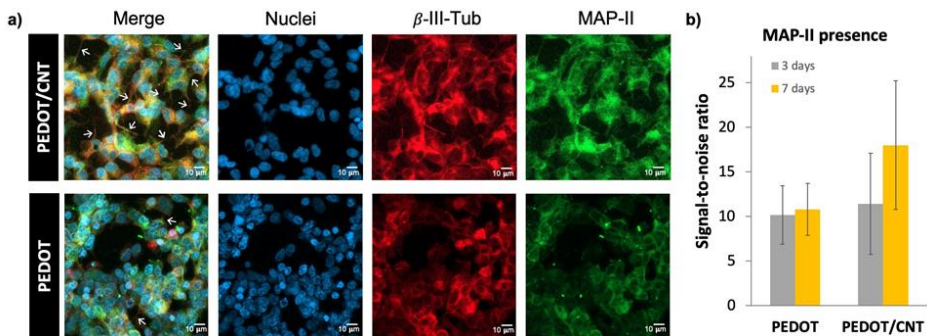
Figure 3.9 a) Staining of the SH-SY5Y cells grown on the PEDOT and PEDOT/CNT scaffolds after 7 days. Neurites elongations are pointed with arrows. **b)** Intensity signal-to-noise ratio of amount of MAP-II expressed on the incubated cells, taken from the immunostaining images.

3.3 Conclusions

In this chapter, we have succeeded prepare conducting porous scaffold of PEDOT and PEDOT/CNT by electropolymerizaton method, using 3D electrode-templates on ITO coated-PET slides. The reaction was optimized in order to obtain stables self-standing conducting PEDOT and PEDOT/CNT scaffold after the sucrose removal. The composition of the scaffolds was determined using TGA, obtaining PEDOT percentages between 45 and 60 wt%. PEDOT/CNT scaffolds showed a grain-like homogeneous internal structure as well as containing pores size between 100-250 µm, while PEDOT scaffolds present totally opened porous macrostructures without tridimensionality. Higher magnification images revealed

the presence of CNT due to brush-like assembly along the internal surface of the whole structure. The correspondence of this brush-like structures to CNT was corroborated by XPS. The presence of CNT within the lattices of the sacrificial crystal sugar electrodes, allow the polymerization in the tridimensional Z axys, allowing the manufacturing of thicker scaffolds. Moreover, it has an impact in the conductivity, thus PEDOT/CNT scaffolds presented five times higher conductivity than PEDOT scaffolds (values compared in 0.01 Hz frequency), which represents an increase above 10 times in terms of conductivity.

The scaffolds prepared were incubated with neuroblastoma SH-SY5Y cells for 3 and 7 days. In general, high confluence was observed with the calcein-M staining in both scaffolds. However, neurons on PEDOT/CNT scaffolds presented different morphology analyzed with F-actin staining and SEM. This results showed neuron-like elongations and abundant cell-to-cell contacts for both PEDOT and PEDOT/CNT scaffold surfaces, although they were longer and more numerous in the material containing CNTs. In addition, larger and more amount of lamellipodia was observed for the CNT-based scaffolds, indicating better adhesion to the substrate. Moreover, some round-shaped cells were attached to the PEDOT scaffolds, indicating that some of this cells were not able to expand and differentiate without the presence of the CNT. Finally, β-III-Tub and MAP-II staining typically used in the evaluation of neural differentiation, shows more and larger elongated neurites in the cells incubated on PEDOT/CNT scaffolds, confirming the differentiation into mature neuronal cells. On the other hand, markers in PEDOT scaffolds was not as significant. We suggest that the improved differentiation and maturation observed in PEDOT/CNT scaffolds results from the excellent tight interaction between the cells and the CNT, having a crucial importance on the conductivity of the material and the nanoscale cylindrical shape.
Overall, we have designed and constructed a novel conducting biomaterial able to differentiate SH-SY5Y cells, without using any chemicals or neurothophic factors.

This study provided insights for future applications of CNT-containing 3D scaffolds in neural bioapplications as potent modulators of cell behavior.

3.4 Experimental section

3.4.1 Fabrication and optimization of PEDOT and PEDOT/CNT scaffolds

Template manufacture and electropolymerization

The crystal sugar template support was produced in a multi-stage process, very similar to the previous reported in the Chapter 1. Summarized, 250 mg of crystal sugar grain were mashed and sifted within sizes of 100 µm and 250 µm (Fisher Scientific Inc.). Then CNTs (15 mg) and the sieved sucrose (500 mg) were mixed and shaken overnight. In order to make the electrodes, 150 mg of the mixture was mixed with 10 µL of MilliQ water, homogenized and deposited onto a ITO coated PET electrode.

Working as well counter electrodes were manufactured on ITO coated PET slides with different dimensions, thus 5x30 mm for square electrodes and 20x20 mm for cylinder electrodes. First, the working area of the ITO slide (5x5 mm for squares, 5x20 mm for cylinder) was cover with the paste of sucrose/CNT, covered area ranging from 25 and 50 mm2 depending on the geometry. The paste was well pressed to enforce the connection and interaction with the ITO electrode. PDMS homemade mold with the desired dimensions was used to ensure the tridimensional template.

Electropolymerization

Reaction was performed in a 3 electrode chamber where Ag/AgCl(KCl 3M) as the reference electrode and tetrabutylammonium hexafluorophosphate (TBAPF$_6$, 0.1M) as supporting electrolyte in acetonitrile as solvent. Before the reaction, the solution was purged with nitrogen. The electropolymerization was performed at a

constant potential mode. The electrodeposition was modulating as the follow: voltage (1V, 1.2V and 1.4V vs Ag/AgCl), time of reaction (between 2h and 16h), and EDOT monomer concentration (from 0.05M to 0.5M). After the reaction was complete, 2h or 16h, the scaffold was immersed into MilliQ water overnight to dissolve sucrose, resulting in a self-standing architecture with interconnected micro-channels and holes. As control sample, PEDOT scaffolds without CNT were polymerized in the following conditions: 1.2V, 0.1M EDOT during 2h.

Conductivity measurements

In a first attempt, relative conductivity between PEDOT and PEDOT/CNT scaffolds were evaluated using Impedance Electrochemical Spectroscopy (EIS) in a configuration two-electrode cell using PBS buffer as supported electrolyte in order to simulate as much as possible physiological conditions. To carry out the measurement, the self-standing scaffold was used as working electrode and ITO coated on PET as counter electrode. Additionally, in order to measure more accurately the electrical conductivity of the neat material, four-point probe was employed. For that purpose, PEDOT and PEDOT/CNT scaffolds were detached from the ITO electrode, mashed and dispersed in water (20 mg/mL). The dispersion was drop casting in a12 mm diameter circular coverslip. Due to their powder nature and it poor dispersability, the deposited material formed clusters, thus comparative conductivity was evaluated in $\Omega \cdot m$ and not in S/cm.

3.4.2 Cell culture

Cell morphology and differentiation staining

The scaffolds incubated with cells during 3 and 7 days were washed once with PBS fixed with paraformaldehyde (4%) during 20 min, afterwards scaffolds were washed again twice with PBS. Then, the cells in the scaffolds were permeabilized with 0.2% Triton X-100 in PBS for 20 min at 37 ºC, and blocked for 30 min with PBS containing 0.1% Tween20, 5% bovine serum albumin. Within the F-actin

filament staining, scaffolds were incubated for 30 min with complete media containing Actin Red 555 Ready Probes Reagent (1:10 dilution, Invitrogen) in darkness. For differentiation, the scaffolds were incubated with anti-beta-III tubulin monoclonal antibody [EP1569Y] conjugated to Alexa Fluor 647 (1 μg·mL-1 dilution, abcam, cat. N. ab190575) in 0.1% Tween20 PBS at 4ºC in a humidified chamber for 20 h. Then, media was aspirated, and cells were incubated with Actin Green 488 Ready Probes Reagent (1:10 dilution, Invitrogen) for 30 min in the dark and 50nM 2-(4-amidinophenyl)-1H -indole-6-carboxamidine (DAPI) was added for nuclei stain.

Confocal imaging

Stained scaffolds with cells were covered with PBS in a 50 mm-diameter ≠1.5 optical glass bottom dish (Cellvis). 16 μm-Z-stack images were taken in a light scanning microscope (ZeissNLO 880) with the Plan-Apochromat 20x/0.8 M27 objective lens employing the excitation/emission wavelengths of 633nm/650-735nm for AF647, 561 nm/610-715 nm for Actin Red 555 and 405 nm/415-475 nm for DAPI and 488 nm/500-600 nm for Actin Green 488 and Calcein-AM. For imaging the scaffolds, 458 nm/441-471 nm or 633nm/ 620-650 nm were used in reflection mode. For live imaging at 5%CO_2, 37ºC and 100% humidity, an insert chamber for temperature and atmosphere control was employed. For image processing, maximum intensity Z-projection images were generated using ZEN 2.3 software. For the quantification of beta-III-tubulin stain, fluorescent images were analyzed using ImageJ program (National Institutes of Health, USA).

During the analysis, the cytoplasm regions were selected, and nuclei were subtracted. The fluorescent intensity of the pixels localized in the cytoplasm was averaged for each condition (signal). The fluorescent intensity of the pixels localized in areas outside the cells was also averaged (noise). Results are expressed as a signal to noise ratio. More than 20,000 pixels were analyzed for each condition.

3.5 References

(1)   Iqbal, S.; Ahmad, S. Recent Development in Hybrid Conducting Polymers: Synthesis, Applications and Future Prospects. *J. Ind. Eng. Chem.* **2018**, *60*, 53–84. https://doi.org/https://doi.org/10.1016/j.jiec.2017.09.038.

(2)   Heinze, J.; Frontana-Uribe, B. A.; Ludwigs, S. Electrochemistry of Conducting Polymers--Persistent Models and New Concepts. *Chem. Rev.* **2010**, *110* (8), 4724–4771. https://doi.org/10.1021/cr900226k.

(3)   Otero, T. F.; Martinez, J. G. Electro-Chemo-Biomimetics from Conducting Polymers: Fundamentals{,} Materials{,} Properties and Devices. *J. Mater. Chem. B* **2016**, *4* (12), 2069–2085. https://doi.org/10.1039/C6TB00060F.

(4)   Daneshvar, E. D.; Smela, E. Characterization of Conjugated Polymer Actuation under Cerebral Physiological Conditions. *Adv. Healthc. Mater.* **2014**, *3* (7), 1026–1035. https://doi.org/10.1002/adhm.201300610.

(5)   Sharma, M.; Waterhouse, G. I. N.; Loader, S. W. C.; Garg, S.; Svirskis, D. High Surface Area Polypyrrole Scaffolds for Tunable Drug Delivery. *Int. J. Pharm.* **2013**, *443* (1–2), 163–168. https://doi.org/10.1016/j.ijpharm.2013.01.006.

(6)   Kim, D.-H.; Richardson-Burns, S. M.; Hendricks, J. L.; Sequera, C.; Martin, D. C. Effect of Immobilized Nerve Growth Factor on Conductive Polymers: Electrical Properties and Cellular Response. *Adv. Funct. Mater.* **2007**, *17* (1), 79–86. https://doi.org/10.1002/adfm.200500594.

(7)   Poppendieck, W.; Hoffmann, K.-P. Coating of Neural Microelectrodes with Intrinsically Conducting Polymers as a Means to Improve Their Electrochemical Properties BT - 4th European Conference of the International Federation for Medical and Biological Engineering; Vander Sloten, J., Verdonck, P., Nyssen, M., Haueisen, J., Eds.; Springer Berlin Heidelberg: Berlin, Heidelberg, 2009; pp 2409–2412.

(8)   Leprince, L.; Dogimont, A.; Magnin, D.; Demoustier-Champagne, S.

Dexamethasone Electrically Controlled Release from Polypyrrole-Coated Nanostructured Electrodes. *J. Mater. Sci. Mater. Med.* **2010**, *21* (3), 925–930. https://doi.org/10.1007/s10856-010-4008-6.

(9) Richardson-Burns, S. M.; Hendricks, J. L.; Martin, D. C. Electrochemical Polymerization of Conducting Polymers in Living Neural Tissue. *J. Neural Eng.* **2007**, *4* (2), L6–L13. https://doi.org/10.1088/1741-2560/4/2/L02.

(10) Strakosas, X.; Wei, B.; Martin, D. C.; Owens, R. M. Biofunctionalization of Polydioxythiophene Derivatives for Biomedical Applications. *J. Mater. Chem. B* **2016**, *4* (29), 4952–4968. https://doi.org/10.1039/C6TB00852F.

(11) Wong, J. Y.; Langer, R.; Ingber, D. E. Electrically Conducting Polymers Can Noninvasively Control the Shape and Growth of Mammalian Cells. *Proc. Natl. Acad. Sci.* **1994**, *91* (8), 3201–3204. https://doi.org/10.1073/pnas.91.8.3201.

(12) Garner, B.; Hodgson, A. J.; Wallace, G. G.; Underwood, P. A. Human Endothelial Cell Attachment to and Growth on Polypyrrole-Heparin Is Vitronectin Dependent. *J. Mater. Sci. Mater. Med.* **1999**, *10* (1), 19–27. https://doi.org/10.1023/a:1008835925998.

(13) Ibanez, J. G.; Rincón, M. E.; Gutierrez-Granados, S.; Chahma, M.; Jaramillo-Quintero, O. A.; Frontana-Uribe, B. A. Conducting Polymers in the Fields of Energy, Environmental Remediation, and Chemical–Chiral Sensors. *Chem. Rev.* **2018**, *118* (9), 4731–4816. https://doi.org/10.1021/acs.chemrev.7b00482.

(14) Martin, C. R. Template Synthesis of Electronically Conductive Polymer Nanostructures. *Acc. Chem. Res.* **1995**, *28* (2), 61–68. https://doi.org/10.1021/ar00050a002.

(15) Martin, C. R. Nanomaterials: A Membrane-Based Synthetic Approach. *Science (80-.).* **1994**, *266* (5193), 1961–1966. https://doi.org/10.1126/science.266.5193.1961.

(16) Zhang, J.; Li, X.; Guo, W.; Hreid, T.; Hou, J.; Su, H.; Yuan, Z.

Electropolymerization of a Poly(3,4-Ethylenedioxythiophene) and Functionalized, Multi-Walled, Carbon Nanotubes Counter Electrode for Dye-Sensitized Solar Cells and Characterization of Its Performance. *Electrochim. Acta* **2011**, *56* (9), 3147–3152. https://doi.org/https://doi.org/10.1016/j.electacta.2011.01.063.

(17)   Liu, M.; Wen, Y.; Li, D.; He, H.; Xu, J.; Liu, C.; Yue, R.; Lu, B.; Liu, G. Electrochemical Immobilization of Ascorbate Oxidase in Poly(3,4-Ethylenedioxythiophene)/Multiwalled Carbon Nanotubes Composite Films. *J. Appl. Polym. Sci.* **2011**, *122* (2), 1142–1151. https://doi.org/10.1002/app.34257.

(18)   Bhandari, S.; Deepa, M.; Srivastava, A. K.; Lal, C.; Kant, R. Poly(3,4-Ethylenedioxythiophene) (PEDOT)-Coated MWCNTs Tethered to Conducting Substrates: Facile Electrochemistry and Enhanced Coloring Efficiency. *Macromol. Rapid Commun.* **2008**, *29* (24), 1959–1964. https://doi.org/10.1002/marc.200800550.

(19)   Xu, F.; Liu, Y.; Ding, G.; Deng, M.; Chen, S.; Wang, L. Three Dimensional Macroporous Poly(3,4-Ethylenedioxythiophene) Structure: Electrodeposited Preparation and Sensor Application. *Electrochim. Acta* **2014**, *150,* 223–231. https://doi.org/https://doi.org/10.1016/j.electacta.2014.10.114.

(20)   Alegret, N.; Dominguez-Alfaro, A.; Mecerreyes, D. 3D Scaffolds Based on Conductive Polymers for Biomedical Applications. *Biomacromolecules* **2019**, *20* (1), 73–89. https://doi.org/10.1021/acs.biomac.8b01382.

(21)   Janáky, C.; Visy, C. Conducting Polymer-Based Hybrid Assemblies for Electrochemical Sensing: A Materials Science Perspective. *Anal. Bioanal. Chem.* **2013**, *405* (11), 3489–3511. https://doi.org/10.1007/s00216-013-6702-y.

(22)   George, J. H.; Nagel, D.; Waller, S.; Hill, E.; Parri, H. R.; Coleman, M. D.; Cui, Z.; Ye, H. A Closer Look at Neuron Interaction with Track-Etched

Microporous Membranes. *Sci. Rep.* **2018**, *8* (1), 15552. https://doi.org/10.1038/s41598-018-33710-6.

(23) Yang, M.; Xiang, G.; Yu, D.; Yang, G.; He, W.; Yang, S.; Zhou, G.; Liu, A. Hsa_circ_0002468 Regulates the Neuronal Differentiation of SH-SY5Y Cells by Modulating the MiR-561/E2F8 Axis. *Med. Sci. Monit.* **2019**, *25*, 2511–2519. https://doi.org/10.12659/MSM.915518.

(24) Xicoy, H.; Wieringa, B.; Martens, G. J. M. The SH-SY5Y Cell Line in Parkinson's Disease Research: A Systematic Review. *Mol. Neurodegener.* **2017**, *12* (1), 10. https://doi.org/10.1186/s13024-017-0149-0.

(25) Encinas, M.; Iglesias, M.; Liu, Y.; Wang, H.; Muhaisen, A.; Ceña, V.; Gallego, C.; Comella, J. X. Sequential Treatment of SH-SY5Y Cells with Retinoic Acid and Brain-Derived Neurotrophic Factor Gives Rise to Fully Differentiated, Neurotrophic Factor-Dependent, Human Neuron-like Cells. *J. Neurochem.* **2000**, *75* (3), 991–1003. https://doi.org/10.1046/j.1471-4159.2000.0750991.x.

(26) Agholme, L.; Lindström, T.; Kågedal, K.; Marcusson, J.; Hallbeck, M. An in Vitro Model for Neuroscience: Differentiation of SH-SY5Y Cells into Cells with Morphological and Biochemical Characteristics of Mature Neurons. *J. Alzheimers. Dis.* **2010**, *20* (4), 1069–1082. https://doi.org/10.3233/JAD-2010-091363.

CHAPTER 4
3D PRINTING SCAFFOLDS
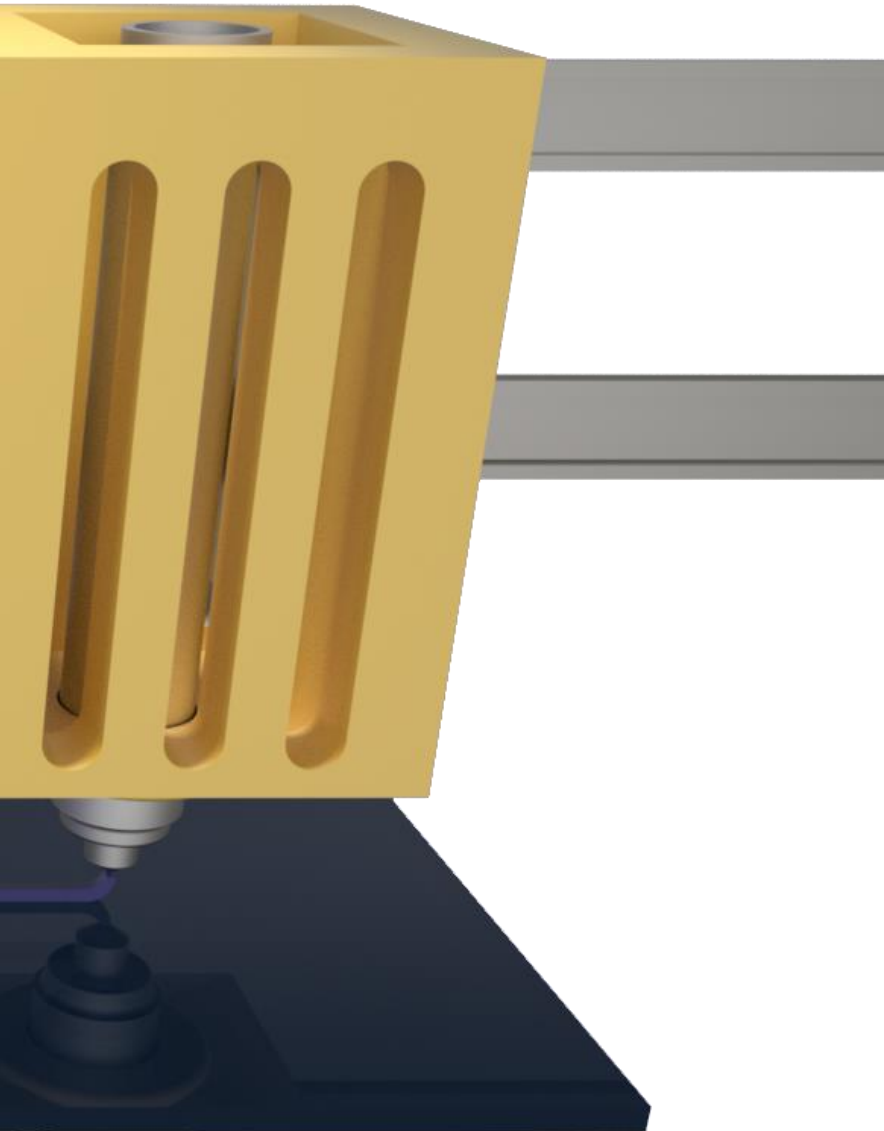
Chapter 4: 3D printed scaffolds

4.1. Introduction

The third approach has consisted on the synthesis of a new polymer for additive manufacturing instead of the use of carbon nanotubes to hold and support the tridimensional structure.

Additive manufacturing (AM), which refers to all technologies that build 3D objects by adding layer-upon-layer of materials by the use of computer-assisted design manufacture, represent a new and versatile technology for fabrication of objects controlling its shape and functionality. As recently highlighted by Nelson *et al.*, "the future of additive manufacturing will depend on new polymeric materials that are specifically designed for these technologies".[1] Thus, the polymer has a dominant role within the tailored features required in applications as tissue engineering,[2]

98

aerospace, biomedical devices,[3,4], soft-robotics or energy.[5,6] For instance, next generation tissue engineering structures are looking for the development of vascularization structures and/or 3D printable conducting polymers for electroactive cells.[7]

PEDOT represents one the most popular electronic conducting polymer since it is commercially available, has high conductivity, and stability, however, it presents important limitations as its insolubility and infusibility, which limits drastically its processability. As we remarked in the introduction, PEDOT normally requires the use of stabilizers or other isolating polymers to improve its limitations. Thus the early attempts to process PEDOT by additive manufacturing methods were unsuccessful.

In the recent past two years some approaches have appeared, but new approaches required to be developed. In fact, in 2019 Zhao *et al.* designed PEDOT/PSS inks with very promising rheological characteristics that can be malleable by AM. This method uses direct ink printing to create dry and wet hydrogel that are conductive at the microscale structures and can be used for the manufacturing of neural electrodes in rats.[8] As the example described in the chapter 1, PEDOT:PSS can be patterned by light based printing as SLA. Zhang *et al.* crosslinked PEDOT/PSS with PEG-diacrylate to create very conductive structured hydrogels with future applications in tissue engineering.[9]

However, apart from these examples, PEDOT has not been printed using commonly AM technologies based on polymer melting methods, such as filament fused fabrication (FFF) or direct ink writing (DIW).[10] Only recently, it has been reported the employment of extrusion followed by fiber spinning to fabricate PEDOT/Nafion composites.[11]

On the other hand, one of the most well-known materials use in FFF method is polylactide (PLA) because of its excellent biocompatibility and biodegradability.[12] Therefore, PLA was selected to be used as PEDOT support in order to develop conductive materials with the melting ability throughout 3D printing.

For this reason, in this chapter we have addressed the challenge in manufacturing tridimensional conductive structures throughout the synthesis and characterization of the graft copolymers PEDOT-g-PLA with melting properties that allow its printability by direct ink writing throughout melting extrusion for the first time.

4.2. Results and discussion

4.2.1. Synthesis of the PLA macromonomer

Three different PLA macronomers of molecular weights between 7000 and 24000 g/mol by organocatalyzed ring-openning polymerization (ROP) of L,L-lactide initiated by EDOT-methanol in bulk conditions was prepared. (see **Table 4.1**)

Figure 4.1 presents the reaction using a mixture of non-eutectic organocatalyst as 1,8-Diazabicyclo[5.4.0]undec-7-ene (DBU) and benzoic acid (BA). This type of organocatalytic reaction has been studied by our group for lactide enantioselective ROP[13] or polyols copolymerizations[14,15] among others, resulting in high temperature stability and successfully catalyst performance.

First catalyst mixture was prepared as follows,[16] BA was placed in a flask with ether until the acid was totally dissolved. Then, DBU base was added dropwise obtaining a white salt. After that, the salt was filtered and washed with excess of ether and dried under vacuum. Secondly, DBU:BA organocatalyst prepared (5 mol %), lactide and hydroxy methyl EDOT-methanol was inserted in a vial with a

magnetic stirrer. The reaction was sealed and inserted into a preheated oil bath at 130 °C and followed by ^{1}H NMR. After 1.5 h, 90% conversion was achieved and the molecular weight was confirmed by relative intensities of tiophene proton signals at 6.4 ppm and PLA methyl group at 5.2 ppm (

Figure 4.1c). Finally, a white powder was collected and purified through precipitation in methanol and dried under vacuum at RT for 24h. Moreover, MALDI-Tof show the average mass of the polylactic repeating unit across the distribution of molecular weight (144 m/z) (

Figure 4.1a-b).
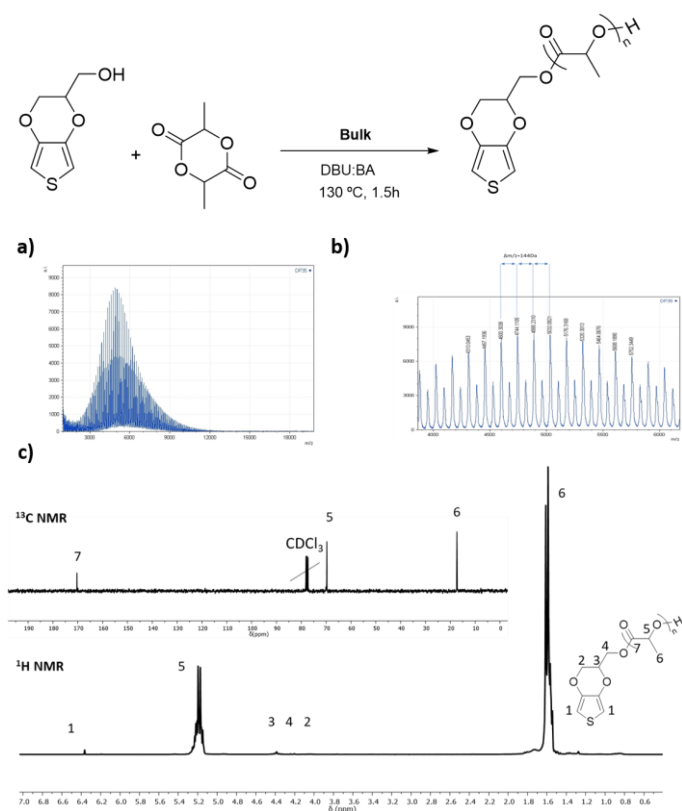
Figure 4.1 Synthesis route of PLA macromonomers synthesized throughout ROP in bulk, using hydroxyl methyl EDOT as initiator and lactide as precursor. **a)** MALDI-TOF of the macromonomer 1a indicating a monomodal mass profile distribution b) Magnification of MALDI-TOF window where 144kDa sequences appeared due to PLA chains repetition and **c)** ^{1}H NMR/^{13}C NMR presented the correspondence PLA macromonomer shifted peaks.

Table 4.1 Characteristics in terms of polydispersity and molecular weight measured. Synthetic conditions carried out in bulk at 130ºC, 1.5 h and DBU:BA organocatalyst.

Entry	Mn,th	Mn, exp SEC	Mn, exp NMR	Mw / Mn
PLA$_{7K}$	5100	7100	7200	1,65
PLA$_{10K}$	10100	8300	10200	1,47
PLA$_{25K}$	20300	13800	24300	1,37

Mn, th = Theoretical number-average molecular weight
Mn, exp, SEC = Experimental number-average molecular weight calculated with SEC using PS standards
Mn, exp, NMR = Experimental number-average molecular weight calculated with NMR
Mw / Mn= Dispersity calculated by SEC

4.2.2 Synthesis and characterization of the graft copolymer

PEDOT-g-PLA copolymers were synthesized by oxidative copolymerization between EDOT and PLA macromonomer (**Figure 4.2**). This strategy has been widely reported for the synthesis of graft copolymers between different conductive and thermoplastic polymers.[17–20] The oxidative copolymerization consists of an oxidation reaction between EDOT and the macromonomers using FeCl$_3$ in chloroform.
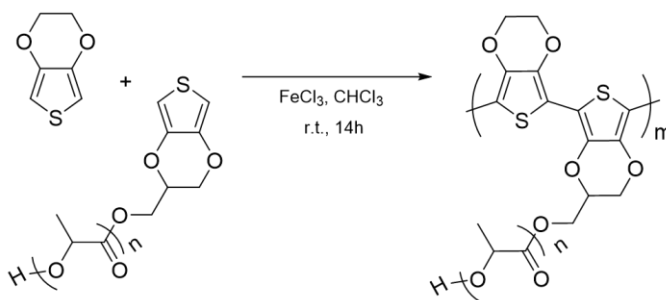
code	PLA Mn (g/mol)	Feed w_{PEDOT}	Reaction Yield (%)	Final w_{PEDOT}	σ (µS/cm)
1	7100	5	50	7	5,1
2	8300	5	60	5	1,81
3	8300	10	38	7	8,91
4	8300	20	25	40	20
5	13800	5	53	5	2,9
6	13800	10	40	34	15,0

a PLA macromonomers molecular weight calculated by ^{1}HNMR

b Weight fraction of EDOT in the reaction feed.

c Weight fraction of PEDOT in the products as measured by TGA

d Electrical conductivity measured by four-point probe

Figure 4.2 (Top) Synthesis Reaction of PEDOT-g-PLA; (Bottom) Characteristics of each copolymer (entry) referred to reaction yield, copolymer composition and conductivity.

Figure 4.3a shows the typical blue dispersion obtained after the oxidative polymerization reaction, which present the UV bipolaron absorption bands in the near-IR, which is very representative of conducting PEDOT. After the reaction, PEDOT-g-PLA copolymers were purified by precipitation and recovered as powder. The composition of the copolymers could be estimated comparing the relative intensity of the carbonyl group in PLA (1754 cm^{-1}) and the tiophene in PEDOT (985 cm^{-1}), as can be observed in **Figure 4.3b**. Furthermore, thermal

stability and weight loss at 400 ºC present proportional weight loss compared with the increasing PEDOT within the copolymers (**Figure 4.3c**). Hence, by developing a calibrating line where weight loss was plotted versus PEDOT percentage, composition PEDOT-g-PLA copolymers could be estimated (see **Figure 4.3d**).

As it was expected, electrical conductivities measured by four-point probe (4PP) of the different PEDOT-g-PLA presented similar values in the range of other copolymers reported in literature.[19,20] In all the cases, the conductivity values were in the order of µS/cm and moreover, the conductivity of the copolymers presents composition dependence. These values are low for applications as transistors for cutaneous electrodes,[4] but are good enough for conductive scaffolds in tissue engineering applications.
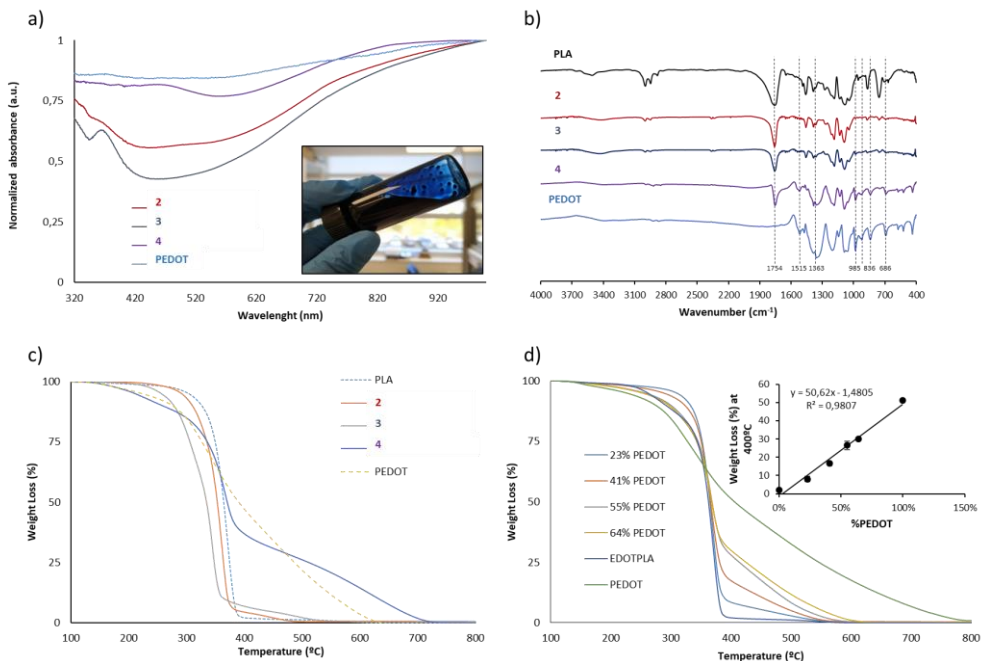
Figure 4.3 a) UV/Vis of different PEDOT-g-PLA copolymers **b)** Infrared spectra of different graft copolymers with 5, 7 and 40% PEDOT percentages compared with it respective PEDOT and PLA macromonomer (PLA$_{10K}$) **c)** TGA of the homonymous copolymers and **d)** TGA of the blends formed for the calibration line

The copolymer morphology of different PEDOT compositions was observed by TEM. In **Figure 4.4**, PEDOT that was synthesized as control sample under the same conditions, and showed powdery appearance with particle sizes close to 1 micron. When PLA is increased in the copolymers, the graft shows lower concentration of particles and smaller size, below 100 nm. Moreover, films were prepared by solvent casting and its topography was observed by SEM. Interestingly, whereas the PEDOT and the 40:60 wt% PEDOT-g-PLA (**3**) copolymer film show an inhomogeneous aspect, the copolymer 5:95 wt% PEDOT-g-PLA (**2**) shows a homogeneous surface. Hence, the last copolymer presents a similar aspect as the PLA macromonomer, suggesting that compositions that may show similar printing properties than the well-known PLA.
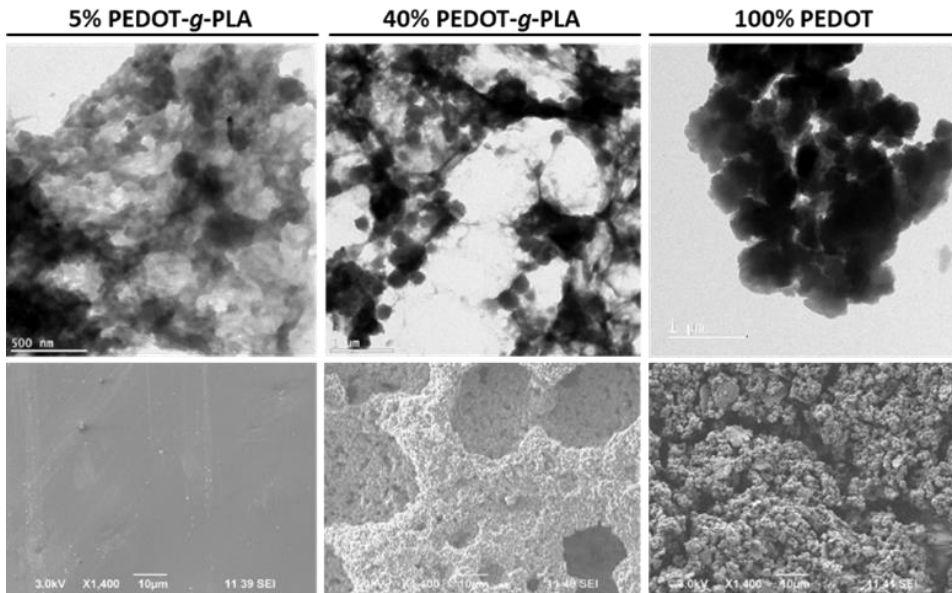
Figure 4.4 TEM images for different PEDOT composition in the graft copolymer (top) and SEM images prepared by drop casting for film of same PEDOT-g-PLA composition (bottom)

After the morphological experiments, we performed the rheological measurements, expecting that not all the compositions presented similar behavior. Therefore, rheological experiments were carried out at 110 ºC above the melting temperature of macromonomers and copolymers. In **Figure 4.5**, complex viscosity (η*) of starting macromonomers and PEDOT-g-PLA copolymers at 0.1Hz are comparatively presented. Complex viscosity shows values higher than 10000 Pa·s for PEDOT percentages above 7%, that correspond to solid-like behavior. Moreover, η* between 10000 and 1000 Pa·s present a transition between solid and liquid that indicate some impediments to its flow. Finally, macromonomers and copolymers with η* ranged between 1 and 100 represent the most suitable compositions, Hence, as can be observed, these compositions are the most suitable for flowing and further printability test.
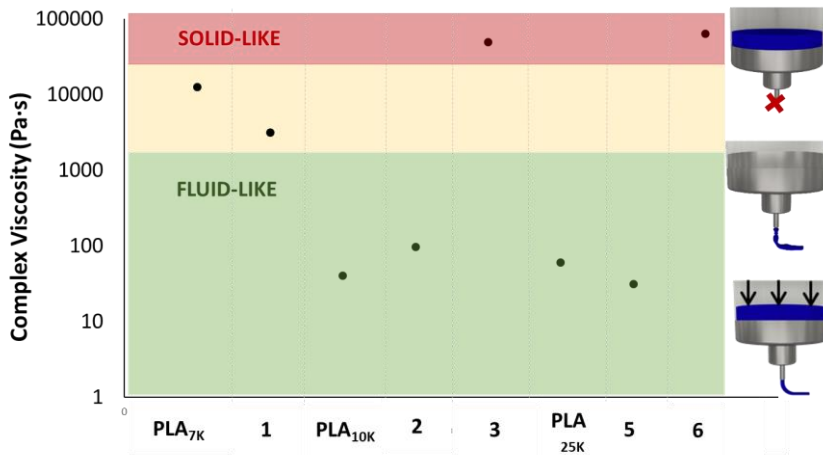
Figure 4.5 Complex viscosity value at 0.1Hz of copolymers and macro-monomers at 110ºC measured in frequency studies

3D printing tests were carried out by direct ink writing (DIW) throughout melting extrusion that consist on warming up the polymer until the melting temperature is reached and extruded by the action of compressed air. Hence, PEDOT-g-PLA inside the metallic extruder and the procedure was followed. As other 3D printing methods, ME deposits the melted polymer layer by layer until obtaining the final object. Some pictures of the different structures printed are presented in **Figure 4.6**, demonstrating good resolution of the printing process.
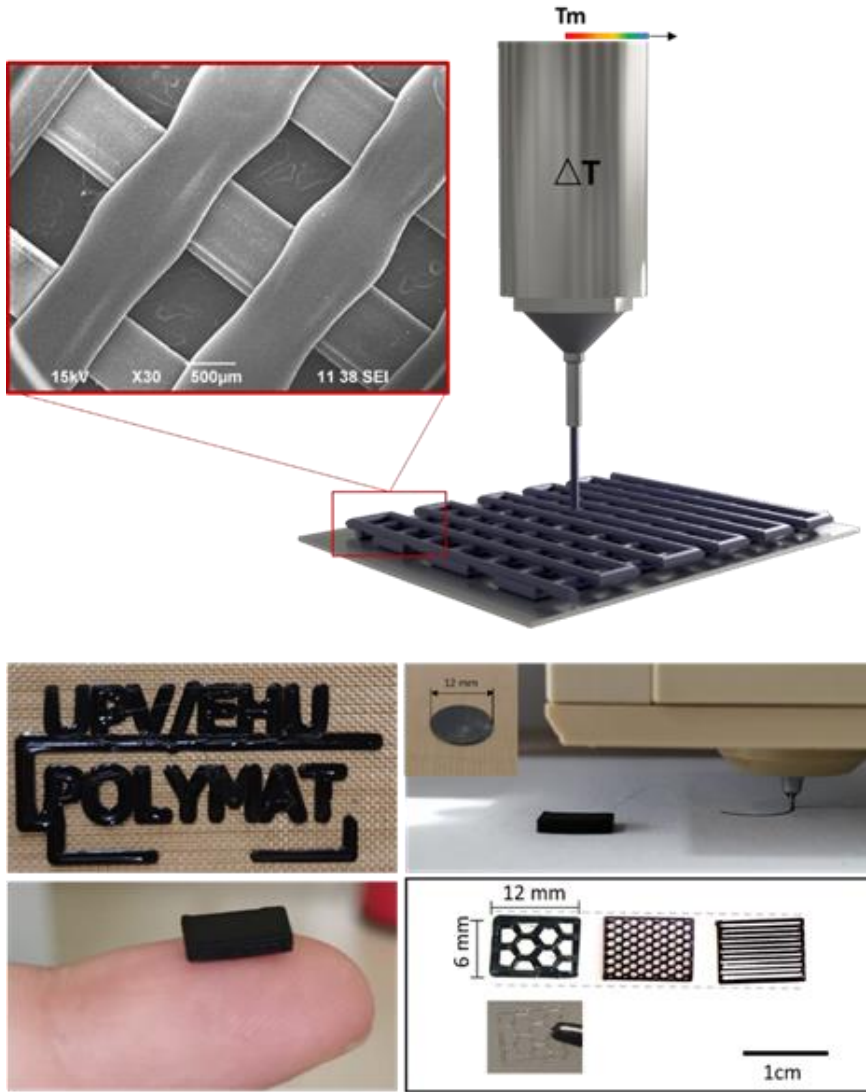
Figure 4.6 SEM image of a printed micro pattern (Upper Left image). Different geometries printed by melting extrusion including patterns used for biocompatibility tests (Bottom)

Interlayer of the printed compositions is presented in **Figure 4.7**. Compositions in the solid-like behavior were impossible to make flow due to its high viscosity. Compositions that present transitions behavior as PEDOT-g-PLA (copolymer **1**) required higher pressures and the use of a physical input (piston). Besides, its copolymers use to block thinner tips decreasing the printing quality due to larger nozzle, *i.e.*, 0.5 mm inner diameter was needed. In the opposite way, copolymer that presented lower complex viscosity PEDOT-g-PLA (copolymer **5**), required lower pressures. However, the high molecular weight makes the layer expand during deposition, thus partially losing its shape. Finally, correlated to complex viscosity measurement, 5:95 wt% PEDOT-g-PLA (copolymer **2**) presented the best performance during the printing. Due to its easy flow, printing presented high controlled shape besides the smaller nozzle used (0.2 inner diameter). Neverthless, slightly layer contraction was observed. Copolymer **2** clearly presented the best printing performance; therefore, it was chosen for it use as patterning of neonatal cardiomyocytes co-cultures.
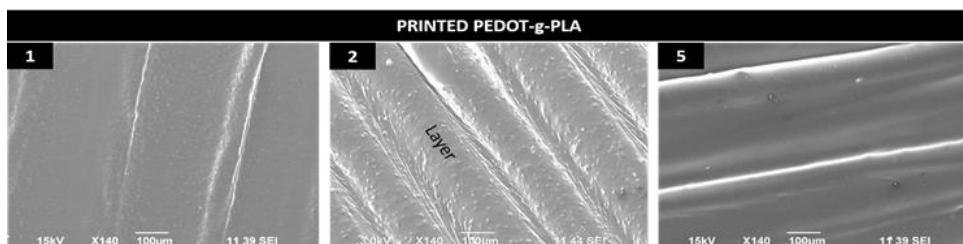
Figure 4.7 SEM images of the 3D printed PEDOT-g-PLA copolymers.

4.2.3 Cardiomyocytes and cardiac fribroblast patterning

Interestingly, previous works have demonstrated that PEDOT-PLA possess dual biocompatibility and electronic conductivity, which is very useful in cell culture of bidimensional films with stem cells[20] or electrospun fibers with skin fibroblasts. [21]

The selected PEDOT-g-PLA copolymer **2** patterned in hexagonal and striped shapes for cardiomyocytes and cardiac fibroblast co-cultures. As it is demonstrated in the literature, cardiomyocytes present elongation, maturation and better function cultured on specific shapes.[7,22,23] Hence, the performance of non-conducting PLA and conductive PEDOT-g-PLA patters was compared. The cell growth and function were compared along the material and between the interstices of hexagonal (1-5 mm diagonal) and stripped pattern structure (200-400 μM space). Differences in the surface morphology between printed PLA and PEDOT-g-PLA can be observed in the **Figure 4.8**.
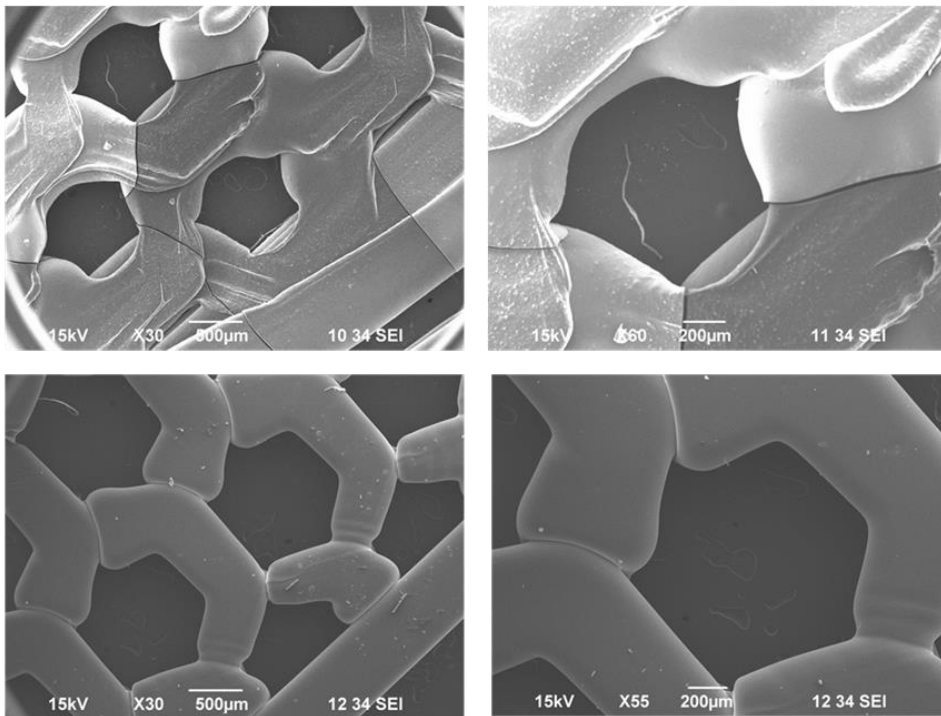
Figure 4.8 SEM images that correspond to hexagonal patterns of medium molecular weight 5%PEDOT-g-PLA copolymer 2 (top) and medium molecular weight macromonomer PLA_{10K} (bottom)

Primary cardiomyocytes (CMs) and cardiac fibroblasts (CF) isolated from neonatal mice 1-3 days old pups were cultured on the prepared patterned scaffolds for 7 days. Gelatin-coated coverslips were used as control. In general, good biocompatibility was observed, and co-culture was grown in all the substrates evaluated. Our patterns have been designed to guide the maturation of the growing cells, there are two areas where cells grow: (i) in the interstices generated within the patterned lines and (ii) on top of the printed material.

Regarding the growth within the interstices, we observe at first glance that both cardiac myocytes and fibroblasts grow as in controls in both linear and hexagonal patterns. However, the most significant difference between the macromonomers and copolymers patterns reside in the ability of the cells to produce fibrous extracellular matrix (ECM) within the interstices of the conductive patterns. Moreover, this pre-tissue is actively beating, suggesting the presence of viable and functional cardiomyocytes. Such fibers are not present in the PLA patterns.

The morphology of the cultured cells was analyzed by staining the sarcomere of the CM with alpha-actinin, and the CF microtubules with anti-vimentin. The fluorescent images of **Figure 4.9** corroborate the attachment of cardiomyocytes on the fibrous ECM generated. These cells present a mature phenotype, with a rectangular shape and linear and organized sarcomere. Furthermore, fibrous large elongations of fibroblasts and abundant cell-to-cell contacts are also clearly distinguished in PEDOT-g-PLA interstices. This suggests that the Fb are able to maintain their typical morphology and their structural supporting function, thus corroborating the potential of our material to facilitate the generation of artificial tissue. On the other hand, the cardiac cells grown within PLA patterned interstices show star-like cardiomyocytes and not-elongated fibroblasts, which are the typical shapes of unmatured cultured neonatal cardiac cells. Regarding the growth on the printed material, the exhibition of fibroblasts is abundant and extend in both PLA and PEDOT-g-PLA surfaces. However, presence of cardiomyocytes observed on

the PEDOT-containing substrate is much higher, suggesting a better attachment of the CMs on the conductive substrate.
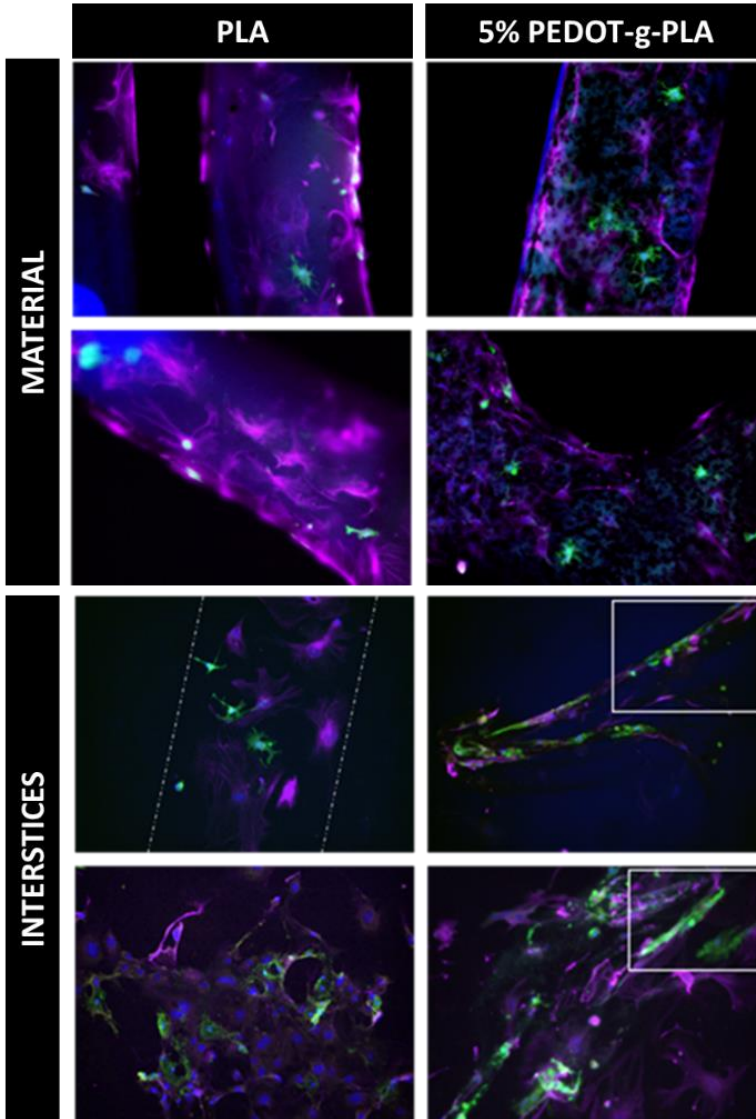
Figure 4.9 Immunofluorescence images of CMs and CFs co-cultures grown on printed PLA and PEDOT-g-PLA patterns for 7 days. Antibody staining against α-

actinin (green) and vimentin (pink) label CMs and CFs, respectively, with nuclei labelled using DAPI (blue)

4.3. Conclusion

In conclusion, in this chapter we have described a new PEDOT copolymer that possess conducting properties beside as it can be printed by direct ink writing throughout melting extrusion, improving one of the main disadvantages of PEDOT: procesability. Hence, a series of graft copolymers with different molecular weight between PEDOT and a different *Mn* tailored PLA were synthesized. The PEDOT-g-PLA copolymers were characterized by FTIR, TGA, UV/Vis confirming the successful copolymerization and the presence of the polytiophene. TEM and SEM evaluated the impact of the copolymer composition at the nanoscopic level showing that at high PEDOT content confer higher particles size as well as less homogeneous films. Complex viscosity by sweep frequency oscillatory studies at the melting temperature suggest two different behaviors, solid-like behavior for higher PEDOT percentages and liquid-like for lower than 7wt%. In line with this observation and the microscopy analysis, copolymers with liquid-like behavior were able to flow and further printed by melt extrusion while the rest present some difficulties. Hence, the best copolymer performance PEDOT-g-PLA (**2**) was patterned in hexagonal and striped shapes for cardiomyocytes and cardiac fibroblast co-cultures. Good biocompatibility was observed and tissue like structure composed of cardiomyocytes supported with fibroblast were developed in PEDOT-g-PLA patterns while random growth was observed in the PLA as control. Moreover, beating of the cardiomyocytes confirmed their correct function. Overall, this chapter have presented as a proof of concept for the manufacture of designed shapes patterns of a novel conducting and biocompatible PEDOT/PLA that was 3D printed by direct ink writing.

4.4. Experimental part

4.4.1 Synthesis of the macromonomer

Nuclear magnetic resonance spectroscopy (NMR)

[1]H and [13]C Nuclear Magnetic Resonance (NMR) Spectroscopies. ^{1}H NMR spectra were used for analyzing the macromonomer conversions. ^{13}C NMR spectra was used for determining tacticity of the PLA.

4.4.2 Synthesis, characterization and printability of the graft copolymers

Fourier transform Infrared spectroscopy (FTIR)

Infrared spectra were recorded at room temperature with a Thermo scientific model Nicolet 6700 FT-IR spectrometer and KBr pellets were used for solid-state IR spectroscopy applying 64 scans in transmission mode. The mixture was morter in a concentration of 2 mg copolymer respect 2 gr of KBr and it was mixed until the homogenize. Finally, the mixture was compressed forming a slightly black pellets.

UV-Vis spectroscopy

UV-Vis-NIR absorption spectra were recorded with a Perkin-Elmer UV/Vis/NIR Lambda 950 spectrometer. In order to avoid saturation absorbance, a solution of 0.5 mg copolymer was diluted in 10 mL of chloroform ($CHCl_3$). The dispersion was sonicated during 15 min and then measured in a quartz cuvette.

Scanning electron microscope (SEM)

Measurements were performed on JEOL JSM-6490LV at 5kV, running in a point by point scanning mode. Previously, cylindrical coverslip with 11 mm diameter were introduced in isopropanol and sonicated during 15 min in order to remove impurities, solvent was evaporated at room temperature. 25 mg of grafting PEDOT

was solubilized in 1 mL of chloroform. After obtain a totally disperse solution, they were sonicated for 15 minutes and drop-casted in a cylindrical glass coverslip. The solvent was evaporated at room temperature. The samples were placed on an aluminum holder and fixed with double-side carbon tape. The samples were introduced in the SEM chamber and evaluated at different magnifications.

Conductivity

The measurements of conductivity were performed on a four-point probe Ossila Sheet using more than three different zones of the film more than three times. For this purpose, 100 µL of each dispersion were drop-casted in glass coverslips and dried at room temperature. The samples were prepared in the same way as SEM samples. First, the thickness of the drop casting was measured using a digital caliper. Then the electrical conductivity was calculated using equipment throughout the thickness of the sample.

Rheology measurenment

Strain and frequency oscillatory experiments were carried out in an ARES rheometer (Rheometrics) at the melting temperature of the copolymers or macromonomers, i.e 110 ºC. Frequency sweeps studies of the different samples were carried out from 0.1 to 100 Hz at constant strain. Alumminium plates of 25 mm of diameter was employed.

3D Printing

The printing process was carried out in a 3D-Bioplotter (Developer Series, EnvisionTEC, Gladbeck, Germany) and the printing geometries were originally designed in Autodesk Inventor 2019. Typically, the printing of the samples was performed at a temperature of 110 °C, with 0.001 mm of maximun resolution, and a maximum pressure of $4 \cdot 10^5$ Pascal. In this study, needles with an inner diameter of 0.4 mm were used.

4.4.3 Cell culture of cardiomyocytes

Isolation and in vitro culture of ventricular cardiomyocytes from neonatal mice (NMVMS)

Primary neonatal mouse ventricular cardiomyocytes (NMVMs) were isolated from 1 to 3-day-old C57BL/10SCSNJ mouse pups, following the Pierce Primary Isolation Kit from Promega. Briefly, ventricles were separated from the atria using scissors, dissociated in HBFF buffer (calcium and bicarbonate-free Hanks buffer with Hepes), and digested with two specific enzymes provided by the Kit manufacturer for 30 mins. Special media for cardiomyocytes enrichment was prepared with Minimum Essential Media (DMEM), supplemented with 5% fetal bovine serum (FBS) and 0.5% Pen/Strep. Myocytes that were either in solution or lightly attached were then separated from the adherent stromal cells by gentle mechanical disaggregation and subsequently plated at a density of $2 \cdot 10^5$ cells/ml in primary petri dishes (Falcon) or in multi-chambered slides coated with 0.1% gelatin (Sigma). The resultant NMVMs were cultured (90k cells per sample) in 2D gelatin-coated plates (2D gelatin controls) or on the 3D printed patterned substrates. After the first 24h, culture medium was changed; afterwards, cell culture medium was changed every 3 days. All the experiments have been performed according to the Biodonostia Animal Care and Use Committee guidelines.

Immunofluorescence

NMVMs were fixed in PBS containing 4% PFA for 15 min at room temperature. Cells were permeabilized at room temperature, with 1% Triton X-100 for 90 min, blocked with 2% BSA in PBS for 45 min and incubated overnight with α-sarcomeric actinin 1:400 (Sigma), to assess the contractile apparatus of NMVMs, and Vimentin 1:400 (Millipore), a cytoskeleton marker commonly used for fibroblast staining, prepared in 2% BSA. Goat anti-mouse antibody conjugated to Alexa

Fluor 488 (Molecular Probes) and Goat anti-chicken antibody conjugated to Alexa Fluor 647 (Invitrogen) were used as secondary antibody 1:400, respectively. Each sample was stained with Hoechst 1:2000 to counter-staining the nuclei. Representative immunofluorescence images were acquired using an ECLIPSE Ti-S/L100 microscope (Nikon) equipped with a 20×S-Fluor objective and attached to a lambda-DG4 illumination system.

4.5 References

(1)   Narupai, B.; Nelson, A. 100th Anniversary of Macromolecular Science Viewpoint: Macromolecular Materials for Additive Manufacturing. *ACS Macro Lett.* **2020**, *9* (5), 627–638. https://doi.org/10.1021/acsmacrolett.0c00200.

(2)   Dominguez-Alfaro, A.; Alegret, N.; Arnaiz, B.; González-Domínguez, J. M.; Martin-Pacheco, A.; Cossío, U.; Porcarelli, L.; Bosi, S.; Vázquez, E.; Mecerreyes, D.; Prato, M. Tailored Methodology Based on Vapor Phase Polymerization to Manufacture PEDOT/CNT Scaffolds for Tissue Engineering. *ACS Biomater. Sci. Eng.* **2020**, *6* (2), 1269–1278. https://doi.org/10.1021/acsbiomaterials.9b01316.

(3)   Williamson, A.; Rivnay, J.; Kergoat, L.; Jonsson, A.; Inal, S.; Uguz, I.; Ferro, M.; Ivanov, A.; Sjöström, T. A.; Simon, D. T.; Berggren, M.; Malliaras, G. G.; Bernard, C. Controlling Epileptiform Activity with Organic Electronic Ion Pumps. *Adv. Mater.* **2015**, *27* (20), 3138–3144. https://doi.org/10.1002/adma.201500482.

(4)   Leleux, P.; Johnson, C.; Strakosas, X.; Rivnay, J.; Hervé, T.; Owens, R. M.; Malliaras, G. G. Ionic Liquid Gel-Assisted Electrodes for Long-Term Cutaneous Recordings. *Adv. Healthc. Mater.* **2014**, *3* (9), 1377–1380. https://doi.org/10.1002/adhm.201300614.

(5)   Pekkanen, A. M.; Mondschein, R. J.; Williams, C. B.; Long, T. E. 3D Printing Polymers with Supramolecular Functionality for Biological Applications.

117

Biomacromolecules **2017**, *18* (9), 2669–2687. https://doi.org/10.1021/acs.biomac.7b00671.

(6) Sanchez-Rexach, E.; Johnston, T. G.; Jehanno, C.; Sardon, H.; Nelson, A. Sustainable Materials and Chemical Processes for Additive Manufacturing. *Chem. Mater.* **2020**, *32* (17), 7105–7119. https://doi.org/10.1021/acs.chemmater.0c02008.

(7) Vunjak-Novakovic, G.; Tandon, N.; Godier, A.; Maidhof, R.; Marsano, A.; Martens, T. P.; Radisic, M. Challenges in Cardiac Tissue Engineering. *TISSUE Eng. PART B-REVIEWS* **2010**, *16* (2), 169–187. https://doi.org/10.1089/ten.teb.2009.0352.

(8) Yuk, H.; Lu, B.; Lin, S.; Qu, K.; Xu, J.; Luo, J.; Zhao, X. 3D Printing of Conducting Polymers. *Nat. Commun.* **2020**, *11* (1), 1604. https://doi.org/10.1038/s41467-020-15316-7.

(9) Heo, D. N.; Lee, S.-J.; Timsina, R.; Qiu, X.; Castro, N. J.; Zhang, L. G. Development of 3D Printable Conductive Hydrogel with Crystallized PEDOT:PSS for Neural Tissue Engineering. *Mater. Sci. Eng. C* **2019**, *99*, 582–590. https://doi.org/https://doi.org/10.1016/j.msec.2019.02.008.

(10) Fantino, E.; Roppolo, I.; Zhang, D.; Xiao, J.; Chiappone, A.; Castellino, M.; Guo, Q.; Pirri, C. F.; Yang, J. 3D Printing/Interfacial Polymerization Coupling for the Fabrication of Conductive Hydrogel. *Macromol. Mater. Eng.* **2018**, *303* (4), 1700356. https://doi.org/10.1002/mame.201700356.

(11) Hofmann, A. I.; Östergren, I.; Kim, Y.; Fauth, S.; Craighero, M.; Yoon, M.-H.; Lund, A.; Müller, C. All-Polymer Conducting Fibers and 3D Prints via Melt Processing and Templated Polymerization. *ACS Appl. Mater. Interfaces* **2020**, *12* (7), 8713–8721. https://doi.org/10.1021/acsami.9b20615.

(12) Gkartzou, E.; Koumoulos, E. P.; Charitidis, C. A. Production and 3D Printing Processing of Bio-Based Thermoplastic Filament. *Manuf. Rev.* **2017**, *4*. https://doi.org/10.1051/mfreview/2016020.

(13)   Sanchez-Sanchez, A.; Rivilla, I.; Agirre, M.; Basterretxea, A.; Etxeberria, A.; Veloso, A.; Sardon, H.; Mecerreyes, D.; Cossío, F. P. Enantioselective Ring-Opening Polymerization of Rac-Lactide Dictated by Densely Substituted Amino Acids. *J. Am. Chem. Soc.* **2017**, *139* (13), 4805–4814. https://doi.org/10.1021/jacs.6b13080.

(14)   Basterretxea, A.; Jehanno, C.; Mecerreyes, D.; Sardon, H. Dual Organocatalysts Based on Ionic Mixtures of Acids and Bases: A Step Toward High Temperature Polymerizations. *ACS Macro Lett.* **2019**, *8* (8), 1055–1062. https://doi.org/10.1021/acsmacrolett.9b00481.

(15)   Basterretxea, A.; Gabirondo, E.; Jehanno, C.; Zhu, H.; Flores, I.; Müller, A. J.; Etxeberria, A.; Mecerreyes, D.; Coulembier, O.; Sardon, H. Polyether Synthesis by Bulk Self-Condensation of Diols Catalyzed by Non-Eutectic Acid–Base Organocatalysts. *ACS Sustain. Chem. Eng.* **2019**, *7* (4), 4103–4111. https://doi.org/10.1021/acssuschemeng.8b05609.

(16)   Coady, D. J.; Fukushima, K.; Horn, H. W.; Rice, J. E.; Hedrick, J. L. Catalytic Insights into Acid/Base Conjugates: Highly Selective Bifunctional Catalysts for the Ring-Opening Polymerization of Lactide. *Chem. Commun.* **2011**, *47* (11), 3105–3107. https://doi.org/10.1039/C0CC03987J.

(17)   Mecerreyes, D.; Stevens, R.; Nguyen, C.; Pomposo, J. A.; Bengoetxea, M.; Grande, H. Synthesis and Characterization of Polypyrrole-Graft-Poly(ε-Caprolactone) Copolymers: New Electrically Conductive Nanocomposites. *Synth.   Met.   **2002**,   *126*   (2),   173–178. https://doi.org/https://doi.org/10.1016/S0379-6779(01)00503-3.

(18)   Marina, S.; Mantione, D.; ManojKumar, K.; Kari, V.; Gutierrez, J.; Tercjak, A.; Sanchez-Sanchez, A.; Mecerreyes, D. New Electroactive Macromonomers and Multi-Responsive PEDOT Graft Copolymers. *Polym. Chem.* **2018**, *9* (27), 3780–3790. https://doi.org/10.1039/C8PY00680F.

(19)   da Silva, A. C.; Augusto, T.; Andrade, L. H.; Córdoba de Torresi, S. I. One Pot Biocatalytic Synthesis of a Biodegradable Electroactive

Macromonomer Based on 3,4-Ethylenedioxytiophene and Poly(l-Lactic Acid). *Mater. Sci. Eng. C* **2018**, *83*, 35–43. https://doi.org/https://doi.org/10.1016/j.msec.2017.09.007.

(20)   da Silva, A. C.; Semeano, A. T. S.; Dourado, A. H. B.; Ulrich, H.; Cordoba de Torresi, S. I. Novel Conducting and Biodegradable Copolymers with Noncytotoxic Properties toward Embryonic Stem Cells. *ACS Omega* **2018**, *3* (5), 5593–5604. https://doi.org/10.1021/acsomega.8b00510.

(21)   Chang, H. C.; Sun, T.; Sultana, N.; Lim, M. M.; Khan, T. H.; Ismail, A. F. Conductive PEDOT:PSS Coated Polylactide (PLA) and Poly(3-Hydroxybutyrate-Co-3-Hydroxyvalerate) (PHBV) Electrospun Membranes: Fabrication and Characterization. *Mater. Sci. Eng. C* **2016**, *61*, 396–410. https://doi.org/https://doi.org/10.1016/j.msec.2015.12.074.

(22)   Noor, N.; Shapira, A.; Edri, R.; Gal, I.; Wertheim, L.; Dvir, T. 3D Printing of Personalized Thick and Perfusable Cardiac Patches and Hearts. *Adv. Sci.* **2019**, *6* (11). https://doi.org/10.1002/advs.201900344.

(23)   Dong, R.; Ma, P. X.; Guo, B. Conductive Biomaterials for Muscle Tissue Engineering. *Biomaterials* **2020**, *229*, 119584. https://doi.org/https://doi.org/10.1016/j.biomaterials.2019.119584.

Chapter 5:

Conclusions and

Future Works

The field of tissue engineering requires the generation of new materials and three dimensional platforms such as controlled scaffolds for model studies. Thus, innovative materials with soft mechanical properties, electrical conductivity, controlled shaoe and porosity and biocompatibility are actively searched in this area. This doctoral thesis has address the challenge of manufacturing 3D structures with conducting polymer such as PEDOT using different secondary supporters as CNTs or PLA polyester. As a result of this work, new and innovative materials and manufacturing techniques have been developed and investigated

for tissue engineering applications. Bellow the partial conclusions of each chapter are described.

Chapter 2: The first project of this thesis was based on the modulation of a general technique used to manufacture films in order to produce tridimensional structures composed of PEDOT and CNT. This represented a huge improvement in the methodology since PEDOT, as other conductive polymers, collapse by itself when is introduced into a 3D macrostructure. For this reason, the addition of CNT became crucial in the manufacturing of this 3D material because they can act as a reinforcement within the lattices allowing the formation of self-standing structures. The reaction consists on a vapour phase polymerization (VPP) in a solid-gas environment where EDOT monomer in gas phase is placed in contact with the oxidant in solid; the heterogeneous reaction occurs in presence of the CNT. The compositions of the scaffolds were studied throughout modulating the reaction conditions and resulted to be correlative with the mechanical properties of the material, which presented weakness when less polymer was present inside the structure. Within the reaction, crystal sugar grains were used as porogen; the formation of homogeneous and controlled porosity was studied by microcomputer tomography. It was quite interesting to observe by SEM the CNT distribution, which were placed along the edges of the holes. Moreover, intimate relationship of the PEDOT with the CNT was confirmed using TEM, which enhance the tridimensional conductivity up to ten times respect with control materials formed by composite of isolating polymer and CNT.

Finally, the devices designed were used as scaffold for cell cultures of astrocytes C8-D1A, which are involve in neurogenesis, studied in neural models and present a first step before their use with other neuronal cell lines. The excellent attachment of the cells and growth was corroborated by actinin and calcein tests, as well as SEM.

As further work, this methodology represents an interesting procedure to introduce functionalized carbon nanotubes with specific functional groups which could improve bioconjugation, biocompatibility among others important parameters in TE. Moreover, the extension of this methodology to other nanostructures as graphene, silver nanowires, plastic crystals or nanoparticles can provide improvements in terms of ionic conductivity, mechanical properties or confers new functionalities to the scaffold.
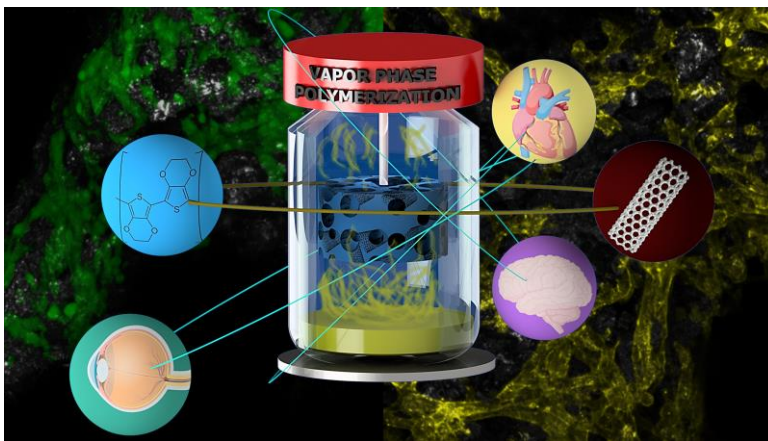
Chapter 3: In the third chapter, a second manufacturing technique was modulated from conventional electropolymerization (EP) to manufacture 3D macrostructures. In this chapter we presented PEDOT/CNT scaffolds avoiding the typical disadvantages as the use of iron based oxidants or strong reaction conditions. The main innovation of this methodology is that we can manufacture real 3D structures thanks to CNT, since they act as nucleation points during the polymerization process in the third dimension. For instances, PEDOT/CNT scaffolds presented more than double size than control PEDOT scaffolds, observation never reported until this day.

PEDOT scaffolds with and without CNT presented differences in their microscope morphology: while PEDOT/CNT scaffolds showed some brush-like structures along the surface similar of the previous scaffolds, PEDOT scaffolds presented a completely smooth topography. Moreover, the presence of tridimensionality in PEDOT/CNT scaffolds resulted in internally connected porous while PEDOT presented a homogeneous opened macrostructure with absence of 3D interconnectivity. The presence of carbon nanotubes improved the conductivity few times than scaffolds in absence of CNT; this result was evaluated by impedance spectroscopy and confirmed by four-point probes.

The scaffolds were used as platforms for spontaneous differentiation of neuroblastoma cell line SH-SY5Y without the addition of any chemical, as typically. Therefore, PEDOT/CNT and PEDOT materials were presented as model structures were neurons can grow and maturate. Moreover, the differentiation was confirmed for PEDOT/CNT scaffolds by the use of different immune assay labeling and SEM morphology evaluation.

As further work, this methodology could be used for the manufacturing of tridimensional structures of conductive polymer derivatives. An improvement in the scaffold functionality could be modulated using different derivativated conductive polymers as bifunctional monomers or PEGylated, among others. This derivative monomer could impact in the mechanical properties due to increment of interconnected conjugated chains and biocompatibility due to presence of PEG moieties. Moreover, as it was introduced in the chapter, drug loading during the polymerization and posterior delivery throughout electrical or chemical changes, (as it was reported in films) could be take into account and study within tridimensional structures evaluating its impacts within *in vitro* or *in vivo* systems..
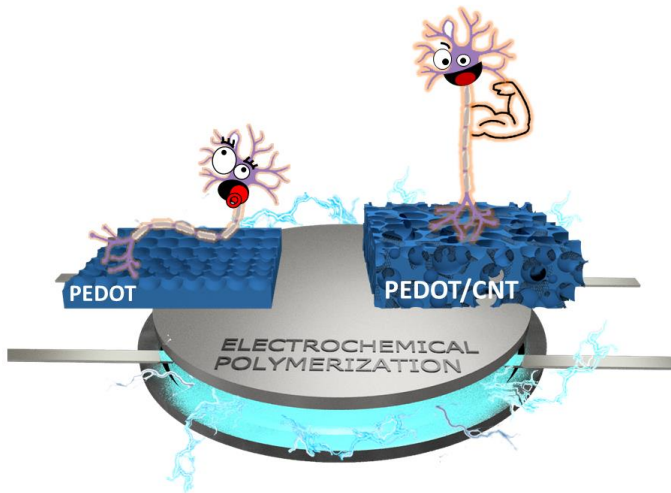
Chapter 4: In the last chapter, we have changed our manufacturing strategy and adapting the thesis to the additive manufacturing megatrend. In this case, we have developed a PEDOT-graft-Polylactide copolymer that could be 3D printed by direct ink writing by melting extrusion. For this purpose, graft copolymers composed by conducting polymer poly(3,4-ethylenedioxythiophene) PEDOT and a biocompatible polymer polylactide (PLA) were designed. The PEDOT-g-PLA copolymers were synthesized by chemical oxidative polymerization between 3,4-ethylenedioxythiophene and PLA macromonomers. PEDOT-g-PLA copolymers with different compositions were obtained and fully characterized. The rheological characterization indicated that copolymers containing bellow 10wt% of PEDOT showed the right complex viscosity values are suitable for 3D printing. The 3D printing tests using the direct ink writing (DIW) methodology was successful and allowed to print different shapes with high resolution (200-300 µm). The conductive and biocompatible printed patterns of PEDOT-g-PLA showed excellent cell growth and maturation of neonatal cardiac myocytes co-cultured with fibroblasts.

In the future, this graft copolymer strategy can be extended to other copolymers such as PEDOT-g-Poly(e-caprolactone). Moreover, printing improvements in stability or conductivity can be achieved using carbon nanomaterials as CNT that can show a beneficial effect in the bioactivity and mechanical properties of the scaffolds.

PEDOT-*g*-PLA
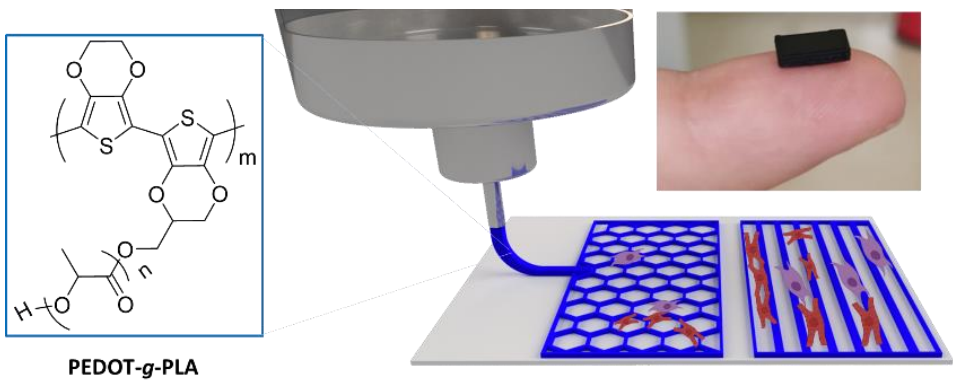
Resumen

El campo de la ingeniería de tejidos (TE) requiere la generación de nuevas plataformas tridimensionales como implantes o materiales tridimensionales para estudios de modelos. Para que estas estructuras cumplan todos los requisitos y mimeticen el tejido nativo se requieren propiedades mecánicas blandas, conductividad eléctrica, porosidad controlada y biocompatibilidad. Esta tesis doctoral ha abordado el desafío de fabricar estructuras 3D con el polímero conductor PEDOT que generalmente colapsa al formar estructuras tridimensionales. Por ello, y para conseguir solventarlo, se han utilizado materiales como soportes secundarios, tal que nanotubos de carbono (CNT) y poliésteres de alto peso molecular. Como resultado de este trabajo, se han desarrollado, caracterizado y aplicado en el campo nuevos e innovadores materiales y sus respectivas técnicas de fabricación. Estos materiales y sus métodos de fabricación

representan la primera piedra para crear materiales conductores y mejorar sus propiedades intrínsecas.

En el **capítulo 2**, se ha modificado una técnica usada generalmente para la fabricación de films de polímeros conductores con el objetivo de producir estructuras tridimensionales conductores. Para ello se ha utilizado una mezcla de CNT y PEDOT que permite su crecimiento tridimensional ya que PEDOT es un polímero de bajo peso molecular que presenta grades limitaciones en este sentido. Por esta razón, la incorporación de CNT presenta un papel crucial en la fabricación de este material 3D porque pueden actuar como refuerzo dentro de los intersticios permitiendo la formación de estructuras autoportantes. La metodología consiste en una polimerización en fase vapor (VPP) donde el monómero EDOT en fase gaseosa se pone en contacto con el oxidante en sólido produciendo el polímero PEDOT. Se ha realizado una importante caracterización de las estructuras generadas, determinando composiciones, propiedades mecánicas, porosidad, topología y conductividad del material. Además, sus propiedades se compararon con estructuras sintetizadas anteriormente que ya han sido testadas y corroboradas para el ámbito de la regeneración de tejido neuronal.

Con el fin de evaluar su potencial uso en ingeniería del tejido, se realizaron cultivos celulares con astrocitos, dado que son células que forman parte de la glía, brindando soporte y nutrientes a las neuronas, por lo que tienen una función esencial en la regeneración del tejido neuronal. Además, que representan un modelo ideal para probar su biocompatibilidad y el potencial de estas estructuras tridimensionales para prótesis neurales y lesión de la médula espinal.

En el **tercer capítulo** se ha modulado otra conocida técnica de fabricación de films por método electroquímico. De esta manera se han fabricado estructuras tridimensionales de PEDOT/CNT evitando desventajas como el uso de oxidantes

o fuertes condiciones de reacción. Una de las principales observaciones que hemos hecho con esta metodología es que se pueden fabricar estructuras realmente con tridimensionalidad gracias al uso de CNT, ya que éstos actúan como puntos de nucleación 3D durante el proceso de polimerización. Sin embargo, en este caso se pudieron fabricar estructuras compuestas sólo de PEDOT, echo que nos ayudó a observar que dichas estructuras poseen la mitad de altura a las homónimas y usando idénticas condiciones de síntesis que las anteriormente citadas de PEDOT/CNT. Al igual que en el anterior capítulo, se hizo una profunda caracterización del material y fue aplicado en la diferenciación de células neuronales.

Generalmente, para la diferenciación espontánea de la línea celular de neuroblastoma SH-SY5Y se utiliza la adición de compuestos químicos como factores de crecimiento u otros. En este trabajo, se ha realizado la misma labor de diferenciación sin el uso de estos compuestos y con el uso exclusivo de las plataformas tridimensionales de PEDOT/CNT y PEDOT. Por lo tanto, estas estructuras se presentaron como estructuras modelo donde las neuronas pueden crecer y madurar. Esta diferenciación se corroboró con el uso de estudios de inmunofluorescencia específicos para neuronas maduras además de la observación específica membranas celulares estiradas y correcta morfología.

Finalmente, en el **capítulo 4** se ha cambiado de estrategia de manera que en lugar de usar nanotubos de carbono, se ha utilizado un polímero de alto peso molecular que además tiene buenas propiedades en impresión 3D. Para ello se ha realizado un macromonomero a medida de PLA que posee al final de la cadena una unidad de EDOT. En un segundo paso, mediante una copolimerización oxidativa se ha insertado en diferentes porcentajes PEDOT. Técnicas como la absorbancia, el infrarrojo, y la TGA se utilizaron para corroborar la unión covalente del PEDOT al macromonómero. Además, como era de esperar, PEDOT afecta de

forma importante a la consistencia y composición del material. Además, esto tiene una incidencia directa a la capacidad del material de formar estructuras continuas tipo film tal y como lo hace el PLA. Finalmente, todas las composiciones que presentaban viscosidades complejas adecuadas, se imprimieron. El copolímero que presentó mejor calidad y resolución de capa fue el que se utilizó para fabricar patrones específicos para el cultivo de cardiomiocitos extraídos de ratones.

Por lo tanto, patrones con forma hexagonal y lineal fueron utilizados para la alineación y maduración de cocultivos de fibroblastos y cardiomiocitos. Observamos que PEDOT ayuda a crear una matriz extracelular entre los intersticios y las estructuras impresas que permiten la maduración de los cardiomiocitos y como consecuencia la mejora de la funcionalidad biológica que se observó a través de la observación de latidos.

List of figures

Chapter 1: Conducting scaffolds for tissue engineering

Chapter 2: Vapor phase polymerization scaffolds

Chapter 3: Electropolymerized scaffolds

Chapter 4: 3D printing scaffolds

List of acronyms

TE	Tissue engineering
CP	Conducting polymer
PEDOT	3,4 poly (ethylenedioxitiophene)
CNM	Carbon nanomaterial
CNT	Carbon nanotube
CP	Conducting polymer
VPP	Vapour phase polymerization
EP	Electro polymerization
ME	Melting extrusion
SEM	Scanning electron microscopy
TEM	Transmission electron microscopy
EIS	Electrochemical impedance spectroscopy
μCT	Micro-computer tomography
YM	Young's modulus
C8-D1A	Astrocytes cell line
LDH	Lactate dehydrogenase
SH-SY5Y5	Neuroblastoma cell line
AM	Additive manufacturing
FFF	Fused filament fabrication

PEDOT-g-PLA	Graft copolymer of PEDOT y PLA
FTIR	Fourier transform infrared spectroscopy
UV/vis	Ultraviolet-visible spectroscopy
CF	Cardiac fibroblast
NMR	Nuclear magnetic resonance
PDMS	Polydimethylsiloxane
PEDOT:PSS	Poly(3,4-ethylenedioxythiophene):poly(styrenesulfonate)
WE	Working electrode
CE	Counter electrode
Ref	Reference electrode
FPP	Four point probe

Publications related with the thesis

The results presented in this thesis have been published and listed below:

Chapter 1:

1. 3D Scaffolds Based on Conductive Polymers for Biomedical Applications
    Nuria Alegret, Antonio Dominguez-Alfaro, and David Mecerreyes
    Biomacromolecules, **2019** 20 (1), 73-89

2. Conductive Polymers Building 3D Scaffolds for Tissue Engineering
    Nuria Alegret, Antonio Dominguez-Alfaro, and David Mecerreyes
    Chapter 10 In Redox Polymers for Energy and Nanomedicine; The Royal
    Society of Chemistry, **2021,** pp 383–414

Chapter 2:

3. Tailored Methodology Based on Vapor Phase Polymerization to
    Manufacture PEDOT/CNT Scaffolds for Tissue Engineering
    Antonio Dominguez-Alfaro, Nuria Alegret, Blanca Arnaiz, Jose M.
    González-Domínguez, Ana Martin-Pacheco, Unai Cossío, Luca Porcarelli,
    Susanna Bosi, Ester Vázquez, David Mecerreyes, and Maurizio Prato
    ACS Biomaterials Science & Engineering **2020** 6 (2), 1269-1278

4. Three-Dimensional Conductive Scaffolds as Neural Prostheses Based on Carbon Nanotubes and Polypyrrole
Nuria Alegret, Antonio Dominguez-Alfaro, Jose M. González-Domínguez, Blanca Arnaiz, Unai Cossío, Susanna Bosi, Ester Vázquez, Pedro Ramos-Cabrer, David Mecerreyes, and Maurizio Prato
ACS Applied Materials & Interfaces **2018** 10 (50), 43904-43914

Chapter 3:

5. Towards Spontaneous Neuronal Differentiation of SH-SY5Y Cells using Novel 3D Electropolymerized Conductive Scaffolds.
Dominguez-Alfaro, A.; Alegret, N.; Arnaiz, B; Salsamendi, M.; Mecerreyes, D. and Prato, M.
In revision to ACS Applied Materials & Interfaces

6. Dominguez-Alfaro, A.; Alegret, N.; Gomez, I. J.; Mecerreyes, D. and Prato, 2D and 3D Immobilization of Carbon Nanomaterials Throughout PEDOT Derivative Co-Polymerization. (Submitted to Polymers)

Chapter 4:

7. 3D Printable Conducting and Biocompatible PEDOT-graft-PLA co-polymers by Direct Ink Writing
Antonio Dominguez-Alfaro, Elena Gabirondo, Nuria Alegret, Claudia Leon, Robert Hernandez, Ainara Vallejo-Illarramendi, Maurizio Prato and David Mecerreyes.
Submitted to ACS Macro Letters

Papers in progress:

8. Review about 3D printing of conducting polymers, ACS Applied Polymer Material

9. Direct ink writing for 3D Printable PEDOT-g-PCL copolymers

Curriculum Vitae

Antonio Dominguez-Alfaro

antoniodominguezalfaro@gmail.com

Education

2015-January 2020 **PhD student** in Applied chemistry and polymeric materials, co-supervised by prof. David Mecerreyes and prof. Maurizio Prato, University of the Basque Country, San Sebastian (Spain). *3D Structures Based on Carbon Materials and Conducting Polymers for Electroresponsive Cell Cultures*

Secondment at the Complex flow of complex fluids, Rice University, Matteo Pasquali group, Houston (Texas), from October to December of 2017

2012-2013 **MSc in Chemistry**
MSc thesis: Synthesis and characterization of diodes of energy transfer with antennas of two-photon excitation, supervised by prof. Uwe Pischel

2013-Not defended **MSc in Industrial Engineering**
MSc thesis: Development and Manufacturing of orthesis for bone regeneration using commercially available 3D printing (pending defense), supervised by prof. Juan Mora

2006-2012 **BSc in Chemical Engineering** (Ingenieria Tenica Industrial en quimica), University of Huelva (Spain).
BSc thesis: Chemical modification of fluorophores with spermine supervised by prof. Uwe Pischel

Experience

Self-employed in 3D printing projects

Languages and skills

Spanish (native), English (B2), Italian (B1)

Mastery of Microsoft Office programs (Word, Excel, PowerPoint)

Knowledge of design and manufacturing of 3D printed parts

Awards, Grants, and Pubblic Engagment

2019	Pint of Science, Oral presentation "El tamaño importa: Nanotecnología" Silvestri, A. and Dominguez-Alfaro, A.
2019	Science Week, Oral presentation "El tamaño importa: Nanotecnología", Alegret, N. and Dominguez-Alfaro, A.
2018 - 2019	Participation International Day of Women and Girls in Science, CIC biomaGUNE
2018	Chillida Prize, Prize conceded to the best Table of Content published within the year in the Innovative Polymers Group
2016	10 Finalist within "XI Concurso ideas de negocio" University of Seville

Publications during the thesis

1. **Dominguez-Alfaro, A**.; Alegret, N.; Gomez, I. J.; Mecerreyes, D. and Prato, 2D and 3D Immobilization of Carbon Nanomaterials Throughout PEDOT Derivative Co-Polymerization. (Submitted to Polymers)

2. **Antonio Dominguez-Alfaro,** Elena Gabirondo, Nuria Alegret, Claudia Leon, Robert Hernandez, Ainara Vallejo-Illarramendi, Maurizio Prato and David Mecerreyes. 3D Printable Conducting and Biocompatible PEDOT-graft-PLA co-polymers by Direct Melting Extrusion (Submitted to ACS Macro Letters)

3. **Dominguez-Alfaro, A**.; Alegret, N.; Arnaiz, B; Salsamendi, M.; Mecerreyes, D. and Prato, M. Towards Spontaneous Neuronal Differentiation of SH-SY5Y Cells using Novel 3D Electropolymerized Conductive Scaffolds. (Submitted to ACS Applied Mater. Interfaces)

4. Nuria Alegret, **Antonio Dominguez-Alfaro** and David Mecerreyes, Book Chappter: Conductive Polymers for Tissue Engineering, in Redox Polymers for Energy and Nanomedicine Book, 2020, The Royal Society of Chemistry, 2021, pp 383–414

5. **Dominguez-Alfaro, A**.; Alegret, N.; Arnaiz, B.; González-Domínguez, J. M.; Martin-Pacheco, A.; Cossío, U.; Porcarelli, L.; Bosi, S.; Vázquez, E.; Mecerreyes, D.; Prato, M.

Tailored Methodology Based on Vapor Phase Polymerization to Manufacture PEDOT/CNT Scaffolds for Tissue Engineering. ACS Biomater. Sci. Eng. 2020, 6 (2), 1269–1278. https://doi.org/10.1021/acsbiomaterials.9b01316

6. Luque, G. C., Picchio, M. L., Martins, A. P. S., **Dominguez-Alfaro, A.**, Tomé, L. C., Mecerreyes, D., Minari, R. J. Elastic and Thermoreversible Iongels by Supramolecular PVA/Phenol Interactions. Macromol. Biosci. 2020. https://doi.org/10.1002/mabi.202000119.

7. Gazzi, A.; Fusco, L.; Orecchioni, M.; Ferrari, S.; Franzoni, G.; Yan, J. S.; Rieckher, M.; Peng, G.; Lucherelli, M. A.; Vacchi, I. A.; Chau, N. D. Q.; Criado, A.; Istif, A.; Mancino, D.; **Dominguez, A.**; Eckert, H.; Vázquez, E.; Ros, T. Da; Nicolussi, P.; Palermo, V.; Schumacher, B.; Cuniberti, G.; Mai, Y.; Clementi, C.; Pasquali, M.; Feng, X.; Kostarelos, K.; Yilmazer, A.; Bedognetti, D.; Fadeel, B.; Prato, M.; Bianco, A.; Delogu, L. G. Graphene, Other Carbon Nanomaterials and the Immune System: Toward Nanoimmunity-by-Design. J. Phys. Mater. 2020, 3 (3), 34009. https://doi.org/10.1088/2515-7639/ab9317.

8. Minudri, D., Mantione, D., **Dominguez-Alfaro, A**., Moya, S., Maza, E., Bellacanzone, C., Antognazza, M. R., Mecerreyes, D. Water Soluble Cationic Poly(3,4-Ethylenedioxythiophene) PEDOT-N as a Versatile Conducting Polymer for Bioelectronics. Adv. Electron. Mater. 2020. https://doi.org/10.1002/aelm.202000510

9. Benitez-Martin, C.; Li, S.; **Dominguez-Alfaro, A**.; Najera, F.; Pérez-Inestrosa, E.; Pischel, U.; Andréasson, J. Toward Two-Photon Absorbing Dyes with Unusually Potentiated Nonlinear Fluorescence Response. J. Am. Chem. Soc. 2020, 142 (35), 14854–14858. https://doi.org/10.1021/jacs.0c07377.

10. A. Dominguez-Tello, **A. Dominguez-Alfaro**, J.L. Gómez-Ariza, A. Arias-Borrego, T. G.-B. Effervescence-Assisted Spiral Hollow-Fibre Liquid-Phase Microextraction of Trihalomethanes, Halonitromethanes, Haloacetonitriles, and Haloketones in Drinking Water. J. Hazard. Mater. 2020. https://doi.org/10.1016/j.jhazmat.2020.122790.

11. Alegret, N.; **Dominguez-Alfaro, A**.; Mecerreyes, D. 3D Scaffolds Based on Conductive Polymers for Biomedical Applications. Biomacromolecules 2019, 20 (1), 73–89. https://doi.org/10.1021/acs.biomac.8b01382.

12. Peña, B.; Maldonado, M.; Bonham, A. J.; Aguado, B. A.; **Dominguez-Alfaro, A**.; Laughter, M.; Rowland, T. J.; Bardill, J.; Farnsworth, N. L.; Alegret Ramon, N.; Taylor, M. R. G.; Anseth, K. S.; Prato, M.; Shandas, R.; McKinsey, T. A.; Park, D.; Mestroni, L. Gold Nanoparticle-Functionalized Reverse Thermal Gel for Tissue Engineering Applications. ACS Appl. Mater. Interfaces 2019, 11 (20), 18671–18680. https://doi.org/10.1021/acsami.9b00666.

13. Alegret, N.; **Dominguez-Alfaro, A**.; González-Domínguez, J. M.; Arnaiz, B.; Cossío, U.;

Bosi, S.; Vázquez, E.; Ramos-Cabrer, P.; Mecerreyes, D.; Prato, M. Three-Dimensional Conductive Scaffolds as Neural Prostheses Based on Carbon Nanotubes and Polypyrrole. ACS Appl. Mater. Interfaces 2018, 10 (50), 43904–43914. https://doi.org/10.1021/acsami.8b16462

14. Alegret, N.; **Dominguez-Alfaro, A**.; Salsamendi, M.; Gomez, I. J.; Calvo, J.; Mecerreyes, D.; Prato, M. Effect of the Fullerene in the Properties of Thin PEDOT/C60 Films Obtained by Co-Electrodeposition. Inorganica Chim. Acta 2017, 468. https://doi.org/10.1016/j.ica.2017.04.059

Conferences

Oral contributions:

1. Reunión Bienal de la RSEQ 2019 –Donosti- 26th-30th May 2019
   "Innovatives Methodologies to Develop Porous 3D Scaffolds Based on PEDOT and CNT for Tissue Engineering"
   Dominguez-Alfaro, A.; Alegret, N.; Arnaiz, B.; Mecerreyes, D. and Prato. M

2. Jóvenes Investigadores en Polímeros (JIP) – Tarragona - 5th-8th June 2017
   "Effect of the fullerene in the properties of thin PEDOT/C60 films obtained by coelectrodeposition."
   Dominguez-Alfaro, A; Alegret, N.; Salsamendi, M.; Mecerreyes, D. and Prato, M.

Poster contributions:

1. ChemOnTubes –Biarritz- 22th-26th April 2018
   "Innovatives Methodologies to Develop Porous 3D Scaffolds Based on PEDOT and CNT for Tissue Engineering"
   Dominguez-Alfaro, A; Alegret, N.; Arnaiz, B..; Mecerreyes, D. and Prato, M.

2. Congreso del Grupo Especializado en Polímeros (GEP) –Punta Umbría- 24th-27th September 2018
   "Vapor Phase Polymerization method to develop 3D scaffolds based on PEDOT/CNT for electroactive tissue regeneration"
   Dominguez-Alfaro, A; Alegret, N.; Arnaiz, B..; Mecerreyes, D. and Prato, M.

Collaboration and funding